Title

Human Induced Pluripotent Stem Cell- and mRNA-based Gene Therapy Strategies for Treatment of Arginase Deficiency

Permalink

https://escholarship.org/uc/item/9gd7r3d8

Author

Truong, Brian

Publication Date

2019

Peer reviewed|Thesis/dissertation

UNIVERSITY OF CALIFORNIA

Los Angeles

Human Induced Pluripotent Stem Cell- and mRNA-based Gene Therapy Strategies for

Treatment of Arginase Deficiency

A dissertation submitted in partial satisfaction of the requirements for the degree

Doctor of Philosophy In Molecular and Medical Pharmacology

by

Brian Truong

2019

ABSTRACT OF THE DISSERTATION

Human Induced Pluripotent Stem Cell- and mRNA-based Gene Therapy Strategies for

Treatment of Arginase Deficiency

by

Brian Truong

Doctor of Philosophy in Molecular and Medical Pharmacology

University of California, Los Angeles, 2019

Professor Gerald S. Lipshutz, Chair

Urea cycle disorders are incurable enzymopathies that affect nitrogen metabolism and typically lead to hyperammonemia. Arginase deficiency is caused by biallelic mutations in ARG1, the final step of the urea cycle, and results biochemically in hyperargininemia and the presence of circulating guanidino compounds while clinically is notable for developmental delays, spastic diplegia, psychomotor function loss, and uncommonly, death. There is currently no completely effective medical treatment available. Current medical treatments for urea cycle disorders are only marginally effective, and for proximal disorders, liver transplantation is effective but limited by graft availability.

Restoring Ureagenesis in Hepatocytes by CRISPR/Cas9-mediated Genomic Addition to

Arginase-Deficient Induced Pluripotent Stem Cells

Advances in human induced pluripotent stem cell research has allowed for the genetic modification of stem cells for potential cellular replacement therapies. In this study, we demonstrate a universally-applicable CRISPR/Cas9-based strategy utilizing exon 1 of the

hypoxanthine-guanine phosphoribosyltransferase locus to genetically modify and restore arginase activity, and thus ureagenesis, in genetically distinct patient-specific human induced pluripotent stem cells and hepatocyte-like derivatives. Successful strategies restoring gene function in patient-specific human induced pluripotent stem cells may advance applications of genetically modified cell therapy to treat urea cycle and other inborn errors of metabolism.

Lipid Nanoparticle Targeted mRNA Therapy as a Treatment for the Inherited Metabolic Liver Disorder Arginase Deficiency

While preclinical strategies have been demonstrated, disadvantages with viral-based episomal-expressing gene therapy vectors include the risk of insertional mutagenesis and limited efficacy due to hepatocellular division and patient-specific genetically modified cell therapies suffer from lengthy preparation time where patients with urea cycle disorders (UCDs) are at continued risk for progressive intellectual decline. Recent advances in mRNA codon optimization, synthesis, and encapsulation within biodegradable liver-targeted lipid nanoparticles (LNPs) have potentially enabled a new generation of rapidly applicable and safer, albeit temporary, treatments to restore liver metabolic function in patients with UCDs including arginase deficiency. In this study, we applied such technologies to successfully treat an arginase deficient murine model. Mice were administered LNP encapsulating human codon-optimized *ARG1* mRNA every 3 days and demonstrated 100% survival with no evidence of hepatotoxicity. Plasma ammonia, arginine, and glutamine demonstrated good control and near-normal ureagenesis was measured. These results suggest that h*ARG1* mRNA delivery by liver-targeted nanoparticles may be a viable gene-based therapeutic for the treatment of arginase deficiency.

The dissertation of Brian Truong is approved.

Samson A. Chow

April D. Pyle

Donald B. Kohn

Gerald S. Lipshutz, Committee Chair

University of California, Los Angeles

2019

DEDICATION

This is dedicated to my parents, Minh and Thu Truong, and my brothers, Johnny, Vu, and Alan

Truong, who have supported me throughout my life and career.

TABLE OF CONTENTS

LIST OF TABLES AND FIGURES

CHAPTER ONE

CHAPTER TWO

ACKNOWLEDGEMENTS

EDUCATION

B.S.	University of California, Los Angeles
2014	Major: Molecular, Cell, and Developmental Biology
	Departmental Honors

AWARDS AND HONORS

2016-2017	Interdisciplinary Training Grant in Virology and Gene Therapy (National Institute of Health)
2014	Graduate Dean's Scholar Award
2013	Initiative for Maximizing Student Diversity Scholars
	CARE Science, Engineering, and Math Summer Program for Undergraduate Research
	Undergraduate Research Fellows Program
	Academic Advancement Program's Robina Riccitiello Scholarship
2010	Scholarship Recognition Award

PUBLICATIONS

Truong B, Allegri G, Liu XB, Burke KE, Zhu X, Cederbaum SD, Haberle J, Martini PGV, and Lipshutz GS. (2019) Lipid Nanoparticle Targeted mRNA Therapy as a Treatment for the Inherited Metabolic Liver Disorder Arginase Deficiency. (2019) PNAS doi: 10.1073/pnas.1906182116.

Liu XB, Haney J, Nieto GC, Lambert JR, Otero-Garcia M, **Truong B**, Gropman A, Sillero MC, Cederbaum SD, and Lipshutz GS. Hepatic Arginase Deficiency Fosters Dysmyelination and Synaptic Abnormalities During Postnatal CNS Development that is Reversed by Arginase 1 Gene Transfer. (2019) JCI Insight doi: 10.1172/jci.insight.130260

Khoja S, Nitzahn M, Hermann K, **Truong B**, Borzone R, Willis B, Rudd M, Palmer DJ, Ng P, Brunetti-Pierri N, and Lipshutz GS. (2018) Conditional Disruption of Hepatic Carbamoyl Phosphate Synthetase 1 in Mice Results in Hyperammonemia without Orotic Aciduria and Can be Corrected by Liver-Directed Gene Therapy. Mol Genet Metab 124(4): 243-253. doi: 10.1016/j.ymgme.2018.04.001.

Vega-Crespo A, **Truong B**, Shoenberg BE, Ciminera AK, Larson BL, Anderson DG, and Byrne JA. (2018) Adult Stem Cell Subsets from Human Dermis. J Stem Cell Res Ther 8:2. doi: 10.4172/2157-7633.1000411.

Angarita S, **Truong B**, Khoja S, Nitzahn M, Rajbhandari R, Zhuravka I, Duarte S, Lin M, Lam A, Cederbaum SD, and Lipshutz GS. (2018) Human Hepatocyte Transplantation Corrects the

Inherited Metabolic Liver Disorder Arginase Deficiency in Mice. Mol Genet Metab doi: 10.1016/j.ymgme.2018.04.005.

Lee P*****, **Truong B***, Vega-Crespo A, Gilmore WB, Hermann K, Kingman S, Tang JK, Chang KM, Lam A, Shoenberg B, Cederbaum SD, Pyle AD, Byrne JA, and Lipshutz GS. (2016) Restoring Ureagenesis in Hepatocytes by CRISPR/Cas9-mediated Genomic Addition to Arginase-Deficient Human Induced Pluripotent Stem Cells. Mol Ther- Nuc Acids doi: 10.1038/mtna.2016.98. ***contributed equally**

Mavila N, Trecartin A, Spurrier R, Xiao Y, Hou X, James D, Fu X, **Truong B**, Wang C, Lipshutz GS, Wang KS, and Grikscheit TC. (2016) Functional Human and Murine Tissue-Engineered Liver is Generated from Adult Stem/Progenitor Cells. Stem Cells Trans Med doi: 10.5966/sctm.2016-0205.

Vega-Crespo A, **Truong B**, Hermann K, Awe J, Chang K, Lee P, Schoenberg B, Wu L, Byrne J, and Lipshutz GS. (2016) Investigating the Functionality of an OCT4-Short Response Element in Human Induced Pluripotent Stem Cells. Mol Ther-Methods and Clinical Development doi:10.1038/mtm.2016.50.

Awe JP, Gschweng EH, Vega-Crespo A, Voutila J, Williamson MH, **Truong B**, Kohn DB, Hasahara N, and Byrne JA. (2015) Putative Immunogenicity Expression Profiling Using Human Pluripotent Stem Cells and Derivatives. Stem Cells Trans Med doi: 10.5966/sctm.2014-0117.

INTRODUCTION

Urea cycle disorders (UCDs) are rare enzymopathies with an incidence of 1:35,000 births resulting in approximately 113 new cases per year in the United States [1]. UCDs result from a deficiency in one of six hepatic enzymes or two mitochondrial transporters that regulate nitrogen metabolism and urea production and are typically classified as inborn errors of metabolism [1-4]. They are a significant cause of inherited hyperammonemia and afflicted infants and newborns are at substantial risk of recurrent brain injury and death. Severity of the UCD is influenced by the enzyme's position in the urea cycle as deficiencies in more proximal enzymes such as carbamoyl phosphate synthase I (CPS1), ornithine transcarbamylase (OTC), argininosuccinic acid synthetase (ASS1), and argininosuccinic acid lyase (ASL) result in ammonia and metabolite accumulation within the first few days of life while a deficiency in arginase I (ARG1), the last enzyme, uncommonly causes hyperammonemia in patients [5]. Excessive plasma ammonia is neurotoxic, resulting in central nervous system injury including intellectual disabilities, seizures, and loss of psychomotor function [1-4, 6]; they also live with continued nitrogen vulnerability. However, the exact mechanism by which ammonia causes brain damage continues to be under investigation; current theories implicate that increased glutamine accumulation, by condensation of excess ammonia and glutamate by glutamine synthetase, causes osmotic stress to astrocytes and cerebral edema [5, 7]. Additional factors also likely play a role as clinical outcomes of proximial UCDs with more severe hyperammonemia phenotypes do not seem to differ from the more distal UCDs [8]. Treatment strategies for specific urea cycle disorders vary, but generally involve dietary protein restriction and emergency treatments for acute hyperammonemic episodes by dialysis or pharmacologic intervention using nitrogen scavengers such as sodium phenylacetate and sodium benzoate [5]. Liver transplantation for treatment of UCDs, though curative, has generally only been recommended for patients suffering from neonatal onset of OTC and CPS1 deficiency or

patients where conventional treatment strategies fall short [5, 9]. However, liver transplants are severely limited in availability and patients can suffer from short- and long-term consequences of immunosuppression [10].

Arginase deficiency (MIM#207800) is an uncommon autosomal recessive disorder (estimated incidence of 1:950,000 in the United States [1]) that results from loss of ARG1 (EC 3.5.3.1). ARG1 is the final enzyme of the urea cycle completing the major metabolic pathway for the disposal of excess nitrogen in terrestrial mammals. Along with red blood cells, the cytosolic enzyme is most prevalent in hepatocytes hydrolyzing arginine into ornithine, which then re-enters the cycle, while nitrogen, in the form of urea, is excreted as waste in the urine [11]. The typical presentation of arginase deficiency is different than that of the other UCDs with onset of symptoms typically in late infancy. Outcomes include microcephaly, seizures, loss of ambulation, clonus, spastic diplegia, intellectual disability (from mild to severe), growth deficiency and failure to thrive [3, 12]; the exact cause of these neurologic manifestations and the progressive intellectual decline is not known but is hypothesized to be related to hyperargininemia and the accumulation of guanidino compounds (as putative neurotoxins) found in the plasma, urine and cerebrospinal fluid of these patients [13-18]. Unlike the other enzyme deficiencies of the urea cycle, hyperammonemia is uncommon [19] and thus patients typically avoid the severe nitrogen vulnerability and catastrophic crises that occur in the other UCDs. However, the neurological decline is progressive and unrelenting, and the mainstay of current day therapy, which includes provision of a very strict protein-restricted diet, amino acid supplementation, and the administration of nitrogen scavengers [3, 12], only partially alleviates the disorder as there exists no medical therapy that is completely efficacious. While liver transplantation has not been commonly employed for patients with this disorder, long-term follow-up of two patients who underwent liver transplantation showed normalization of plasma arginine and guanidino compounds with lack of progressive neurological decline [20, 21], further supporting methods of normalization of plasma arginine levels as tenets of therapy.

2

With the advent of transgenic technology, the development of gene therapies for treatment of inherited monogenic disorders have significantly advanced over the last two and a half decades. Broadly applicable, gene therapy strategies have been investigated for a wide range of disorders including hemoglobinopathies such as beta-thalassemia and sickle cell anemia, primary immune deficiencies such as X-linked SCID and adenosine deaminase deficiency, bleeding disorders such as hemophilia A and B, and liver metabolic disorders such as UCDs [22, 23]. Viral vectors such as the adenovirus, γ-retrovirus, lentivirus, and adeno-associated virus (AAV) have long been the vehicles of choice for the delivery of genetic cargo to restore enzymatic function to cells [24]. However, advantages and disadvantage of each viral vector must be evaluated depending on disease context. Our group, like other groups investigating gene therapy strategies for treatment of liver metabolic disorders, have veered away from using the highly immunogenic adenovirus despite its high hepatotropism and large genetic cargo capacity (~7.5 kb) in place of AAV with its minimal immunogenic response despite its limited genetic cargo capacity (~4 kb) [24]. After developing a mouse model of arginase deficiency that recapitulates several pathobiological aspects of the human condition such as hyperargininemia, hyperammonemia, plasma amino acid profile abnormalities, and mental impairment [25], our group has been successful in demonstrating pre-clinical application of viral-based gene therapy approaches for treating the disorder [26-28]. However, our studies have revealed significant challenges associated with using episomal-based viral vectors for direct systemic *in vivo* genetic delivery mainly highlighted by loss of episomal vector copy number in the rapidly dividing hepatic neonatal murine liver [28]. Therefore, our group has focused on developing novel gene therapy approaches for treatment of arginase deficiency that avoid the complications arising from use of viral vectors.

Liver transplantation has evidence to be the only long-term and curative treatment for UCDs that eliminate the need for daily restrictive diets and absolves the fear of stressors potentially initiating a life threatening hyperammonemic crises [5]. Though uncommonly

3

employed, liver transplantation has been demonstrated to be curative in two patients of arginase deficiency [20, 21]. However, due to the extremely limited availability, liver transplantations are often restricted to severe cases such as neonatal onset of CPS1 and OTC deficiency. Therefore, a potential alternative to liver transplantation is hepatocyte transplantation. Hepatocytes can be isolated from donor livers unsuitable for liver transplantation or from liver segments I and IV available after split liver transplantation [29]. For treatment of UCDs, the majority of the native liver remains functional while transplanted hepatocytes would serve as a living cellular source of full urea cycle function capable of engrafting, expanding and growing with the patient. Hepatocyte transplantation has some theoretical advantages compared to liver transplantation including being less invasive, being less costly, allowing for multiple transplants, the availability of cryopreserved cells, and multiple patients can be treated with a single donor organ [29]. However, in addition to the still quite limited availability of donors, long-term efficacy of these grafts is still being investigated and optimized as insufficient engraftment and graft rejection currently limits their widespread clinical application [29].

Therefore, a potential alternative source for cells could be patient-specific human induced pluripotent stem cell (hiPSC)-derived hepatocyte-like cells (HLCs). Since the demonstration that human fibroblasts could be reprogrammed to a pluripotent stem cell state by overexpression of four defined transcription factors (*OCT4*, *SOX2*, *KLF4*, and *cMyc*), the field of disease modeling and especially, personalized regenerative medicine was revolutionized [30, 31]. Furthermore, researchers invested significant time and resources to elucidate the molecular pathways and examine applicability and optimization of available differentiation protocols to drive hiPSCs down specific disease-relevant cell lineages such as retinal pigment epithelium for age-related macular degeneration [32], neurons for Parkinson's disease [33], cardiomyocytes for heart disease [34], and especially, hepatocytes for liver metabolic disorders and liver disease [35-39]. These hiPSC-derived HLCs demonstrate phenotypic similarities to endogenously derived hepatocytes and can be successfully transplanted and contribute to liver function in

4

various animal models [40]. Additionally, as these hiPSC-derived HLCs would be autologously transplanted back into the same patient, this would theoretically preclude the need for life-long immunosuppression. Thus, with the advancements made to progress the ability to differentiate an unlimited supply of functional hiPSC-derived HLCs, comes the question of whether these cells can be used to treat inherited liver metabolic disorders such as UCDs. However, as these hiPSCs would continue to possess the inherited genetic mutation, methods to restore functional enzyme expression need to be explored.

Conventional randomly integrating viral and non-viral approaches to genomically modify hiPSCs for gene correction are either inefficient or can result in insertional mutagenesis and malignant transformation [41]. The clustered regularly interspaced short palindromic repeats (CRISPR)/Cas9 system is adapted from a prokaryotic immune system response where foreign genetic material is recognized by CRISPR spacers and is removed from the bacterial genome [42]. The engineered CRISPR/Cas9 system contains: 1) a guide RNA including a scaffold sequence required for Cas9 endonuclease-binding and a spacer sequence that binds to the desired genomic target and 2) the Cas9 endonuclease that facilitates nuclease activity [43-45]. Using this CRISPR/Cas9 system, genomic modification, by site-specific homologous recombination at well-defined loci, can efficiently introduce transgenic elements to safe harbor chromosomal loci in hiPSCs and thereby minimize safety concerns. Furthermore, recent studies have demonstrated the feasibility of CRISPR/Cas9-mediated genomic modification of hiPSCs and subsequent differentiation to disease-relevant cell types such as muscle cells, neural lineages, and HLCs [46-48].

Though promising, generating a large population of patient-specific hiPSC-derived HLCs that have been genomically modified for restored enzyme function can take up to several months beginning from a patient skin punch biopsy. However, if recognized at the time of typical symptom presentation, UCD patients may undergo irreversible progressive intellectual decline during this period even with current mainstay treatment strategies. Therefore, RNA-based

therapeutics may serve as a readily available source of enzymatic function to bridge the gap until the cellular therapy is available. Though *in vivo* delivery of mRNA to sites of missing enzyme function is not a new concept, recent advances have been made to increase efficiency and efficacy of this treatment modality to become clinically relevant [49]. Delivery of unmodified mRNA elicits a cellular innate immune system response as Toll-like receptors can recognize single stranded mRNA in the endosome [49]. Therefore, many investigators have turned to developing chemically modified mRNA. These chemically modified mRNAs often contain modified 5' caps, modified nucleosides such as pseudouridine and 5-methylcytidine, sequence codon optimization, and optimized 3' untranslated regions that altogether help avoid innate immunity, aid in mRNA stability, and increase translatability [49]. Even still, it is required to encapsulate the mRNA in order to protect and efficiently deliver the mRNA to target cells or sites *in vivo*.

Lipid nanoparticles (LNPs) are lipid-based particles that have been formulated to encapsulate nucleic acids for research and drug delivery purposes. Therapeutically, LNPs have been demonstrated to encapsulate small interfering RNA, microRNAs, messenger RNA, and DNA. LNPs generally consist of four components: an ionizable cationic lipid that facilitates encapsulation, cellular uptake, and endosomal escape of negatively charged nucleic acids, a helper lipid such as phosphatidylcholine and cholesterol that both provide LNP structural framework, and a coat lipid such as lipid-anchored polyethylene glycol (PEG) that increases blood circulation time and confers immune response evasion properties [50]. Additionally, with the common use of ionizable cationic lipids, resulting liposomes become neutrally charged in the blood circulation and bind to serum proteins such as apolipoprotein E facilitating uptake into target cells with high density of its LDL receptor such as hepatocytes [50]. Therefore, by encapsulating the chemically modified mRNAs with these optimized LNPs, we now have the tools to develop efficacious therapies to deliver enzymatic function to UCD patients.

CHAPTER 1: Restoring Ureagenesis in Hepatocytes by CRISPR/Cas9-mediated Genomic Addition to Arginase-Deficient Induced Pluripotent Stem Cells

Introduction

The urea cycle is the major pathway for detoxification of ammonia and the only pathway for regulating and disposing of excess nitrogen in mammals. Inherited defects in each of its eight steps including six hepatic enzymes and two mitochondrial transporters are known [1]. Though generally considered uncommon, UCDs are a significant cause of inherited hyperammonemia and represent a substantial cause of brain damage and death in afflicted infants and newborns with many cases remaining undiagnosed. For arginase deficiency, patients have a mutation in arginase 1 (ARG1), which regulates the final step of nitrogen removal in the urea cycle converting arginine into urea leading to hyperargininemia. Loss of ARG1 activity results in an inability to remove nitrogen from arginine, but rarely causes symptoms of hyperammonemia. Instead, the cause of the pathogenesis of neurological deterioration in arginase deficiency is not known and is thought to be due to unique biochemical abnormalities such as elevated guanidino compounds, nitric oxide, or glutamine [3, 51-53].

As there is no completely effective treatment for UCDs, the mainstay of therapy is dietary protein restriction, with emergency treatments for hyperammonemia consisting of dialysis, hemofiltration and intravenous administration of nitrogen scavenging drugs [4]. Chronic therapy is minimally effective in reducing plasma ammonia while control of hyperargininemia may delay the onset of symptoms [11, 51] but may not ultimately prevent the progressive and relentless nature of neurocognitive decline. Liver transplantation is the extreme alternative to conventional therapies to prevent progression of neurological injury in UCD patients. However, the demand for liver donors far exceeds the supply, and other avenues, such as genetic modification and cell replacement therapy, need to be explored to treat these disorders.

7

Since the demonstration that human induced pluripotent stem cells (hiPSCs) could be reprogrammed from fibroblasts with four transcription factors (*OCT4*, *SOX2*, *KLF4*, and *cMyc*), hiPSCs have emerged as a potential avenue for patient-specific disease modeling and development of therapy [30, 31, 54-56]. Whereas the difficulty in obtaining primary cell cultures previously hindered progress of disease research, the ability of patient-specific hiPSCs to differentiate into genetically similar somatic cell types of various lineages, such as hepatocytes, allows for the generation of a substantial quantity of patient-specific cells [37, 38]. These hiPSC-derived hepatocytes express liver-specific markers such as albumin (*ALB*), alpha-fetoprotein (*AFP*), and cytokeratin 18 (*CK18*) as well as functionality markers such a1-antitrypsin (*AAT*) and *CYP3A4*, demonstrating their phenotypic similarity to endogenously derived hepatocytes [38]. Reprogramming patient-specific hiPSCs and establishing isogenic and functional derivatives afford the advantage of avoiding the ethical controversy of oocyte-derived embryonic stem cell use and potentially addressing the immunogenicity issues for cell replacement therapies [57].

In this study, we sought to correct the enzyme deficiency, using a universal approach, in multiple arginase-deficient hiPSC lines derived from hyperargininemic patients by using genome editing technology. We delivered CRISPR/Cas9 nickases via nucleofection for gene addition of a full-length codon-optimized human arginase 1 cDNA (ArgO) expression cassette (LEAPR) into Exon 1 of the endogenous hypoxanthine-guanine phosphoribosyltransferase (*HPRT*) locus in hiPSCs [58]. After targeted insertion and puromycin selection (enabled by the LEAPR-derived puromycin N-acetyl-transferase [PAC]), and with confirmation of the presence of the LEAPR cassette in the patient-specific hiPSCs, we demonstrated the restoration of arginase activity in both hiPSCs and differentiated hepatocyte-like cells (HLCs). Additional efforts were also performed to optimize the LEAPR expression cassette and HLC differentiation protocol. An AFP-Reporter/Selection Construct was also developed and investigated to determine if HLCs could be isolated by AFP expression. Lastly, corrected HLCs were transplanted into an immunosuppressed mouse model of hyperarginininemia. Results from this genetic targeting

8

approach potentially offer a widely applicable method to genetically introduce arginase expression in hiPSCs derived from hyperargininemic patients and, on a broader scale, to other single-enzyme inborn errors of metabolism.

Materials and Methods

In vitro derivation and culture of primary human dermal cells

The control human dermal fibroblast cell line (xcHUF1), obtained from UCLA Good Manufacturing Practice (GMP) facility [59], and two disease fibroblast lines (AD2 and AD3) used in this study were obtained from adult skin punch biopsy (after IRB approval and informed consent) and were cultured in methods previously published [54, 60]. One adult disease fibroblast line (GM00954, renamed AD1) was obtained from Coriell Institute for Medical Research (Camden, NJ). All procedures were approved by the Institutional Review Board (IRB #13-001469-AM-00002) and the Embryonic Stem Cell Research Oversight (ESCRO) (ESCRO #2010-010-04A) Committee of the University of California, Los Angeles and informed consent was documented from both patients.

All fibroblast lines were cultured in media consisting of Dulbecco's modified Eagle medium nutrient mixture/F-12 (DMEM/F-12) (Invitrogen, Grand Island, NY), 10% fetal bovine serum (FBS) (Invitrogen), 1x Glutamax (Invitrogen), 1x minimum essential medium nonessential amino acid (Invitrogen) and 1x Primocin (InvivoGen, San Diego, CA). Cells were maintained in a 37°C 5% CO_2 incubator. Media was changed every 1-2 days and cells were passaged with 0.05% trypsin-ethylenediamine tetraacetic acid (EDTA) (Gemini Bio-Products, West Sacramento, CA).

In vitro derivation and culture of human stem cell lines

The control hiPSC line xc-HUF1 and the three disease hiPSC lines (AD1, AD2, AD3) were developed by reprogramming from corresponding parental fibroblast lines via a lentiviral

transduction of a stem cell cassette (STEMCCA) containing the reprogramming factors Oct4, Sox2, Klf4, and c-Myc [61].

Fibroblasts were seeded at a confluency of 10,000 cells/cm^2 prior to transfection. After viral transduction, cells were maintained in a 37°C 5% CO_2 incubator for 3 days in a defined media consisting of DMEM/F-12 (Invitrogen) supplemented with 20% Knockout Serum Replacement (Invitrogen), 1x Glutamax (Invitrogen), 1x Minimal Essential Media Non-Essential Amino Acids Solution (Invitrogen), 1x Primocin (InvivoGen), 1x b-mercaptoethanol (Millipore, Billerica, MA), and 10 mg/mL basic fibroblast growth factor (bFGF) (Biopioneer, San Diego, CA). After 3 days, the cells were passaged with 0.05% trypsin EDTA (Gemini Bio-Products) onto a layer of mouse embryonic fibroblasts (MEFs) (GlobalStem, Rockville, MD) and maintained in culture up to 30 days until putative hiPSC colonies began to form.

All cells were transitioned to and subsequently maintained in feeder-free culture conditions consisting of reduced growth factor Matrigel (BD Biosciences, San Jose, CA) and a 50:50 mix of mTeSR1 media (StemCell Technologies, Vancouver, BC, Canada) and Nutristem (Stemgent, San Diego, CA) supplemented with 1x Primocin (InvivoGen) and 10 mg/mL bFGF. Cells were mechanically passaged every 4 to 5 days, depending on confluency and colony size. To passage the cells, pulled glass pipettes were used to cross-hatch the colonies and to lift the pieces gently for transfer onto new Matrigel-coated plates.

DNA delivery by nucleofection

Cells were prepared for nucleofection by aspirating the media from each well and replacing with 2 ml of mTeSR/Nutristem media supplemented with 10 mM ROCK inhibitor (BioPioneer, San Diego, CA). After 1 hour, the media was again aspirated and replaced with 1 mL Stempro Accutase (Life Technologies) and incubated at 37°C for 4-6 minutes in 1-2 mL of mTeSR1/Nutristem media supplemented with 10 µM ROCK inhibitor in each well to neutralize the Accutase. Cells were then washed and gently scraped into suspension. The cell suspension

was transferred to a sterile 15 mL conical tube and centrifuged for 5 minutes at 80 x g. The supernatant was aspirated and the cells were resuspended in an appropriate volume of mTeSR1/Nutristem media with ROCK inhibitor. 10 ml of the resuspended sample was removed and counted by hemocytometer. Samples planned for nucleofection were prepared as 800,000-1 million cells each. Aliquots were centrifuged for 5 minutes at 80 x g. Supernatant were aspirated and the cells were resuspended in 100 ml of nucleofection solution (Lonza) and placed into nucleofection cuvettes. (Care was taken to carefully resuspend cells to maximize the amount of single cells in suspension and to minimize cell death due to excessive mechanical stress). 1-2 µg of each DNA vector was added and mixed into the nucleofection solution. Controls, 1-2 µg of pMAX-GFP, which is included in the kit, were added to one aliquot of each cell solution. The samples were then securely placed into an Amaxa Nucleofector II (Lonza) and nucleofected using the B-016 program to facilitate cellular DNA vector uptake. The cells were then pipetted into either previously prepared Matrigel-coated plates or directly onto previously prepared plates of MEFs. 72 hours after plating, mTeSR1/Nutristem media was supplemented with 1 µg/ml of puromycin for an additional 72 hours. Following puromycin selection, cells were cultured in mTeSR1/Nutristem media without puromycin. Colonies were expanded until large enough to isolate by mechanical passaging.

Hepatocyte differentiation of induced pluripotent stem cells

To begin hepatocyte differentiation, hiPSCs were passaged at 90% confluency. The next day, the differentiation protocol began as previously published by Song *et. al.* [38]. Briefly, hiPSCs were incubated for 24 hours with Roswell Park Memorial Institute (RPMI) 1640 medium (Life Technologies, Carlsbad, CA), and supplemented with 0.5 mg/ml bovine serum albumin (Sigma-Aldrich, St. Louis, MO), 100 ng/mL Recombinant Human Activin A (Peprotech, Rocky Hill, NJ), and 1x Primocin (Invivogen). On days 2 and 3, 0.1% and 1% insulin-transferrin-selenium (Life Technologies) were added to the previous supplemented RPMI 1640 medium,

respectively. On day 4, hiPSCs were cultured with Hepatocyte Culture Medium (HCM) (consisting of HBM Basal Medium and HCM SingleQuot Kit) (Lonza, Walkersville, MD) supplemented with 30 ng/mL Recombinant Human Fibroblast Growth Factor-4 (FGF-4) (Peprotech), 20 ng/mL Bone Morphogenetic Protein-2 (BMP-2) (Peprotech), and 1x Primocin (Invivogen) for 4 days. The differentiated cells were then cultured in HCM containing 20 ng/ml Recombinant Human Hepatocyte Growth Factor (HGF), 20 ng/mL Recombinant Human Keratinocyte Growth Factor (KGF), and 1x Primocin (Invivogen) for 6 days, and in HCM supplemented with 10 ng/ml Recombinant Human Oncostatin M (OSM) (R&D Systems, Minneapolis, MN), 0.1 mM dexamethasone (Sigma), and 1x Primocin (Invivogen) for the following 5 days. For the last 3 days of the hepatic differentiation, the cells were cultured in DMEM/F:12 (Life Technologies) supplemented with 1x N2, 1x B27, 1x GlutaMAX (Life Technologies), 1x NEAA (Life Technologies), 0.1 mM β-mercaptoethanol (Life Technologies), and 1x Primocin (Invivogen). All media and supplements were filtered prior to use with a 0.22 micron filter and media was changed daily.

Alternatively, hiPSCs were differentiated following the Carpentier *et. al.* protocol until Day 16 [36]. On day 16 of the protocol, the HLCs were cultured an extra 3 days in the "differentiation medium + 10^7 M DEX" and were then cultured 3 days in the "WEM-based maintenance medium" supplemented with 10^7 M DEX. HLCs were collected on Day 22.

Immunocytochemistry

Cells were washed with PBS and fixed with 4% paraformaldehyde (Polysciences, Warrington, PA) in 1x PBS for 15 minutes prior to staining. When necessary, samples were permeabilized in 1% Triton X-100 (Sigma-Aldrich, St. Louis, MO) in PBS for 1 hour at room temperature. Subsequently, all samples were blocked with 5% goat serum (Sigma) in PBS for one hour at room temperature. Primary antibodies were diluted to working concentrations in 5% goat serum; cells were incubated with the primary antibody overnight in 4°C. After incubation,

cells were washed three times with PBS at 5 minutes per wash. Secondary antibodies were diluted in 5% goat serum and cells were incubated for 1 hour at RT. Cells were washed three times with PBS and incubated with 1X DAPI (Thermo, Waltham, MA) for 7 minutes. Fluorescence images were captured with an Axiocam MR Monocolor Camera and AxioVision Digital Image Processing Software (Axio Observer Inverted Microscope; Carl Zeiss, Jena, Germany). The primary and secondary antibodies used for hiPSC and hepatocyte-like cells are listed in Table 1.

Teratoma formation and analysis

Teratomas for the control and disease hiPSC lines were generated by injecting 1 x 10^6 cells (resuspended in Matrigel [BD Biosciences]) subcutaneously into both hind limbs of male severe combined immunodeficient (SCID) mice (Charles River Laboratories, San Diego, CA). Tumors were harvested roughly 1-1.5 months after injection and fixed in 4% paraformaldehyde. Tissues were routinely processed and paraffin-embedded followed by staining with hematoxylin and eosin (H&E). All animal experiments adhered to policies set by the UCLA Animal Research Committee and the UCLA Division of Laboratory Animal Medicine (Protocol #2006-119-22).

Karyotype analysis

hiPSCs were cultured to 95-99% confluency in 25 cm^2 flasks and delivered to Cell Line Genetics, Inc. (Madison, WI) for G-band karyotyping analysis.

Reverse transcription-polymerase chain reaction

RNA was extracted from primary fibroblasts, hiPSCs, and hepatocyte-like cells with a Roche High Pure RNA Isolation Kit (Roche Applied Sciences, Indianapolis, IN) and 10 ng–1 mg was reversed transcribed to cDNA with the Transcriptor First Strand cDNA synthesis kit (Roche Applied Sciences) following the manufacturer's instructions. Primers were designed in

NCBI/Primer-Blast and synthesized by Valugene, Inc. (San Diego, CA) and are listed in Table 2. RT-PCR was performed with 25 ng of cDNA from each sample and each reaction was prepared with 12.5 mL 2x KAPA Fast Genotyping Mix (Kapa Biosystems, Wilmington, MA) and with 10 mM forward and reverse primers and was run on a LightCycler 480 Real-Time PCR System (Roche Applied Sciences). Gels were made with 2% agarose (Bio-Rad Laboratories, Hercules, CA) and 1x SYBR Safe DNA Gel Stain (Life Technologies) in tris-acetate-EDTA (TAE) buffer and run on a PowerPac Basic Power Supply (Bio-Rad, Hercules, CA) at 90v for 30 minutes.

Quantitative reverse transcription polymerase chain reaction

Total RNA was isolated from cultures with a Roche High Pure RNA Isolation Kit (Roche Applied Sciences) and 250 ng-1 mg was reverse transcribed to cDNA utilizing a Transcriptor First Strand cDNA Synthesis Kit (Roche Applied Sciences). Primers for endogenous arginase and human codon-optimized arginase and probes (designed from the Roche Universal Probe Library) were synthetized at Valuegene Inc. (Table 3). Quantitative PCR relative gene expression experiments were performed with 10 ng of cDNA on a LightCycler 480 Real-Time PCR System (Roche) and data was analyzed with LightCycler 480 Software (release 1.5.0.). Triplicate experimental samples were paired using the all-to-mean pairing rule ΔCt value calculation with GAPDH for advanced relative quantification.

Cloning and gene optimization

pUC18-HPRTx1-LHA-hEF1α-ArgO-IRES-PAC-HPRTx1-RHA was cloned by PCR of HPRTx1 (Exon 1)-RHA(Right Homologous Arm) with primers 5-HPRT-RHA-NotI (GCATGCGGCCGCCAGTCAGCCCGCGCGCC) and 3-HPRT-RHA-PstI (CGATCTGCAGCCTGCCGCCCTCGCGT) and restriction enzyme digested with NotI and PstI. HPRTx1-LHA (Left-Homologous-Arm) was synthesized by GeneWiz, removed and isolated from pUC57-Kan by digestion with EcoRI and XbaI. hEF1α-ArgO-IRES-PAC was removed and

isolated from pRRL-hEF1α-ArgO-IRES-PAC with XbaI+NotI digest. Two synthetic polyadenylation sequences [62] were inserted 3' of HPRTx1-LHA and 5' of HPRTx1-RHA by cutting and inserting the sequences with SpeI and NotI, respectively. Oligonucleotides were synthesized by ValueGene and annealed together to create inserts for cloning. Finally, all inserts were ligated together with pUC18 digested by EcoRI and PstI. DNA was introduced into cells by nucleofection (see Supplemental Experimental Procedures for details).

Human codon optimized arginase (*ArgO*) was developed by running the amino acid sequence of arginase 1 through Gene Designer 2.0 software (DNA2.0, Menlo Park, CA) against the *homo sapiens* codon usage table. Once the initial sequence was produced, it was run through NetGene2 (http://www.cbs.dtu.dk/services/NetGene2/) to find any cryptic splice sites. This sequence was then checked for any long repeats in Oligonucleotides Repeat Finder (http://wwwmgs.bionet.nsc.ru/mgs/programs/oligorep/InpForm.htm). Any variations needed to delete splice sites or long repeats were silent mutations that used the next most common codon in the *Homo sapiens* codon usage table.

Junction PCR and sequencing analysis

To verify targeted integration of our donor vector in corrected hiPSCs, each 5' and 3' junction of the integrated vector was analyzed by PCR and DNA sequencing. Reactions were prepared with genomic DNA, 12.5 mL of Phusion High-Fidelity PCR Master Mix (New England BioLabs, Ipwich, MA), 10.25 mL of water, and 1.25 mL of forward and reverse primers for the 3' and 5' ends of Exon 1 of HPRT (Table 4).

For sequencing, PCR bands were extracted and purified using the Wizard SV Gel and PCR Cleanup System (Promega, Madison WI) and the purified products were sent to Laragen (Culver City, CA) for sequencing analysis.

Off Target Analysis

To identify potential introduced mutations at other regions in the genome, off-target binding/cutting of the DNA by the CRISPR/Cas9 nucleases resulting in insertions or deletions (INDELs) was analyzed at the predicted most common sites for each CRISPR/cas9 nickase as determined by the MIT CRISPR Design website (crispr.mit.edu). Each corresponding gDNA region sequence was downloaded from the PubMed genebank. PCR primers were designed using the ThermoFisher primer designer (www.thermofisher.com/oligoperfect.html). Appropriate primers were synthesized by Integrated DNA Technologies (Coralville, IA) to amplify each off-target region. For particularly GC-rich regions, 5% DMSO or Betaine (Sigma) was added. The region on the other HPRT allele was amplified using the same 5'F and 3'R junction PCR primers as was used for junction PCR analysis. Each potential off-target region was amplified by PCR from both the parental and genetically modified gDNA samples of AD1 using the Phusion PCR Master Mix (ThermoFisher). PCR conditions were set according to manufacturer recommendations: 1. 98C 30s, 2. 98C 10s, 3. 57C 30s, 4. 72C 1min, Repeat 2-4 35x, 5. 72C 5 min, 6. 4C hold using Phusion high-fidelity PCR master mix (ThermoFisher). PCR products were run on a 1% agarose gel for approximately 20 minutes at 100V. Bands were extracted using the Wizard SV Gel and PCR Cleanup System, followed manufacturer protocol and were sequenced by Laragen.

To also determine if both HPRT alleles were integrated with the LEAPR construct, we performed quantitative real time PCR (codon-optimized arginase, genomic GAPDH, and genomic HPRT) of each AD line knowing that AD1 and AD3 were XX and AD2 was XY. Knowing this, we reasoned that we should see twice as much genomic HPRT in AD1 and AD3 compared to AD2 (Figure S7 top). In addition, we reasoned that we should see the same amount of codon-optimized arginase expression in all three AD lines relative to GAPDH (Figure S7 middle). Finally, if only one allele was integrated we should detect half as much codon-optimized arginase expression in AD1 and AD3 compared to AD2, relative to HPRT (i.e. 1 copy

of codon-optimized arginase per 2 copies of HPRT in AD1 and AD3 compared to 1 copy of codon-optimized arginase per 1 copy of HPRT in AD2) (Figure S7 bottom).

Functional assay for arginase activity

Arginase activity was measured in cell lysates. 2×10^6–4×10^6 cells were pelleted by low-speed centrifugation and frozen for each sample. Cell pellets were lysed at 20,000 cells/mL in lysis buffer. Primary tissue sample controls were homogenized with 40 mL of lysis buffer/mg of tissue. Lysis buffer was prepared with 0.1% Triton X-100 and 1x HALT protease inhibitor cocktail (Thermo) and urea production was measured as previously performed [27, 28]. Briefly, samples were centrifuged at 100 x g for 5 minutes at 4°C and the supernatant was collected. An activated mixture, consisting of 12.5 mL of 50 mM Tris-Cl (pH 7.5), 12.5 mL of 10 mM MnCl, and 25 mL of the supernatant was incubated at 56°C for 10 minutes. 2.5 mL of the activated mixture was added to 25 mL of 0.5 M arginine (pH 9.7) and incubated at 37°C for 1 hour. After incubation, 72.5 mL ddH$_2$O was added to bring the final volume to 100 mL. 400 mL of an acid mixture, consisting of 1 part H$_2$SO$_4$ (95%), 3 parts H$_3$PO$_4$ (85%), and 7 parts ddH$_2$O, in addition to 25 mL of 9% isonitrosopropiophenone (ISPF) in ethanol, was added to samples and urea standards. Urea standards were prepared at 9.3, 18.7, 37.5, 75, 150, and 300 mg/mL in ddH$_2$O. The final mixture was incubated at 100°C for 45 minutes. After incubation, samples were cooled to room temperature and protected from light for 10 minutes. 200 mL of each sample was aliquoted in duplicate and measured at an optical density of 540 nm in a 96-well plate in a plate reader (Bio-Rad).

Sequencing Analysis

Fibroblasts were cultured in 25 cm^2 flasks and delivered to GeneDx (Gaithersberg, MD) for complete *Arg1* gene sequencing and mutation analysis. Mutations were analyzed in hiPSC and hepatocyte progeny in the UCLA Orphan Disease lab by PCR followed by Sanger

sequencing. Select regions of the *Arg1* gene were amplified by PCR using standard conditions (95° for 2 min [1 cycle]); 94° for 30 sec, 60° for 30 sec, 72° for 1 min [35 cycles]; 72° for 3 min [1 cycle]; hold at 10°). Primer sequences for the c.61C>T variant were as follows: (5'-TTTGCACAAACTACTTGTTCACTG-3'; 5'-TCAGAGTGGGGAGGAAATCA-3'). Primers for the c.365G>A variant were as follows: (5'-AAAACCAAGTGGGAGCATTG-3'; 5'-CCTTCCACCTCCTGAATGTC-3'). Primers for the c.709G>A variant were as follows: (5'-CATGAAATAATGGGTTGCTACTTTT-3'; 5'-TTGCTTCTCTATTACCTCAGATTGTT-3'). Primers for the c.892G>C variant were as follows: (5'-CCATCGGTTACTACCTTTTTCTG-3'; 5'-TCTGAAAGAACAAGTCTTTAGAAGG-3'). An aliquot of each PCR product was confirmed by gel electrophoresis based on its predicted amplicon size. The rest of the PCR product was purified using the QIAquick PCR purification kit (Qiagen) and subjected to bidirectional sequencing using ABI BigDye v3.1 terminators on an ABI 3130xl genetic analyzer (Applied Biosystems, Foster City, CA). The sequence traces at each location were manually analyzed for the presence of a variant using the SequenceScanner v.1 software (Applied Biosystems, Foster City, CA) in comparison to the GenBank reference sequence NM_000045.3.

Statistical Analysis

All collected data was analyzed with the SPSS (Armonk, NY) statistical package (Version 21.0). Results were expressed as mean ± standard deviation (SD) and p values were determined using a one-way ANOVA to examine significance across comparisons. Error bars represent SD.

Results

Derivation of patient-specific hiPSCs from arginase-deficient dermal fibroblasts

We derived genetically-distinct hiPSC lines from dermal fibroblasts taken from three patients with hyperargininemia. The first disease dermal fibroblast line, AD1, originating from a female argininemic patient, was purchased from Coriell (GM00954). Two additional dermal fibroblast lines, AD2 and AD3, were derived from skin punch biopsies obtained from a male and female patient, respectively. The AD dermal fibroblasts were successfully reprogrammed to hiPSCs using a lentiviral vector expressing a constitutive polycistronic cassette (STEMCCA) encoding the four transcription factors *OCT4*, *SOX2*, *KLF4*, and *cMyc* [54, 60, 63]. Dermal fibroblasts were transduced with the STEMCCA lentivirus and were maintained in culture for 30 days on MEFs before conversion to feeder-free culture conditions. The control hiPSC line (xcHUF1), derived from the dermal fibroblasts of a healthy adult male, was previously established in the lab using the same reprogramming methodology [59].

AD1, AD2, and AD3 hiPSC lines exhibited normal stem cell-like morphology throughout the course of the study. Characterization of the AD hiPSCs included immunophenotyping for common pluripotent stem cell markers, alkaline phosphatase staining, *in vivo* teratoma formation, and karyotype analysis. AD1, AD2, and AD3 hiPSCs stained positive for pluripotency markers: Oct4, NANOG, SSEA-3, SSEA-4, Tra-1-60, Tra-1-81 and all exhibited positive alkaline phosphatase activity (Figure 1-1A). AD hiPSCs were collected and injected subcutaneously into the hindleg of SCID mice for *in vivo* teratoma analysis. Teratoma sections from AD1, AD2, and AD3 were stained with H&E and exhibited formation of gut (endoderm), neuroectoderm (ectoderm), and chondrocyte (mesoderm) derivatives, demonstrating the ability of our hiPSCs to form tissues from all three germ layers (Figure 1-1B). Furthermore, normal karyotypic analyses, with no genomic abnormalities, were detected through G-banding studies of AD1, AD2, and AD3 hiPSC lines (Figure 1-1C). Additionally, the specific arginase mutations were determined for each line (Figure 1-1D). Characterization of all three diseased hiPSCs were compared to

non-diseased controls as xcHUF1 hiPSCs and demonstrated no difference in pluripotency profile (data not shown).

Design of ArgO and vectors for gene correction of hiPSCs

To correct for the mutant *Arg1* gene in our patient-derived AD hiPSCs, we designed a selectable, full-length codon-optimized human arginase cDNA (*ArgO*) expression cassette under the constitutive control of the human elongation factor 1a (hEF1a) promoter, referred to as LEAPR (**L**eft homologous arm-h**E**F1a-**A**rgO-IRES-**P**uro(R)-**R**ight homologous arm), to be inserted into Exon 1 of the HPRT locus (Figure 1-2A). Utilizing CRISPR/Cas9 nickases to bind and cleave Exon 1 of HPRT, we achieved targeted LEAPR addition into this desired site. LEAPR addition and disruption of the HPRT locus allowed for secondary positive clonal selection of successful on-target integration via resistance to 6-thioguanine (6-TG) treatment. Additionally, a puromycin resistance gene encoded within the LEAPR construct afforded the ability to utilize an efficient dual selection method to isolate a clonal population of cells that successfully integrated our vector into the HPRT locus. After dual selection with puromycin and 6-TG, AD1, AD2, and AD3 hiPSCs maintained normal stem cell-like morphology (data not shown).

Evaluation of Targeted Integration and Expression of ArgO into Corrected hiPSCs

After delivery of the LEAPR construct, we performed experiments to verify correct on-target integration into the AD hiPSCs. AD hiPSCs were first dual-selected by two cycles of 1 µg/mL puromycin treatment for 72 hours followed by 6-TG treatment. Dual-resistant cell populations were then clonally selected into three subclones each for all AD hiPSC lines. To analyze the targeted integration of our donor vector into Exon 1 of the HPRT locus, primers were designed to span each junction between the endogenous genome and our inserted vector. For each junction, one primer was designed to bind a region of the genome outside of the

homologous arm region, and another was designed to bind a sequence within our inserted donor vector. Products at both 5' and 3' junction sites demonstrated on-target integration of our LEAPR construct in each of three subclones of the corrected AD1, AD2, and AD3 hiPSC lines (Figure 1-2B). Additionally, sequencing analysis of the junction PCR products showed the seamless transition between donor vector sequence and the endogenous genome sequence of our gene-corrected cell lines at both the 5' and 3' junctions of our gene cassette insert (Figure 1-2C).

To further characterize the targeted integration of LEAPR into the AD hiPSCs, we utilized qRT-PCR to determine whether the LEAPR construct integrated into one or both HPRT alleles in corrected AD1 and AD3 LEAPR hiPSCs and also used sequencing technology to further examine AD1. As AD1 and AD3 are XX and AD2 is XY, qRT-PCR confirmed and demonstrated twice the levels of genomic HPRT (gHPRT) in AD1 and AD3 compared to AD2 relative to genomic GAPDH (gGAPDH) (Figure 1-S4 top). Furthermore, qRT-PCR demonstrated equal amplification of ArgO, a unique element of the LEAPR construct, relative to genomic GAPDH demonstrating an equal number of LEAPR integrations throughout the genomes of AD LEAPR hiPSCs (Figure 1-S4 middle). Finally, qRT-PCR demonstrated AD1 and AD3 with half the level of ArgO compared to AD2, relative to HPRT consistent with the integration of 1 LEAPR copy per 2 HPRT alleles in AD1 and AD3 and 1 LEAPR copy per 1 HPRT allele in AD2 (Figure 1-S4 bottom). We also sequenced the other HPRT allele of AD1 which showed lack of an integration, confirming that only one allele had the integrated donor arginase construct. However, because of nuclease activity at that site, 5 genetic mutations were introduced in the other HPRT allele, the first 4 being silent mutations and the fifth resulting in a serine to phenylalanine amino acid change (data not shown).

Off-target analysis was performed in AD1 LEAPR hiPSCs to determine and quantify potential insertions and deletions (INDELs) due to off-target sequence homology for nickases A and B. High probability sites for off-target nickase binding for each nuclease were determined *in*

silico (probability scores of 1.37, 0.86, and 0.86 for nickase A and 0.58 and 0.58 for nickase B [out of a maximum score of 100]) were examined via sequencing. Analysis demonstrated 0% INDELs at all sites (Figure 1-S3A and 1-S3B).

Arginase levels were examined in the LEAPR-corrected hiPSC lines by measuring RNA expression via qRT-PCR and functionality via urea production (i.e. restoring ureagenesis). After puromycin and 6-TG selection, corrected hiPSCs (n = 3) expressed significantly higher RNA levels (p < 0.001) of codon optimized arginase compared to wild type arginase RNA levels in uncorrected AD hiPSCs, demonstrating on-target integration and expression in all three corrected hiPSC lines. The integration of *ArgO* increased arginase mRNA levels in AD1, AD2, and AD3 hiPSCs to 57%, 92%, and 46% (replicates of n = 3 per sample) respectively when compared to wild type arginase levels in human fetal liver (Figure 1-3A). Additionally, all corrected AD hiPSCs exhibited a significant increase (p < 0.001) in urea production itself (i.e. functional activity) when compared to their uncorrected counterparts (Figure 1-3B). Functionality of corrected AD1 hiPSCs increased to 102% (p = 0.021) of that measured in human fetal liver levels (Figure 1-3B). Varying degrees of recovery were observed in AD1, AD2, and AD3 corrected lines; however, the lowest recorded recovery level was still 71% of the primary fetal liver (Figure 1-3B). Taken together, these data demonstrate 1) a high specificity of integration into Exon 1 of the *HPRT* target site as well as 2) a high codon optimized arginase RNA expression with substantial functional arginase enzyme activity in hiPSCs.

Directed differentiation of human pluripotent cells into hepatocyte-like cells

Using a previously published protocol [38], we differentiated the corrected AD1, AD2, and AD3 hiPSCs, their uncorrected counterparts, and control xcHUF1 hiPSCs into HLCs. After 21 days, we assessed expression of specific liver markers and assessed liver cell-specific functions of our derivatives. Morphology of the genetically modified AD1 LEAPR HLCs

22

resembled both that of their uncorrected counterparts (AD1 WT HLCs) and primary human hepatocytes (PHHs) (shown in Figure 1-4A; AD2 and AD3 shown in Figure 1-S1A).

At the end of the final differentiation stage, we characterized the expression of hepatic markers in our derivatives. Similar to the PHH control, LEAPR-corrected AD1, AD2, and AD3 derivatives stained positive for albumin (Figure 1-4A for AD1 and Figure 1-S1A for AD2 and AD3). The HLCs exhibited expression of *AFP*, whereas the PHH control was essentially negative for *AFP* (Figure 1-4A). This observation is consistent with previous studies demonstrating that PSC-derived HLCs more closely mimic fetal as opposed to adult hepatocytes [64]; that is, mature hepatocytes lose *AFP* expression while more fetal-like hepatocytes continue to express *AFP*. Therefore, we compared RNA expression of multiple hepatic-specific markers of the derivatives to a human fetal liver control. RT-PCR analysis showed that AD1, AD2, and AD3 HLCs all expressed hepatic functional genes including: *ALB, AFP, AAT, CK18, CPS1, CYP3A4, FIX, TF, TDO2,* and *UDP-GT* (Figure 1-4B for AD1 and Figure 1-S1B for AD2 and AD3). PHHs and fetal liver were used as positive controls for the immunostaining and RT-PCR analysis, respectively.

Additionally, we assessed liver-specific functionality of both our genetically modified and unmodified AD1, AD2, and AD3 HLCs. At day 21, we measured glycogen storage via Periodic Acid-Schiff (PAS) staining of all hepatic derivatives. Similar to PHHs, corrected AD1, AD2, and AD3 HLCs stained positive by PAS (Figure 1-4A for AD1 and Figure 1-S1A for AD2 and AD3). These results demonstrate that genetic modification of hiPSCs with our LEAPR construct does not interfere with the capability of the cells to differentiate into HLCs.

Evaluation of arginase expression and functionality in hepatocyte-like cells

We examined codon optimized arginase RNA expression and functionality in the hiPSC-derived HLCs to determine the maintenance of arginase expression after directed differentiation. After the final differentiation step, RNA was collected from LEAPR-corrected

AD1, AD2, and AD3 HLCs and arginase levels were quantified and compared to both corrected

hiPSC and fetal liver levels via qRT-PCR. Hepatic differentiation did result in a decrease in

arginase RNA expression in all three LEAPR-corrected HLC lines compared to undifferentiated

hiPSCs ($p < 0.001$ for AD1, AD2 and AD3) (Figure 1-5A). However, despite the decline in RNA

expression compared to hiPSCs, AD1, AD2, and AD3 HLCs maintained arginase levels of 27%,

39%, and 36% of fetal liver *Arg1* levels (AD1, AD2, and AD3 respectively).

Next, we determined if targeted integration of the LEAPR construct affected expression

of the wild type mutated arginase and other endogenous urea cycle-specific genes in the

hepatocyte-like cells, specifically, carbamoyl phosphate synthase 1 (*CPS1*), which catalyzes the

synthesis of carbamoyl phosphate from glutamine. We measured mRNA levels of *CPS1* in both

uncorrected and corrected hiPSCs and HLCs (Figure 1-S2). Similar to wild-type mutated

arginase mRNA expression, *CPS1* levels were significantly increased post-differentiation in both

uncorrected and corrected lines ($p < 0.01$ for AD1 uncorrected lines; $p < 0.001$ for AD1

corrected, AD2 uncorrected and corrected, and AD3 uncorrected and corrected lines). These

data suggest that the increasing arginase expression with our LEAPR construct in the disease

lines does not negatively impact the expression of other endogenous urea cycle-specific genes.

With the above decline in RNA expression, there was an expected post-differentiation

decline observed in ureagenesis of the LEAPR derivatives ($p < 0.001$ for AD1 and AD3; $p =$

0.001 for AD2 compared to corrected hiPSCs). Importantly, though, all three corrected HLC

lines maintained greater than 40% of the level of urea production (i.e. arginase activity) of fetal

liver (Figure 1-5B).

Optimization of ArgO-expressing vectors

Additional efforts to develop optimized ArgO-expressing vectors with the purpose to

better maintain ArgO expression in post-differentiated LEAPR derivatives were explored. The

minimal ubiquitous chromatin opening element (UCOE) has been shown to prevent silencing of

heterologous promoters in human pluripotent stem cells in lentiviral vectors [65]. Therefore, we cloned an expression cassette encoding ArgO driven by the UCOE and hEF1α promoter (LEAPR+UCOE) combination similarly designed for CRISPR/Cas9 nickase-mediated homologous recombination targeted to exon 1 of HPRT (Figure 1-6A). Though ArgO RNA expression significantly increased after differentiation to HLCs in AD1 hiPSCs modified with the LEAPR+UCOE vector, a similar significant decrease in functionality compared to the LEAPR vector was observed (Figure 1-6B-C).

Optimization of HLC differentiation protocols

Though HLCs obtained from the Song *et. al.* protocol yielded hepatic-like gene expression as examined by ICC and RT-PCR, upon further examination by qRT-PCR, albumin expression was low compared to human fetal liver controls (data not shown). In order to obtain more mature HLCs, protocol modifications and additional protocols were examined. Efforts were made to modify Song *et. al*. protocol by optimization of definitive endoderm induction that improved differentiation, but did not yield appreciable increases in albumin expression (data not shown). HLCs were derived using a modified version of a protocol developed by Carpentier *et. al*. and compared to Song *et. al.* HLCs [36]. Carpentier *et. al.* HLCs yielded improved hepatic morphology and gene expression profiles as demonstrated by significantly increased levels of CPS1 and FAH RNA, but still did not yield high levels of ALB and similar levels of AFP RNA (Figure 1-7A-E). Further modifications of Carpentier *et. al*. HLCs including use of laminin basement substrates additionally did not improve albumin expression (data not shown).

Carpentier *et. al.* HLC gene expression was further examined by qRT-PCR and compared to human fetal liver controls and primary human hepatocytes (PHHs). Carpentier *et. al.* HLCs demonstrated significantly higher levels of AFP and significantly lower levels of ALB RNA compared to fetal liver and PHHs, but demonstrated similar levels of FAH compared to fetal liver (Figure 1-8A-C). Supernatant was collected over the duration of the differentiation

protocol and demonstrated significant increases of secreted albumin over time culminating in 3730 ng/mL of secreted albumin on D22 (Figure 1-8D). Therefore, though RNA levels as assessed by qRT-PCR were low compared to fetal liver and PHHs, secretion of albumin protein was comparable if not higher than the published protocol. Urea cycle enzymes were also assessed and demonstrated a general trend toward a fetal-like profile (Figure 1-8E-K). Therefore, though the current HLC differentiation protocol still produces HLCs with an overall fetal-like profile, the modifications have indicated a step toward hepatic maturity.

Development and examination of an AFP-Reporter/Selection Construct for hepatocyte isolation

The derivation of hiPSCs initiated a push for elucidating the molecular cues to differentiate hepatic lineages for development of patient-specific cell replacement therapeutics for liver and metabolic diseases. Though several groups have derived HLCs demonstrating appropriate phenotypic, morphological, and functional characteristics, inefficiency of derivation, inherent line-to-line variation, and risk for lingering potentially tumorigenic pluripotent stem cells in post-differentiated cultures remain common issues of concern for clinical applications. AFP is a major plasma protein produced by the liver and hepatocytes during fetal development and is not expressed in hiPSCs. Additionally, AFP+ cells derived from hepatic differentiation protocols have been demonstrated to engraft and further mature upon *in vivo* transplantation [66, 67]. We developed a preclinical reporter/selection vector (ARC) encoding an AFP enhancer and promoter driving expression of fluorescent protein tdTomato and blasticidin resistance aimed to isolate AFP+ HLCs from post-differentiated cultures via FACS-Sort and/or *in vitro* antibiotic drug resistance selection (Figure 1-9A). The ARC allows for integration into the adeno-associated virus integration site 1 (AAVS1) safe harbor locus, a widely studied safe harbor site that permits long-term transgene expression [68]. Therefore, we aimed to determine if modifying AD hiPSCs with ARC and post-differentiation selection would lead to populations of HLCs of higher hepatic expression and higher potential for engraftment.

H9 embryonic stem cells (ESCs) were first used to optimize the vector and selection protocols. H9 ESCs were nucleofected with the ARC vector with CRISPR/Cas9 nickases specific for in-frame integration into the AAVS1 safe harbor locus. After purification, clonal expansion, and differentiation into HLCs under established protocols, HLCs were treated with 1.25 µg/mL blasticidin for 72hrs and tdTomato+ populations were quantified via flow cytometry to be 84% while unselected populations were 81% tdTomato+ (Figure 1-9B). Though tdTomato+ enrichment levels have reached up to 89.3% in other experimental runs, blasicidin treatment caused loss of hepatic morphology and gene expression profile as assessed by qRT-PCR compared to the untreated control (Figure 1-9C-F). However, sorting tdTomato+ HLCs through FACS does maintain/improve hepatic gene expression profile compared to the untreated control (Figure 1-9D-F). Though there is a modest improvement of hepatic gene expression after sorting for tdTomato+ HLCs via FACS, this strategy would not be scalable for future clinical applications.

Transplantation of pluripotent stem cell-derived HLCs

To determine *in vivo* efficacy of gene-added hiPSC-derived HLCs for treatment of arginase deficiency, our group established and characterized an immunosuppressed arginase deficient mouse model (FRG-CKO) [69]. In order to demonstrate this model as an appropriate model for upcoming HLC transplantations, PHHs were transplanted by intrasplenic injection and allowed to engraft and repopulate the liver. After the endogenous murine arginase function was disrupted, we demonstrated that the PHH-transplanted mice controlled normal plasma ammonia levels, amino acid profiles, could withstand an exogenous ammonia load, and maintained normal neurological behavior. These studies demonstrated that human hepatocyte repopulation in the murine liver can result in effective treatment of arginase deficiency.

Transplantation of HLCs have been attempted with no success. Using the Song *et. al.* HLC differentiation protocol, $1x10^6$ D21 HLCs derived from AD1 uncorrected (n = 4), AD1

LEAPR C1 (n = 5), AD1 LEAPR C3 (n = 5), and xcHUF1 control hiPSC (n = 8) were transplanted and did not engraft within the liver of FRG-CKO mice leading to death of FRG-CKO mice either during NTBC cycling or after knockout of endogenous arginase. Additionally, D10 HLCs from AD1 LEAPR C3 (n = 10) and D5 definitive endoderm from xcHUF1 (n = 6) were also transplanted and did not engraft. Using the optimized Carpentier *et. al.* differentiation protocol, we transplanted $1x10^6$ D23 HLCs derived from H9 ESCs (n = 5) and could not detect circulating human albumin by D56 indicating a lack of expansion of the transplanted HLCs.

Discussion

Chronic therapy for urea cycle disorders includes dietary restriction to limit nitrogen intake and pharmacological intervention with nitrogen scavenging drugs (e.g. phenylbutyrate). Such substrate restriction is commonly used for treating urea cycle disorders and while it is somewhat effective, this is more prophylactic than curative and patients remain at risk for developing long-term neurological issues due to intermittent hyperammonemia. Gene and stem cell therapy have emerged as promising therapeutic avenues to treat these disorders and prevent the development of hyperammonemia-induced neurological injury [26, 70-73].

Stem cells, specifically hiPSCs, provide an almost inexhaustible source of patient-specific cells that can undergo directed differentiation into various somatic cell types to be used for cellular replacement therapies [74-76]. Due to their therapeutic potential, considerable effort has been aimed into optimizing protocols to genetically modify these cells in order to model diseases and to use in potential cellular therapies [77]. However, despite the promise of utilizing genetically modified hiPSCs for therapeutic studies, the ability to efficiently deliver genes to targeted sites in hiPSCs is hampered by several challenges. Non-viral methods, such as chemical transfection or electroporation, and viral methods, via lentiviruses or adeno-associated virus (AAVs), all suffer from relatively low transfection and transduction efficiencies, transient expression, and off-target integration in the host hiPSC genome [70, 77]. Recently, the

development of highly specific clustered interspaced short palindromic repeats (CRISPRs) and CRISPR-associated (Cas) systems to introduce genes into hiPSCs have begun to address many previous issues surrounding genomic editing of stem cells. Unlike its predecessors, such as zinc finger nucleases (ZFNs) and transcription activator-like effector nucleases (TALENs), CRISPR/Cas9 systems can be produced rapidly and introduced into specific target sites with increased accuracy [58, 78, 79]. As such, recent studies have demonstrated highly efficient genetic correction of hiPSCs utilizing CRISPR/Cas9 for neural and muscular disorders [46].

The goal of the present study was to determine if integration of codon-optimized arginase into three genetically distinct patient-specific hiPSCs could produce *in vitro* enzyme function after differentiation into hepatocyte-like derivatives for potential use in cellular therapy for these patients. Previous gene therapy studies have demonstrated successful reversal of disease manifestations through either treatment of neonatal mice with a helper-dependent adenoviral vector (HDV) [26] or with AAV-expressing arginase [27]. In the former, the transient nature of expression led to loss of arginase function while in the later, long-term survival without neuropathology was achieved; however, with the loss of episomal AAV genomes, the level of arginase expression was low and, therefore, the animals remained nitrogen vulnerable [80]. However, these murine studies were able to determine that long-term survival [27] with normal behavior and learning [81] was possible and that only low levels of hepatic arginase activity, as low as 3.5-5%, were necessary to prevent brain injury and/or death from hyperammonemia or hyperargininemia [80]. Here, we developed a CRISPR/Cas9-based strategy to deliver a codon-optimized version of human arginase 1 into hiPSCs derived from patients with arginase deficiency. Arginase 1 was introduced into Exon 1 of the HPRT locus via a construct containing right and left homologous arms, the human elongation factor 1a promoter, a polyadenylation signal, and puromycin for selection (LEAPR), resulting in substantial arginase enzymatic activity in hiPSCs and in differentiated derivatives.

Cellular HPRT is an enzyme that catalyzes the conversion of hypoxanthine to inosine monophosphate and guanine to guanosine monophosphate in the non-essential purine salvage pathway [82]. Homozygous loss of HPRT function results in Lesch-Nyhan syndrome, which causes an overproduction of uric acid. However, in normal conditions, purine salvage and HPRT do not play a major role in cell growth and proliferation [83]; in therapeutic administration of cells where HPRT is not functional in the large mass of HPRT-positive cells (such as the liver), it is believed that this loss will be inconsequential in purine metabolism. There are certainly desirable selective advantages of utilizing HPRT for integrated cell selection: HPRT-positive cells are sensitive to 6-thioguanine (6-TG), killing cells by post-replicative mismatch repair [84]; additionally, this mechanism allows for secondary selection with 6-TG after HPRT locus disruption [85, 86]. As transfection efficiency of hiPSCs is inherently low, the incorporation of a dual selection method with puromycin and 6-TG allowed us to purify a population of hiPSCs that contained the integrated construct at the targeted site utilizing nucleofection to deliver CRISPR/Cas9 nickases and the LEAPR cassette. In culture, these corrected hiPSCs showed that they maintained proper morphology and pluripotency, and sequencing data and qRT-PCR-based genomic integration quantification confirmed that the constructs integrated into the correct targeted site in a single HPRT allele with no off-target INDELs at high unrelated probable sites. While the data demonstrate that a single X chromosome of each AD line is integrated with the donor construct, we did detect genetic mutations in the other allele of HPRT at the site of nuclease A and B activity.

Importantly, arginase was highly expressed in LEAPR-corrected cells as shown by both qRT-PCR and in urea production from functional arginase activity. After directed differentiation of LEAPR-corrected hiPSCs to the hepatic lineage using the Song *et. al.* protocol, the HLCs were positive for albumin and AFP, stored glycogen, and expressed multiple liver-specific RNAs. However, after further hepatic profiling by qRT-PCR, HLCs derived from Song *et. al.* strongly exhibited fetal-like characteristics. Therefore, efforts were made to optimize the HLC

differentiation protocol where the current protocol is a modified version of Carpentier *et. al.* Though current HLCs are generally still fetal-like, they are a significant improvement upon the previous generation.

To determine if differentiation affected expression and functionality of arginase in the hepatocyte-like cells, we quantified RNA levels and urea production for comparison with their hiPSC counterparts. While RNA levels of LEAPR-derived arginase in HLCs were lower when compared to their hiPSC counterparts, functional arginase expression with urea production for all LEAPR-corrected hepatocyte-like cells remained, and at levels that were previously determined (with AAV-based gene therapy) to be necessary for arginase-deficient mice to survive and be without neurodevelopmental abnormalities. As previous studies by others have shown a decline in transgene expression during differentiation with the use of the hEF1a promoter in embryonic stem cells [87], this in part may explain the decline in expression in the hepatocyte derivatives in this study. Additionally, comparison of wild type mutated arginase and CPS1, another urea cycle enzyme, demonstrated that LEAPR modification does not negatively affect the expression of endogenous promoters of urea cycle enzymes. In aggregate, however, these data demonstrate that genetic modification at the HPRT locus of the arginase-deficient lines had no deleterious effect on their pluripotent capability and overall "stemness"; were not altered by nucleofection, selection, or culture of the hiPSCs; and were able to be differentiated into hepatocytes with restoration of arginase activity and ureagenesis.

Based on these data, integration of arginase 1 via the LEAPR expression construct by targeting the HPRT locus demonstrates the potential for restoring enzymatic activity in cells derived from hyperargininemic patients. Previously, we have shown in a murine model that with relatively low overall hepatic arginase activity establishing ureagenesis at 3.5-5% of normal led to long-term survival with controlled plasma arginine and ammonia; however these animals remained nitrogen vulnerable due to the low level of arginase expression [80]. LEAPR-corrected HLCs across all three lines demonstrated functionality of at least 40% compared to fetal liver;

31

while the hEF1a promoter-based expression, both alone and in combination with the UCOE, did decline with cellular differentiation, arginase expression in our studies remains well above the minimum threshold needed for survival and adequate nitrogen metabolism determined from the prior murine arginase studies [80]. While our present LEAPR construct contains a copy of the selection marker puromycin, an aminonucleoside antibiotic, before clinical applicability alteration of our donor construct to avoid integration of an antimicrobial resistance gene and the potential immunogenicity would be required. This would be accomplished by altering our donor construct by adding flanking *lox*P sites to the puromycin cDNA such that it could excised at the hiPSC stage prior to differentiation to the hepatocyte lineage.

Over the last 30 years, multiple studies including our own for treatment of arginase deficiency, in rodents have shown that adult hepatocyte transplantation can reverse liver failure and can correct various metabolic deficiencies of the liver [69, 88, 89]. While clinical trials of hepatocyte transplantation have demonstrated the long-term safety of cellular administration, only partial correction of metabolic disorders in humans has ever been achieved [90, 91]. In part due to the limited availability of fresh donor hepatocytes of adequate quality, clinical trials, however, have been hampered and reports have been limited in general to case reports involving a few patients at most and generally with no untreated controls [92-95]. While attaining adequate engraftment will need further attention to make such therapies successful for patients with metabolic liver disorders, issues of cellular rejection should be greatly reduced [89] with an hiPSC approach as described herein.

In choosing this approach where cell availability and numbers of hepatocytes will not be a limitation, there are other important implications for treating more common monogenic disorders of the liver. The safe harbor of exon 1 of HPRT could be used in that the efficiency of homologous recombination has been demonstrated here as well as the exogenous gene expression at this locus based on the hEF1a promoter. Targeted therapy of other liver-based

disorders would be easily addressed by substitution of the arginase cDNA from the donor construct with one of the other enzyme cDNA sequences from another metabolic disorder.

This study presents an approach that can be utilized to integrate an optimized cassette into a universal site distant from proto-oncogenes in patient-specific hiPSCs to restore function of abnormal liver enzymes. While we have addressed the restoration and maintenance of transgene expression pre- and post-differentiation, additional studies aimed to repopulate the liver of an established an immunosuppressed conditional arginase deficient mouse model capable of liver repopulation of human primary hepatocytes with corrected hiPSC-derived hepatic-like derivatives have so far been unsuccessful. Therefore, additional studies are required to investigate the *in vivo* therapeutic efficacy of the corrected derivatives to maintain recovered arginase activity after cellular transplantation. However, successful *in vivo* recovery of enzyme function by means of these strategies has the promise to benefit enzyme deficiencies of the urea cycle and other inborn errors of metabolism.
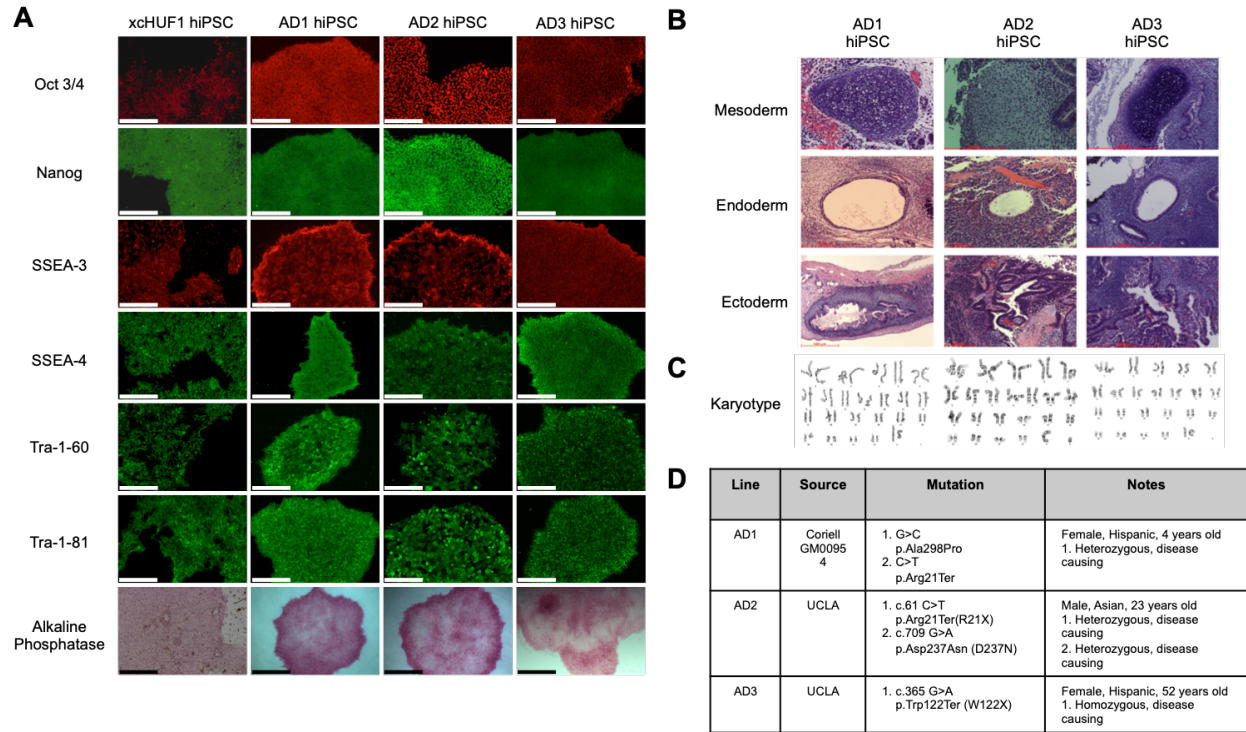
Figure 1-1. Characterization of arginase deficient (AD) hiPSCs. (A) Pluripotency of all three AD hiPSC lines was measured via immunophenotyping. AD1, AD2, and AD3 subclones were positive for octamer-binding transcription factor-4 (OCT3/4), homeobox protein nanog (NANOG), stage-specific embryonic antigens 3 (SSEA-3) and 4 (SSEA-4), tumor-related antigens 1-60 (TRA-1-60) and 1-81 (TRA-1-81), and alkaline phosphatase. AD hiPSCs were compared to a wild type hiPSC line xc-HUF1. (Scale bars for all images are 200 mm except alkaline phosphatase which is 500 mm.) **(B)** AD1, AD2, and AD3 hiPSC lines exhibited normal 46 XX or 46 XY karyotypes, and **(C)** demonstrated the ability to form tissues from all three germ layers: gut (endoderm), chondrocytes (mesoderm), and neuroectoderm (ectoderm). (Scale bars = 200 mm) **(D)** Sequencing analysis reveals specific arginase mutations in each line.
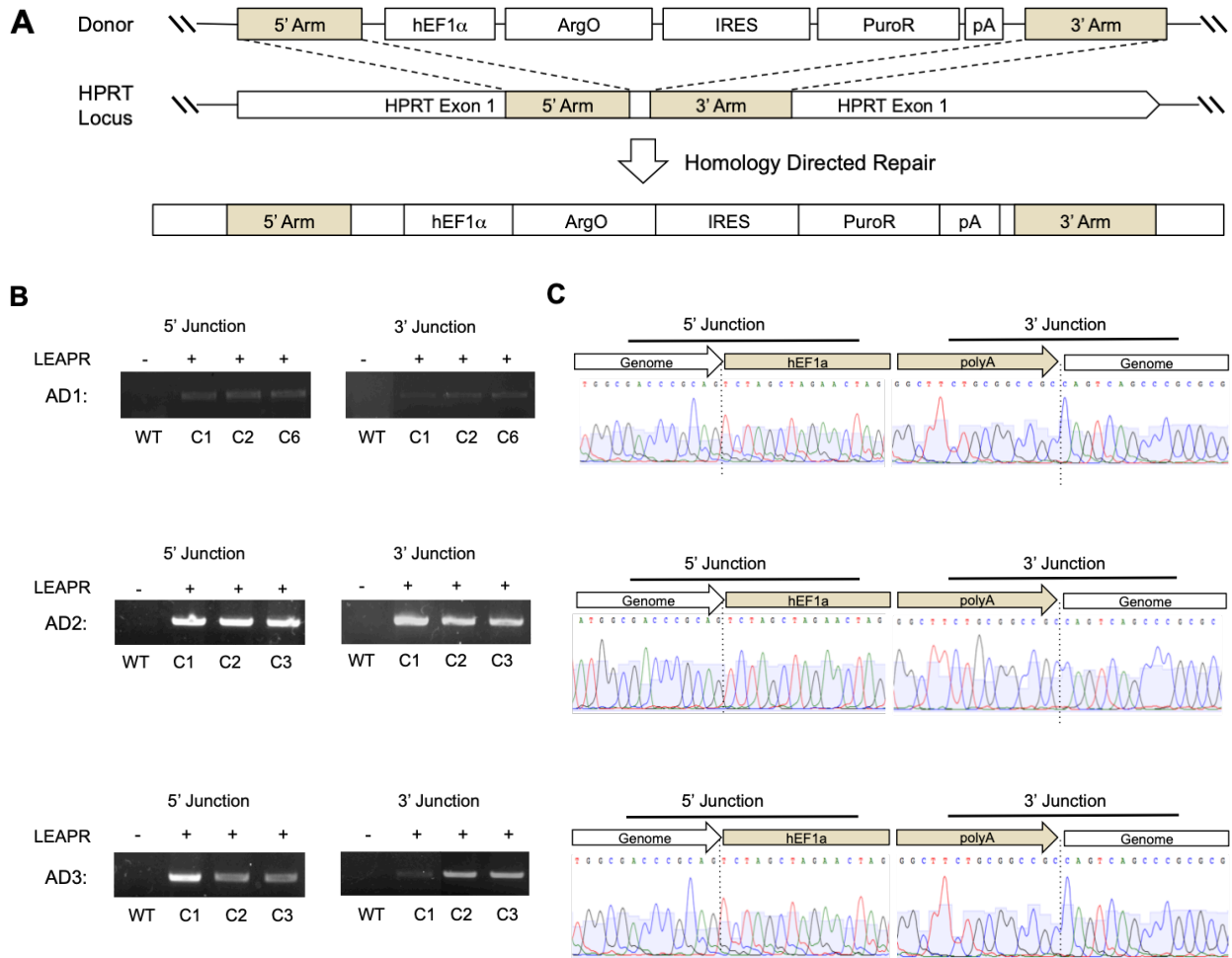
Figure 1-2. Design and integration of LEAPR expression cassette. (A) Design of the LEAPR construct containing the human codon optimized arginase (*ArgO*). **(B)** Junction PCR was performed to determine integration of the construct in both wild-type xcHUF1 and AD1, AD2, and AD3 hiPSCs in Exon 1 of the HPRT site. **(C)** Sequencing analysis was performed on the integration of the construct in AD1, AD2, and AD3 hiPSCs at the target site.
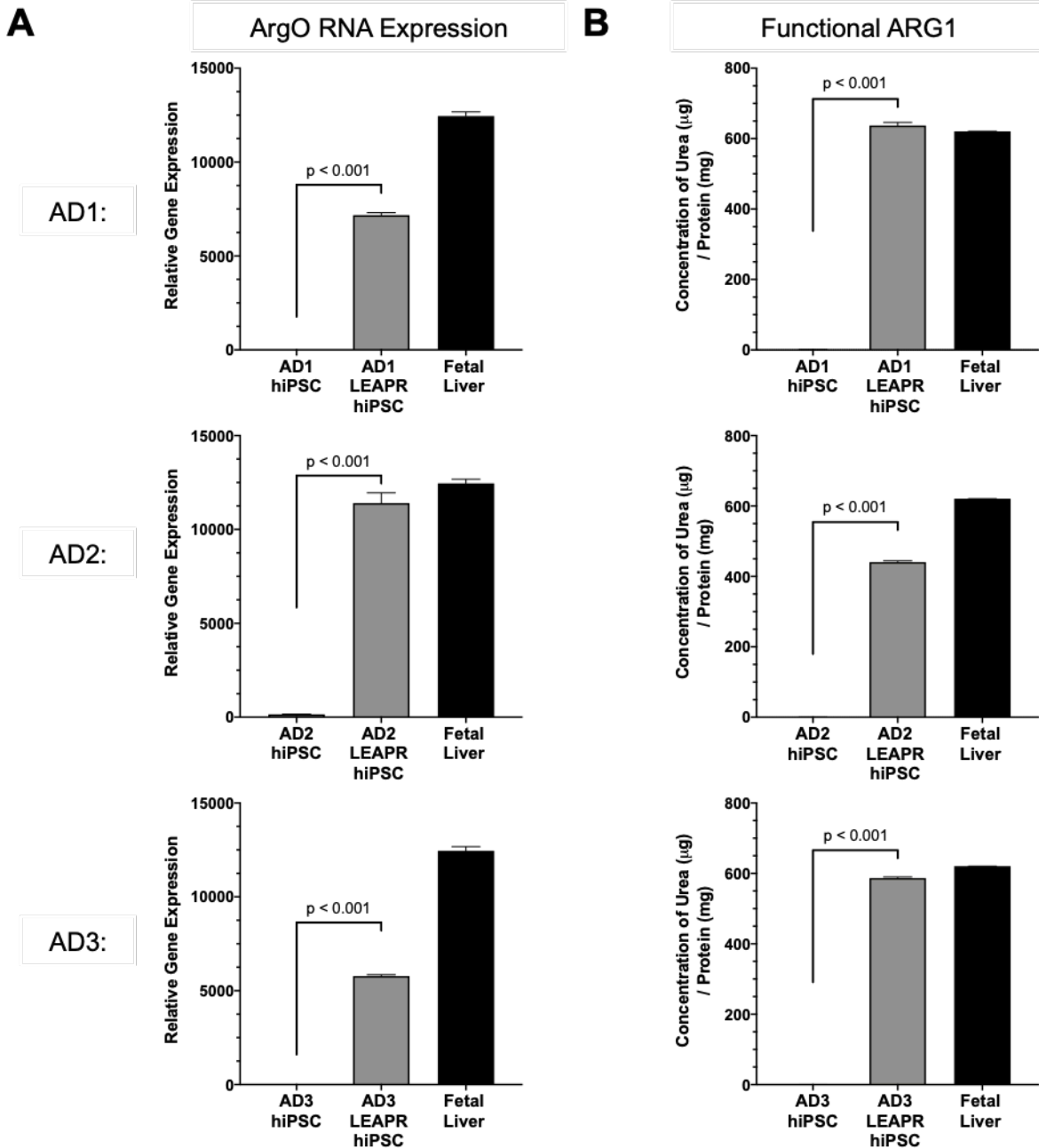
Figure 1-3. Measuring *ArgO* in AD hiPSCs. (A) Relative gene expression of *ArgO*, measured against glyceraldehyde 3-phosphate dehydrogenase (GAPDH), in AD1, AD2 and AD3 uncorrected and corrected hiPSCs was measured by qRT-PCR in technical triplicate (n = 3). **(B)** After integration of *ArgO* in AD hiPSCs, urea production was measured and compared to fetal liver (n = 2). Functionality experiments were performed in technical duplicate. (Data are represented as mean ± SD.)
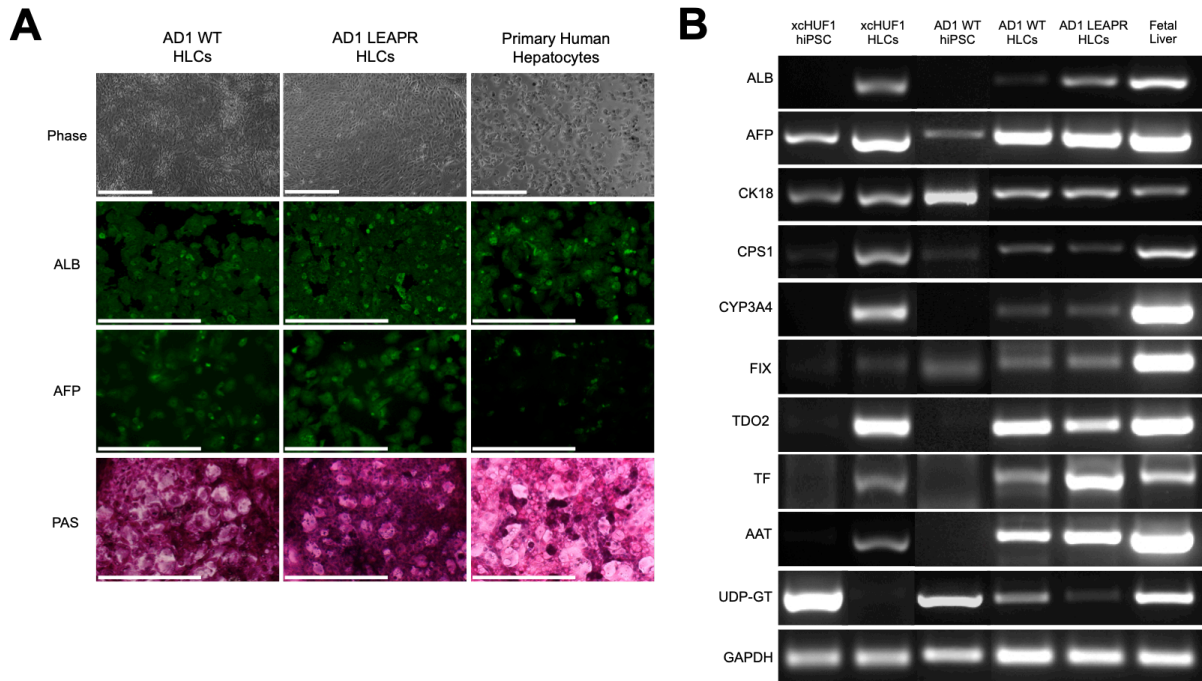
Figure 1-4. Characterization of hepatocyte-like cells (HLCs). (A) Derived uncorrected and corrected (gene added) AD1 HLCs were examined and morphology compared to primary adult hepatocytes *in vitro* (Scale bars = 500 mm). **(B)** Hepatic markers were examined via RT-PCR in uncorrected and corrected AD1 HLCs: alpha 1-antitrypsin (*AAT*), *AFP*, human serum albumin (*ALB*), cytokeratin 18 (CK18), carbamoyl phosphate synthase 1 (*CPS1*), cytochrome p450 3A4 (*CYP3A4*), factor IX (*FIX*), transferrin (*TF*), tryptophan 2,3-dioxygenase (*TDO2*), and uridine diphosphate glucuronyltransferase (*UDP-GT*).
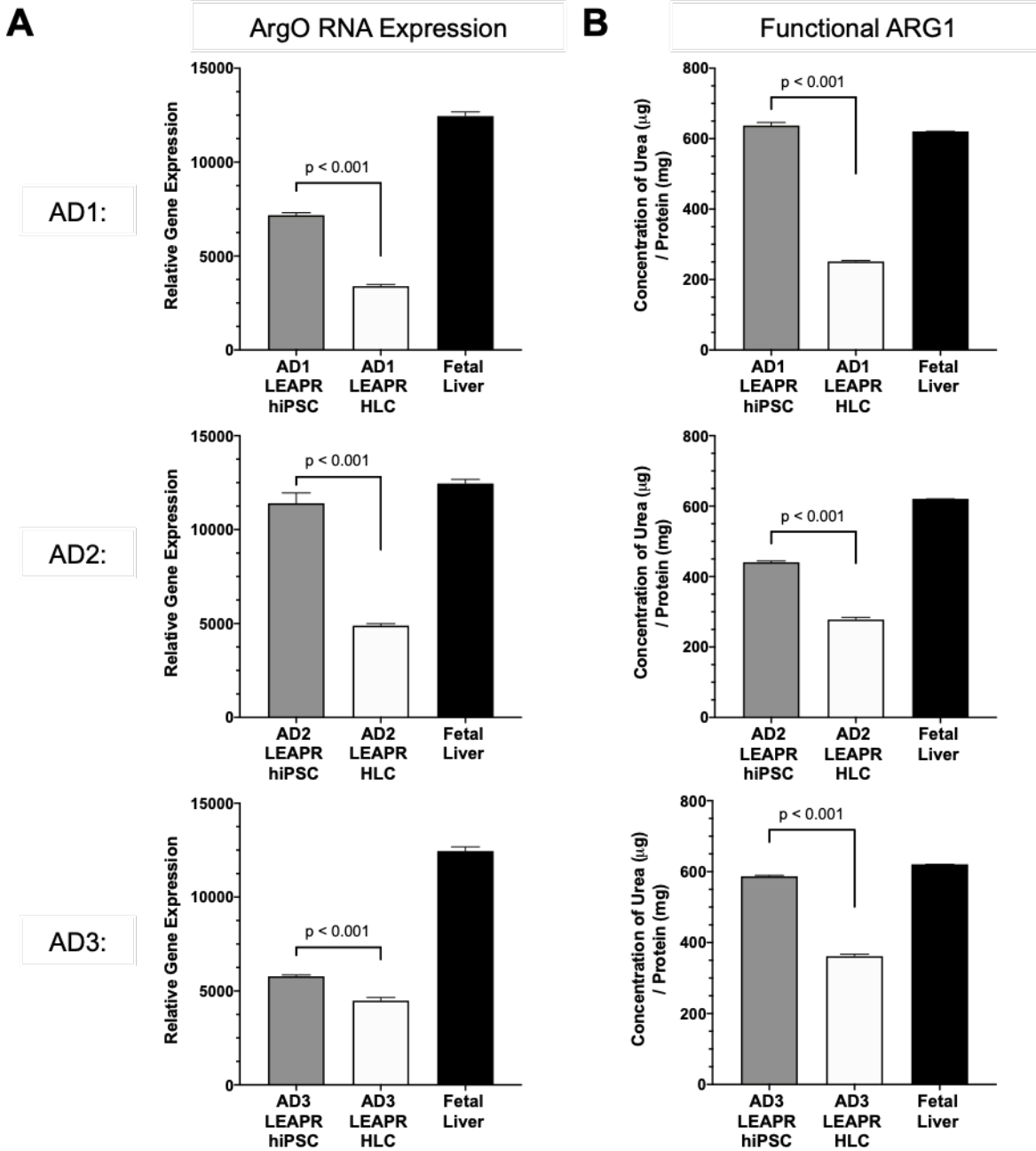
Figure 1-5. Measuring _ArgO_ in AD hepatocyte-like cells (HLCs). (A) Relative gene expression of _ArgO_, measured against glyceraldehyde 3-phosphate dehydrogenase (GAPDH), in AD1, AD2 and AD3 corrected hiPSCs and HLCs was measured by qRT-PCR in technical triplicate (n = 3). **(B)** Urea production was measured and compared to fetal liver (n = 2). Functionality experiments were performed in technical duplicate. (Data are represented as mean ± SD.)
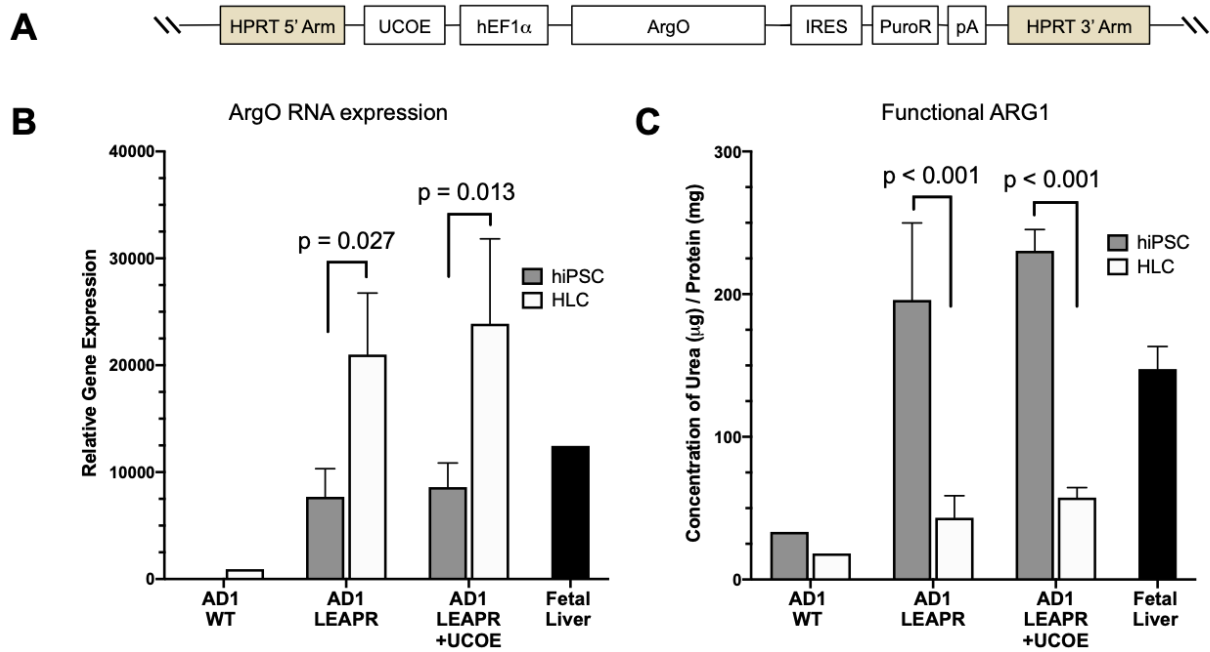
Figure 1-6. Design and expression of LEAPR+UCOE expression cassette compared to LEAPR expression cassette. (A) Design of the LEAPR+UCOE construct containing the ArgO driven by hEF1a and ubiquitous chromatin opening element (UCOE) promoters. **(B)** Relative gene expression of ArgO, measured against glyceraldehyde 3-phosphate dehydrogenase (GAPDH), in AD1 uncorrected, AD1 LEAPR and AD1 LEAPR+UCOE hiPSCs and HLCs was measured by qRT-PCR in technical triplicate (n = 3). **(C)** Urea production was measured and compared to fetal liver (n = 2). Functionality experiments were performed in technical duplicate. (Data are represented as mean ± SD.)
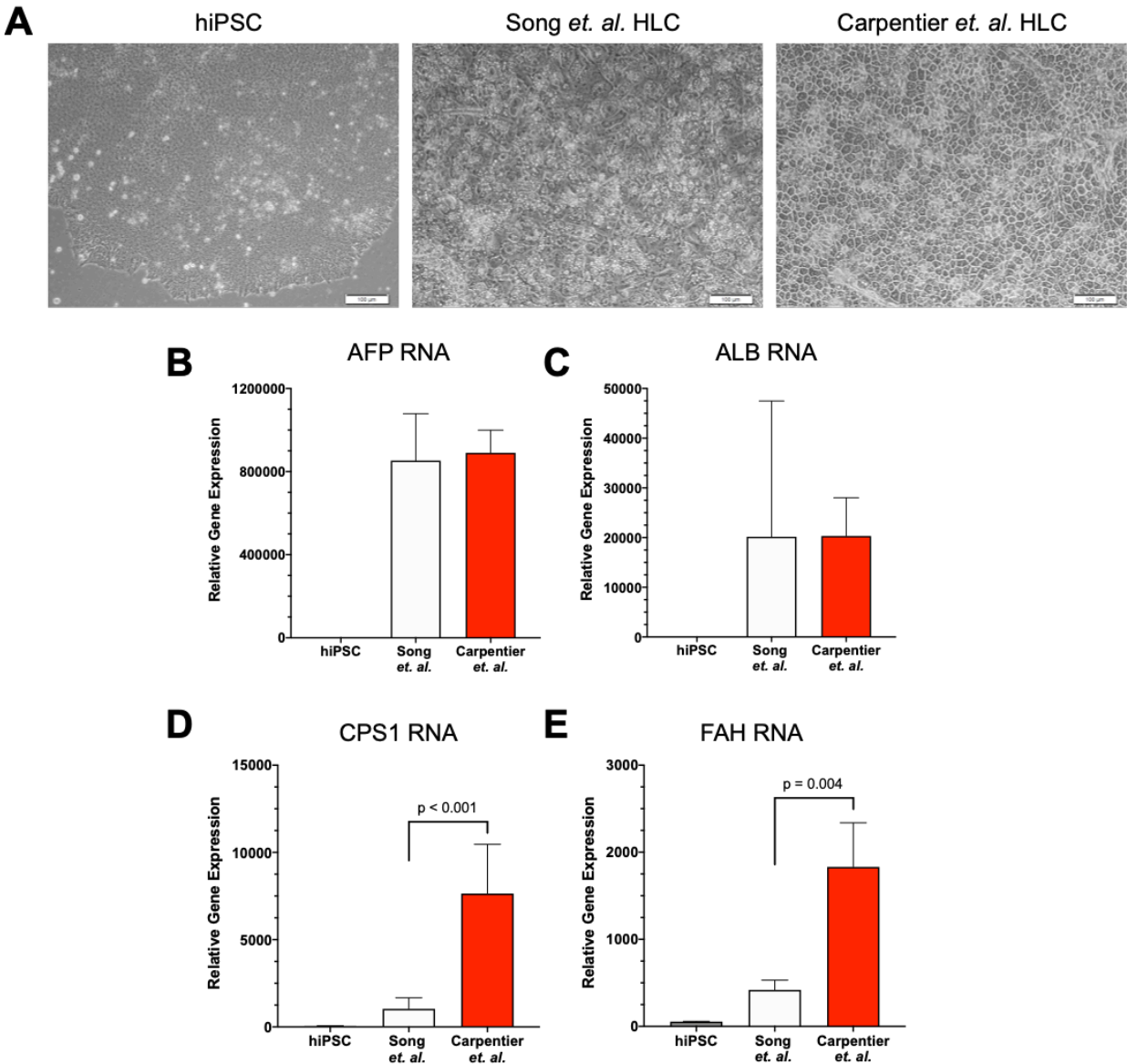
Figure 1-7. Comparison of hepatocyte-like cell (HLC) differentiation protocols. (A) HLCs were generated from the Song *et. al.* and Carpentier *et. al.* protocols and morphology was compared *in vitro* (Scale bars = 100 μm). Relative hepatic gene expression, measured against glyceraldehyde 3-phosphate dehydrogenase (GAPDH), was measured via qRT-PCR in Song *et. al.* and Carpentier *et. al.* HLCs in technical triplicate (n = 3): **(B)** alpha-feto protein (AFP), **(C)** human serum albumin (ALB), **(D)** carbamoyl phosphate synthase 1 (CPS1), and **(E)** fumarylacetoacetate hydrolase (FAH).
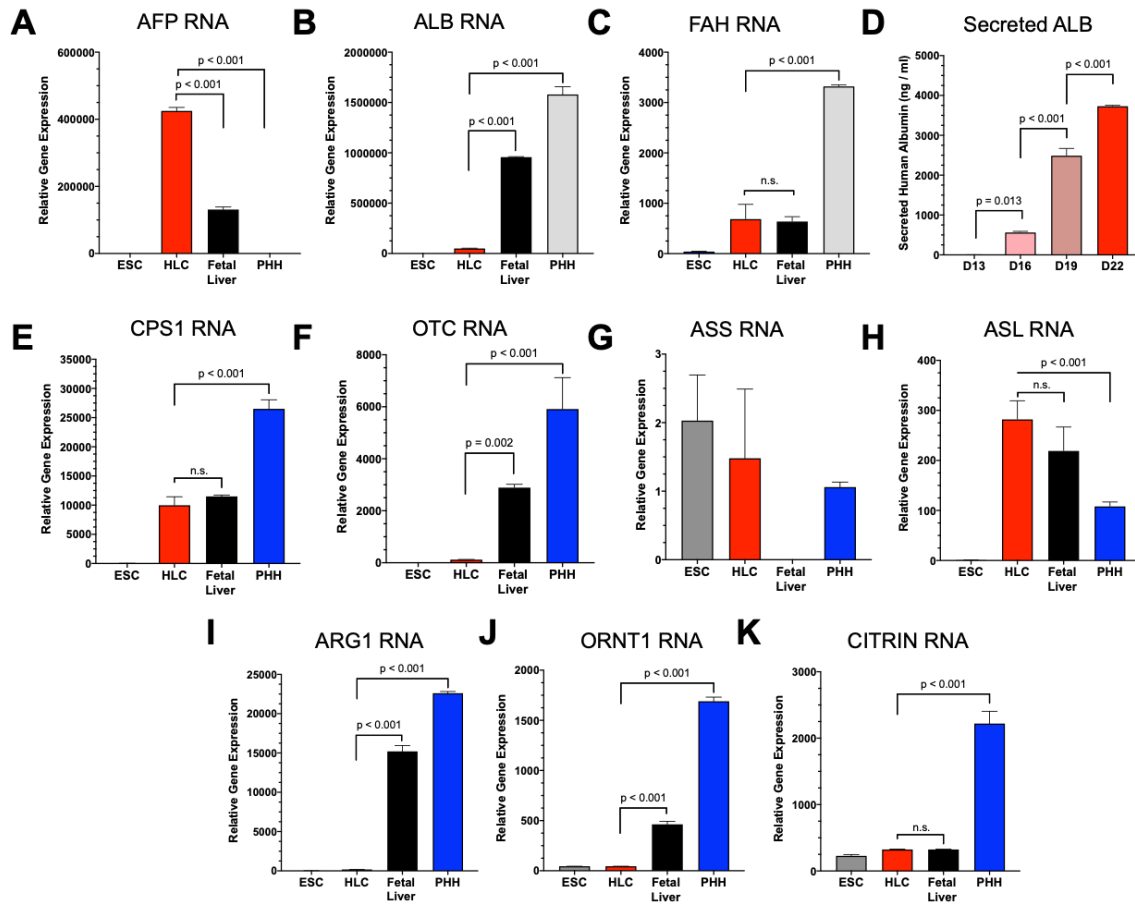
Figure 1-8. Hepatic gene expression profile of Carpentier *et. al*. hepatocyte-like cells. Relative hepatic gene expression, measured against glyceraldehyde 3-phosphate dehydrogenase (GAPDH), was measured via qRT-PCR in Carpentier *et. al.* HLCs in technical triplicate (n = 3) and compared to human fetal liver and primary human hepatocyte controls: **(A)** alpha-feto protein (AFP), **(B)** human serum albumin (ALB), **(C)** fumarylacetoacetate hydrolase (FAH). **(D)** Supernatant throughout the Carpentier *et. al.* HLC differentiation protocol was collected and secreted human albumin was measure via ELISA. Relative urea cycle enzyme gene expression, measured against GAPDH, was measure via qRT-PCR Carpentier *et. al.* HLCs in technical triplicate (n = 3): **(E)** carbamoyl phosphate synthase 1 (CPS1), **(F)** ornithine transcarbamoylase, **(G)** argininosuccinate synthetase (ASS), **(H)** argininosuccinate lyase (ASL), **(I)** arginase 1 (ARG1), **(J)** ornithine translocase (ORNT1), and **(K)** solute carrier family 25, member 13 (CITRIN).
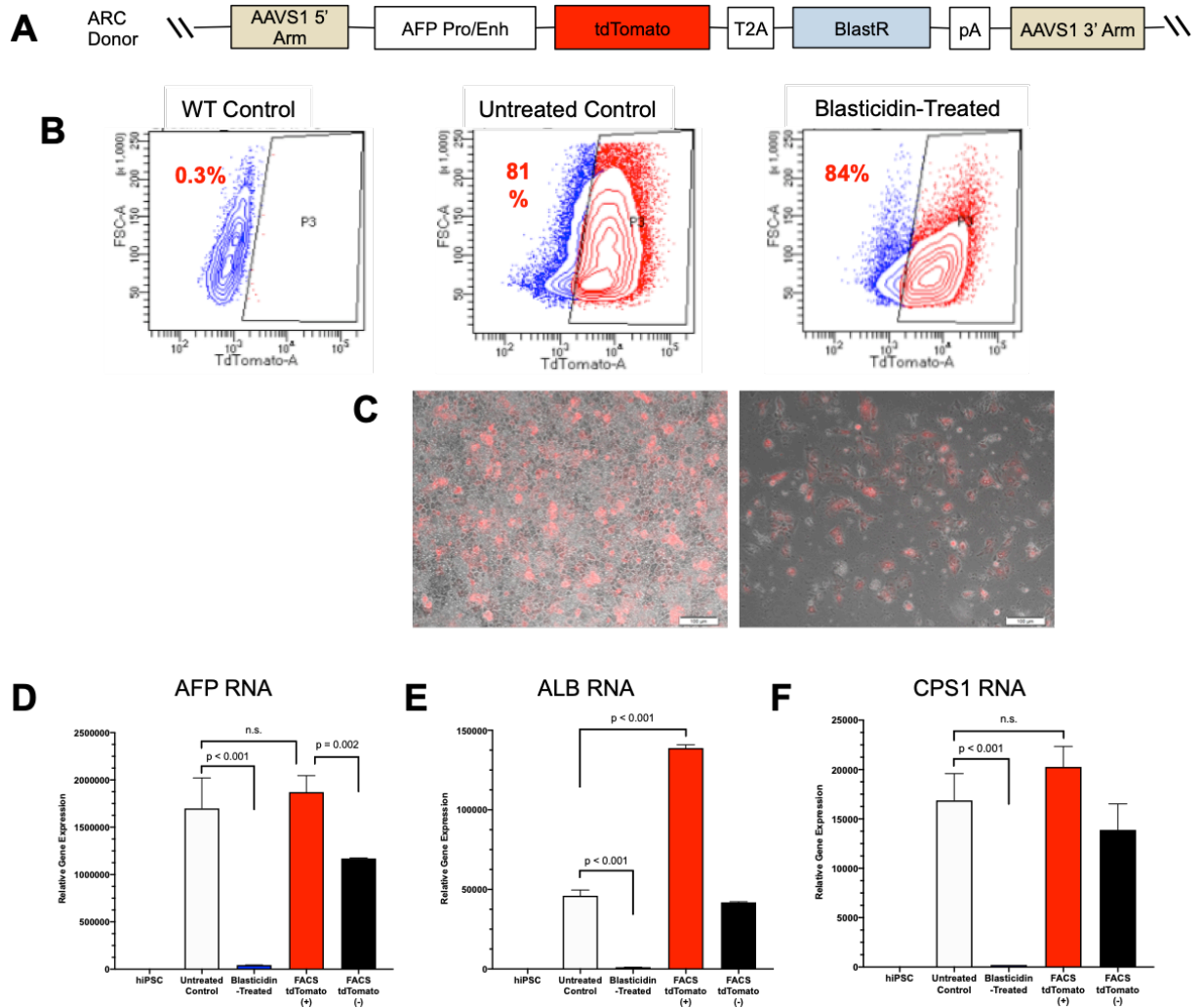
Figure 1-9. Examining the AFP-Reporter/Selection Construct (ARC) for hepatocyte-like cell isolation. (A) Design of the ARC containing an alpha-fetoprotein (AFP) promoter and enhancer driving expression of tdTomato and blasticidin resistance. (B) Flow cytometry was performed on unmodified HLCs (WT Control) and ARC-modified HLCs treated with blasticidin for 72 hrs (Blasticidin-Treated) and untreated (Untreated Control). Percentage illustrates percent of tdTomato-positive HLCs in the population. (C) ARC-modified HLCs untreated and treated with blasticidin were examined for tdTomato fluorescence intensity and morphology. Relative hepatic gene expression, measured against glyceraldehyde 3-phosphate dehydrogenase (GAPDH), was measured via qRT-PCR for (D) alpha-feto protein (AFP), (E) human serum albumin (ALB), and (F) carbamoyl phosphate synthase 1 (CPS1).
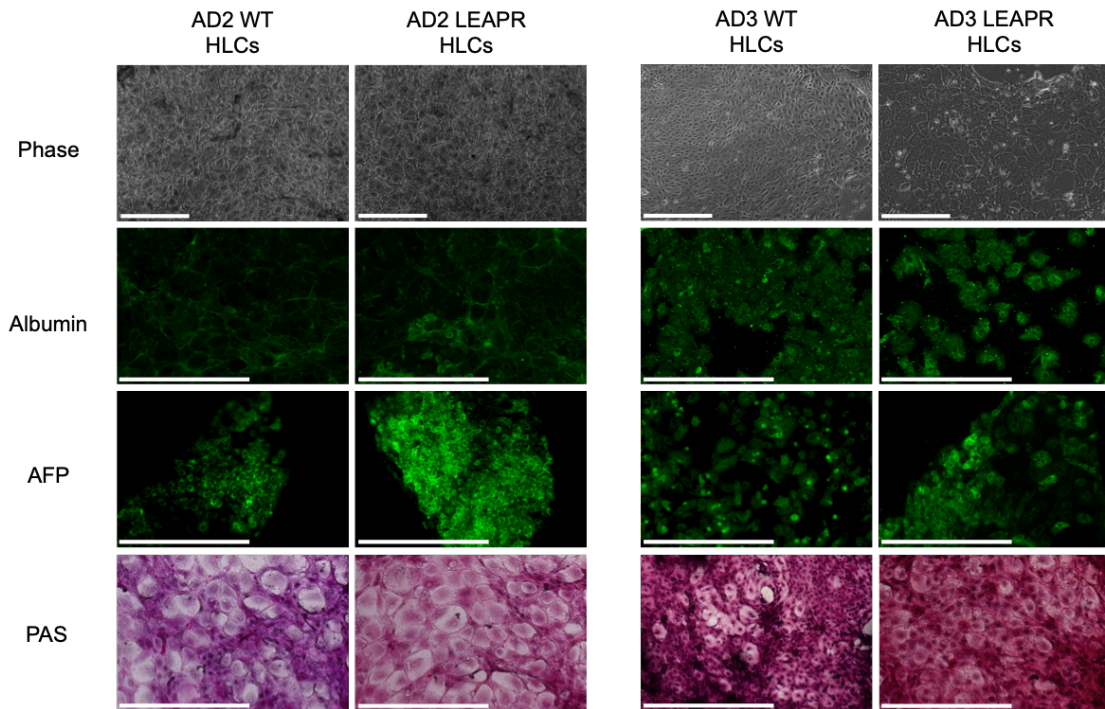
Figure 1-S1A. Characterization of AD2 and AD3 hepatocyte-like cells. Derived uncorrected and corrected AD1 hepatocyte-like were compared to primary adult hepatocytes *in-vitro*. Hepatocyte-like cells were examined for albumin, alpha-fetoprotein (*AFP*), and active glycogen storage, as measured by Periodic Acid Schiff (PAS) staining. (Scale bars = 500 mm)
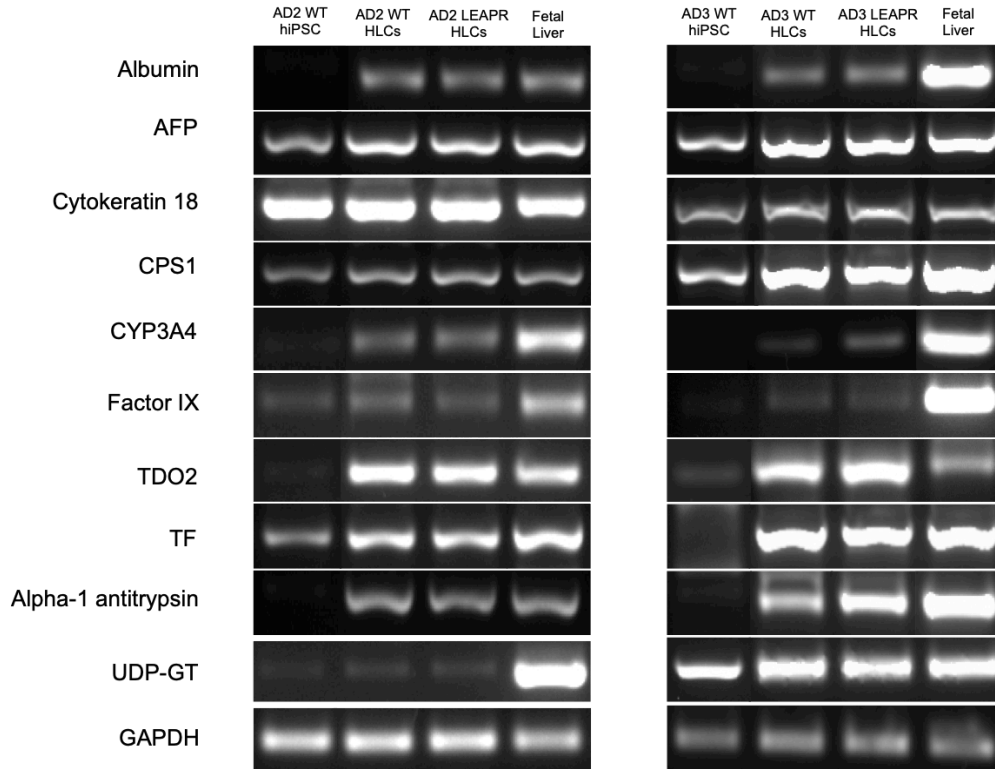
Figure 1-S1B. Characterization of AD2 and AD3 hepatocyte-like cells. Both uncorrected and corrected AD1 hepatocyte-like cells were examined for expression of hepatic markers: alpha 1-antitrypsin (*AAT*), alpha fetoprotein (*AFP*), human serum albumin (*ALB*), cytokeratin 18 (CK18), carbamoyl phosphate synthase 1 (*CPS1*), cytochrome p450 3A4 (*CYP3A4*), factor IX (*FIX*), transferrin (*TF*), tryptophan 2,3-dioxygenase (*TDO2*), and uridine diphosphate glucuronyltransferase (*UDP-GT*). (Mutant refers to endogenous arginase 1 alleles; gene-added refers to CRISPR/Cas9-mediated codon-optimized gene addition.)
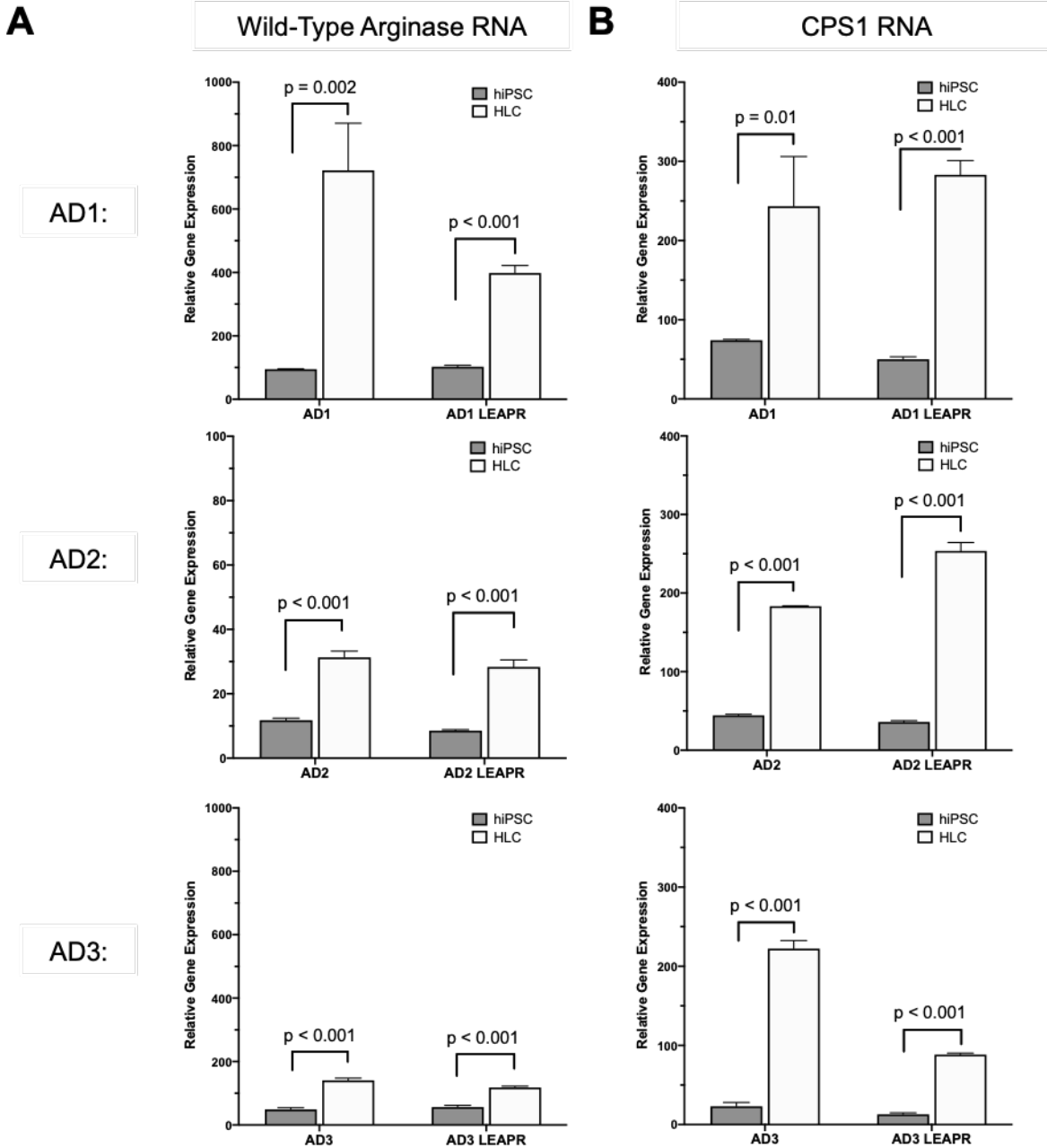
Figure 1-S2. Measuring Wild-type Arg1 and CPS1 levels in uncorrected and corrected hiPSCs and hepatocytes. **(A)** Wild-type Arginase and **(B)** CPS1 mRNA levels were measured in corrected and uncorrected AD1, AD2, and AD3 hiPSCs (n = 3) and hepatocyte-like cells (n = 3) to determine if genetic modification with LEAPR affected the wild-type Arginase and other urea cycle enzymes (Data are represented as mean ± SD)

	Chromosome	Sequence	Primers	Result
Original Nickase A Target	X	GGCGCGCGGGCTGACTGCTCAGG		
Nickase A Off-Target 1	4	TGGGGGCTGGCTGACTGCTCGGG	GTGCAGCCCGAGAACAAC	**No Off Target Integration**
			GACGACCATCAGACAGAGCA	(Reverse Complement)
	Resulting Sequence in AD1 LEAPR			
	TGCTACTTAATGTTGCTGGCTGATGAGTAGCTATGGCTTGTGACAGGAGCCCGAGCAGTCAGCCAGCCCCCAGCCACAGT			
	CAGCCAGACACCTTGACACATATGTTGTGTCATTGTCCCCCTAGTCTGCTGTGCCTGAGCTCAGGCACAGCAGACTAGGGGCA			
	GACAATGACACAACATATGTGTCAAGGTGTCTGGCTGACTGTGGCTGGGGGCTGGCTGACTGCTCGGGCTCCTGTCACAAG			
	CCATAGCTACTCATCAGCCAGCAACATTAAGTAG			
		Chromosome	Sequence	Primers	Result
Nickase A Off-Target 2	18	GGGGAGAGGCCTGACTGCTCTGG	CCAGACCAACAGGCAAAACT	**No Off Target Integration**
			TGGTCAGTGGCACTATTGGA	
	Resulting Sequence in AD1 LEAPR			
	GGGGAGAGGCCTGACTGCTCTGG			
		Chromosome	Sequence	Primers	Result
Nickase A Off-Target 3	X	GGAGGGAGGCCTGACTGCTCCAG	GGAAGGAAGGAAGGAAGGAA	**No Off Target Integration**
			GACCTCCTGGAGCAACTTGA	
	Resulting Sequence in AD1 LEAPR			
	AAGGCTGCTGGGAAAAGGCAACAAGATTGGAGAGGGAGGGAGGCCTGACTGCTCCAGGAAATCATGTGAGTCCCATAGTTCTGT			

Figure 1-S3A. Off target analysis of nickase A for potential insertions or deletions. Sequencing analysis was performed of the three highest probability sites for off-target mutation related to nuclease A. All three sites showed no insertions or deletions.

	Chromosome	Sequence	Primers	Result
Original Nickase B Target	X	GTTATGGCGACCCGCAGCCCTGG		
Nickase B Off-Target 2	10	TGTAAGGCGACCAGCAGCCCCAG	GCCTCTCGTGTCTCTTCACC	**No Off Target Integration**
			GAATGAGCGCTTTTCTCCAG	
	Resulting Sequence in AD1 LEAPR			
	CTAAAATATCTTATTAGTAAAGAGATGGAAGGAGTCCATGTAAGGCGACCAGCAGCCCCAGCCACATACTGGCACAAGGTAGGTGCTC			
	ACGGAG			
		Chromosome	Sequence	Primers	Result
Nickase B Off-Target 3	14	TTGATGACCACCCGCAGCCCAAG	GAGCCTCAGTTTCCTCATCG	**No Off Target Integration**
			TAAGGGGTTGGTGTGGAGAG	(Reverse Complement)
	Resulting Sequence in AD1 LEAPR			
	GTATTCAAAGTATCCTCCCCTTGGGCTGCGGGTGGTCATCAAAGAAGGTAATCTCAATTGTTTAAGGACTCCCCAAGAG			
	CTCTTGGGGAGTCCTTAAACAATTGAGATTACCTTCTTTGATGACCACCCGCAGCCCAAGGGGGAGGATACTTTGAATAC			

Figure 1-S3B. Off target analysis of nickase B for potential insertions or deletions. Sequencing analysis was performed of the highest probability sites for off-target mutation related to nuclease B. These sites showed no insertions or deletions.

46

Figure 1-S4. Determining single integration of LEAPR into HPRT locus in corrected hiPSCs. Relative genomic integrations of LEAPR into the HPRT locus (located on X chromosome) were determined by qRT-PCR (in technical triplicate [n = 3]). Top graph (control) confirmed 2:1 ratio of gHPRT levels (relative to gGAPDH) in AD1 and AD3 (female, XX, i.e. 2 HPRT alleles) compared to AD2 (male, XY, i.e. 1 HPRT allele). Middle graph showed 1:1 ratio of ArgO (relative to gGAPDH) in AD1 and AD3 compared to AD2 demonstrating equal number of LEAPR integrations in the whole genome. Bottom graph showed 1:2 ratio of ArgO (relative to gHPRT) in AD1 and AD3 compared to AD2 demonstrating 1 LEAPR copy per HPRT allele (AD1, AD3 = 1 LEAPR copy/2 HPRT alleles; AD2 = 1 LEAPR copy/1 HPRT allele). (Data are represented as mean ± SD)

47

CHAPTER 2: Lipid Nanoparticle Targeted mRNA Therapy as a Treatment for the Inherited Metabolic Liver Disorder Arginase Deficiency

Introduction

With the development of transgenic technology and the advances of the last two and a half decades in the progress and application of gene therapy to monogenic disorders of the liver, our group has been successful in the development of a mouse model of hyperargininemia [25] along with the pre-clinical application of viral-based gene therapy approaches in treating this enzyme deficiency [26-28]. The beginning of therapy before [96, 97] or shortly after birth [98, 99], before the onset of phenotypic disease, has advantages as early gene therapy has the potential to ameliorate genetic abnormalities before the development of phenotypic disease. For example, initiating therapy shortly after birth has demonstrated that both restoring hepatic arginase activity and controlling hyperargininemia and guanidino compounds leads to normal neurological development, cognitive activity and behavior in Arg1-deficient mice [81, 100].

However, such therapy with episomal viral vectors [as adeno-associated virus (AAV) typically only integrates at a low frequency [101]] is faced with greater challenges in rapidly-dividing tissues and organs than therapy of post-mitotic tissues [102]. In neonates, the rate of hepatocellular proliferation is much higher and affects the maintenance of episomal vector genomes [103, 104] while rapid cellular proliferation in adults is uncommon. For example, individual hepatocytes in the adult mouse liver are replaced once every 180 to 400 days [105, 106] while the neonatal murine liver increases from 50 mg to over one gram in the first 5 postnatal weeks [102]. When administered to neonatal mice this results in a decline in AAV copy number of over 3 logs [102] leaving relatively few arginase-expressing hepatocytes long-term in adult animals and the potential for nitrogen vulnerability [27, 28]. While enzyme replacement has led to successful therapies for a number of other genetic disorders, when tested in arginase-deficient mice, plasma arginine was reduced [19]; however, repeat dosing did

48

not result in improved survival or prevention of weight loss likely due to the inability of the PEGylated enzyme to enter hepatocytes. Additionally, hepatocyte transplantation, though demonstrated to be effective in a murine model of arginase deficiency [69], if sourced from patient-specific genetically modified pluripotent stem cell-derived hepatic-like derivatives, would suffer from lengthy preparation time where patients are at continued risk for progressive intellectual decline. Thus, today, there remains an unmet need for these patients.

mRNA therapy with nanoparticle encapsulation for systemic delivery to hepatocytes has the potential to restore metabolic enzymatic activity for a number of hepatic metabolic disorders [107, 108] including arginase deficiency. Until recently, RNA-based therapeutics have suffered from problems of poor translatability, lack of stability, immune responses, hepatotoxicity [109] and inefficient delivery [107, 110]. Recent advances have improved the stability and translatability of RNAs and have made them immunologically inactive [107]. While the advantages include avoidance of insertional mutagenesis and lack of constitutive gene activation, the use of mRNA technology may also allow for restoration of inaccessible targets [108] such as cytoplasmic arginase activity that was unachievable with PEGylated enzymatic therapy [19].

In this study we encapsulated and systemically administered human codon-optimized *ARG1* mRNA to a conditional knockout murine model of arginase 1 deficiency. We achieved delivery of mRNA to the liver by lipid nanoparticles at therapeutic levels in this preclinical model. We successfully demonstrated high-level hepatic arginase expression and function with restoration of ureagenesis while achieving long-term survival, maintenance of weight, normalization of plasma ammonia and arginine, lack of hepatic guanidinoacetic acid (GAA) (a guanidino compound) and normalization of hepatic arginine without evidence of hepatotoxicity. These findings demonstrate the efficacy of this approach in arginase deficiency.

Materials and Methods

Mouse procedures

Conditional arginase deficient mice on the C57BL/6 background (Jax Stock number 008817) were housed under specific pathogen-free conditions with food and water provided *ad libitum*. All mice were kept according to National Institute of Health guidelines and all experimental procedures were conducted in accordance with guidelines for the care and use of research animals at our institution. At day 0, 8-12 week old animals were intravenously (IV) administered 2.0×10^{11} genome copies of AAV8-thyroxine binding globulin (TBG)-Cre recombinase (University of Pennsylvania Vector Core, Philadelphia, PA) prepared in sterile pharmaceutical grade saline. Male and female mice were distributed evenly throughout the study unless otherwise stated. Scheduled blood collections were taken from the retro-orbital plexus under isoflurane anesthesia. Plasma was frozen immediately and stored at -80°C. Mice were euthanized if they showed symptoms of lethargy, lying on side, or inability to right themselves as signs of hyperammonemia. Beginning day 14 post-AAV8-TBG-Cre recombinase injection, mice were administered IV lipid nanoparticle-encapsulated (LNP)-mRNA prepared at 2 mg/kg in sterile phosphate buffered saline (PBS). One group of mice was injected with LNP-mRNA weekly while two groups were injected every 3 days, one of which also received daily LNP-mRNA loading from day 14 to 21.

mRNA Synthesis and Formulation

h*ARG1* mRNA codon optimization was performed using typical methods in the field [111]. The mRNAs encoding luciferase (*luc*) and h*A RG1* were synthesized *in vitro* by T7 RNA polymerase-mediated transcription using a linearized DNA template that incorporated both the 5' and 3' untranslated regions with a poly-A tail and then purified and formulated for intravenous delivery as previously described [112]. The open reading frame for h*ARG1*:

AUGAGCGCCAAGAGCCGGACCAUCGGCAUCAUCGGCGCCCCCUUCAGCAAGGGCC

AGCCCCGGGGCGGCGUGGAGGAGGGCCCCACCGUGCUCCGCAAGGCCGGCCUCCU

CGAGAAGCUCAAGGAGCAGGAGUGCGACGUCAAGGACUACGGCGACCUCCCCUUC

GCCGACAUCCCCAACGACUCCCCCUUCCAGAUCGUCAAGAACCCCCGCUCCGUCGG

CAAGGCCUCCGAGCAGCUCGCCGGCAAGGUCGCCGAGGUCAAGAAGAACGGCCGC

AUCUCCCUCGUCCUCGGCGGCGACCACUCCCUCGCCAUCGGCUCCAUCUCCGGCCA

CGCCCGCGUCCACCCCGACCUCGGCGUCAUCUGGGUCGACGCCCACACCGACAUCA

ACACCCCCCUCACCACCACCUCCGGCAACCUCCACGGCCAGCCCGUCUCCUUCCUC

CUCAAGGAGCUCAAGGGCAAGAUCCCCGACGUCCCCGGCUUCUCCUGGGUCACCC

CCUGCAUCUCCGCCAAGGACAUCGUCUACAUCGGCCUCCGCGACGUCGACCCCGG

CGAGCACUACAUCCUCAAGACCCUCGGCAUCAAGUACUUCUCCAUGACCGAGGUC

GACCGCCUCGGCAUCGGCAAGGUCAUGGAGGAGACCCUCUCCUACCUCCUCGGCC

GCAAGAAGCGCCCCAUCCACCUCUCCUUCGACGUCGACGGCCUCGACCCCUCCUUC

ACCCCCGCCACCGGCACCCCCGUCGUCGGCGGCCUCACCUACCGCGAGGGCCUCUA

CAUCACCGAGGAGAUCUACAAGACCGGCCUCCUCUCCGGCCUCGACAUCAUGGAG

GUCAACCCCUCCCUCGGCAAGACCCCCGAGGAGGUCACCCGCACCGUCAACACCGC

CGUCGCCAUCACCCUCGCCUGCUUCGGCCUCGCCCGCGAGGGCAACCACAAGCCCA

UCGACUACCUCAACCCCCCCAAG

Bioluminescent imaging (BLI)

Mice were shaved prior to imaging to minimize absorption of light by black fur, then imaged, and

total flux values in photon/s calculated as previously described [102].

Alanine aminotransferase analysis

Alanine aminotransferase (ALT) level determination was performed from plasma samples with a Vet Excel Clinical Chemistry Analyzer (Alfa Wassermann Diagnostic Technologies, West Caldwell, NJ) per the manufacturer's instructions.

Ammonia analysis

Ammonia determination was performed in duplicate from plasma samples per the manufacturer's instructions (Abcam, Cambridge, MA). Prolonged storage of plasma was avoided, and testing was generally performed with all samples simultaneously to avoid any batch effect.

Plasma and liver amino acids

The concentration of amino acids in plasma and liver was determined by high-performance liquid chromatography as previously described [113].

Guanidino Compounds

The concentration of guanidinoacetic acid (GAA) in the plasma and liver was determined by using a normal phase hydrophilic interaction column after analyte derivatization as described [114].

Ammonia challenge and ureagenesis

Mice were fasted for 3-4 hours prior to the beginning of ammonia challenging as previously described [81] using 4 mmol/kg ^{15}N ammonium chloride (^{15}NH$_4$Cl) (Cambridge Isotope Laboratories, Tewksbury, MA). Blood collections were performed immediately before and at 10, 30, and 60 minutes after injection also allowing for ureagenesis determination as described [115].

Functional arginase analysis

Hepatic arginase activity was measured in duplicate from liver tissue lysates as previously described [27].

Histology and Immunohistochemistry

Liver tissues were fixed in 10% (v/v) buffered formalin for 48 hours and then stored in 70% ethanol. Fixed tissue was embedded in paraffin blocks using standard procedures from which 4 µm thick sections were collected on microscope slides. Section deparaffinization, rehydration, antigen retrieval, and permeabilization were performed as previously described [113]. Sections were blocked with 10% (v/v) normal goat serum in PBS for 30 minutes. Sections were then co-incubated with primary antibodies for arginase (Santa Cruz Biotechnology, Dallas, TX sc-20150) and glutamine synthetase (Abcam ab64613) overnight at 4°C. Sections were then co-incubated with fluorescent secondary antibodies donkey anti-goat Alexa Fluor 594 (Invitrogen, Carlsbad, CA A11058) and goat anti-mouse Alexa Fluor 488 (Invitrogen A11001) for 1 hour at room temperature. Section cell nuclei were counterstained with DAPI and mounted with VECTASHIELD Antifade Mounting Medium with DAPI (Vector Laboratories, Burlingame, CA) and then visualized.

Hematoxylin and eosin (H&E) and Masson's trichrome staining were performed by standard methods.

mRNA In Situ Hybridization

mRNA *in situ* hybridization was performed using RNAscope technology on the automated Leica BOND RX autostainer platform using the RNAScope® 2.5 LS Reagent Kit-BROWN from Advanced Cell Diagnostics (Newark, CA). An exclusive target probe with proprietary sequences was designed by ACD to target arginase 1 mRNA. Control probes to the housekeeping gene *Mus musculus* peptidylprolyl isomerase B (Ppib), mRNA (cat no 313918,

ACD) was used as a positive control or the bacterial gene dihydrodipicolinate reductase (DapB) (cat no 312038, ACD) as a negative control was also used as a quality control check for tissues. Slides were processed using a Leica staining protocol per the user manual Document Number 322100-USM (ACD). All images were captured at 20X magnification with the Panoramic 250 Flash II (3DHISTECH, Budapest, Hungary) digital slide scanner.

Electron Microscopy

Four groups of liver tissues were collected and fixed in 4% (v/v) paraformaldehyde (Electron Microscopy Sciences, Hatfield, PA) plus 2.5% (v/v) glutaraldehyde (Thermo Fisher Scientific) in PBS solution at 4°C for several weeks. Each liver sample was prepared for imaging by standard methods. (Details of method are provided in SI Appendix).

RNA Isolation

Total RNA was isolated from approximately 20 mg of homogenized liver tissue with a Roche High Pure RNA Isolation Kit (Roche Applied Sciences, Indianapolis, IN) per manufacturer's instructions.

Residual endogenous murine Arg1 mRNA quantitative RT-PCR

One μg of total RNA was reverse transcribed to cDNA with a Transcriptor First Strand cDNA Synthesis Kit (Roche Applied Sciences) per manufacturer's instructions. Primers for endogenous murine *Arg1* mRNA were designed to bind to the exon 7-8 junction: Forward primer 5'-ACATCACAGAAGAAATTTACAAGACAG / Reverse primer 5'-TGCCGTGTTCACAGTACTCTTC / Amplicon length-113 nucleotides. After cDNA synthesis, quantitative RT-PCR was performed using SsoAdvanced^{TM} Universal SYBR$^{®}$ Green Supermix (Bio-Rad) on MyiQ^{TM}2 Two-Color Real-Time PCR Detection System (Bio-Rad). Transcript levels were analyzed in triplicate using the C_T (threshold cycle) values. Target transcript levels were

normalized to endogenous murine *β-Actin* mRNA and fold enrichment was measured using the $2^{-\Delta\Delta Ct}$ method.

hARG1 mRNA quantitative RT-PCR

Total RNA was diluted to 10 ng/µL in water. LNP-encapsulated mRNA quantification was performed in triplicate with a Taqman™ RNA-to-CT™ 1 Step kit (Thermo Fisher Scientific) per manufacturer's instruction. For relative quantification of h*ARG1* mRNA, sample mRNA quantification was calculated relative to Taqman-validated primer-probe pair for the murine *Gapdh* housekeeping gene (Thermo Fisher Scientific, Catalog No. 4331182, Assay ID No. Hs02786624_g1) using the $2^{-\Delta\Delta Ct}$ method. ARG1 Forward Primer: CAAGGACATCGTCTACATCGG; Reverse Primer: ACCTCGGTCATGGAGAAGTA.

Western blot

Liver tissue was homogenized and 50 µg of protein was transferred, co-incubated with the target primary arginase antibody (Santa Cruz Biotechnology sc-20150) and loading control primary antibody *β*-tubulin (Santa Cruz Biotechnology sc-9104) followed by incubation with secondary HRP-conjugated goat anti-rabbit antibody (Santa Cruz Biotechnology sc-2004).

Statistical analysis

All collected data was analyzed with the GraphPad Prism8 (San Diego, CA) statistical package. Results were expressed as mean ± standard error of the mean (SEM) and p values were determined using one-way ANOVA with Tukey's multiple comparison's test, two-way ANOVA with Sidak's multiple comparison's test, or unpaired T-test when applicable. Error bars represent SEM. $P < 0.05$ were considered significant.

Results

Lipid nanoparticles successfully deliver mRNA to murine livers

The liver is the primary location of nitrogen detoxification and urea cycle function. Therefore, targeted delivery of the LNPs and proper release of the encapsulated mRNA for therapeutic protein translation in the liver is crucial to the potential success of this treatment modality for arginase deficiency. To examine the ability for our engineered LNPs to traffic to the liver we administered a single intravenous (IV) bolus of 2 mg/kg LNP-encapsulated firefly (*Photinus pyralis*) luciferase mRNA (LNP-*luc*) to wild type (WT) conditional arginase deficient mice (Arg1$^{flox/flox}$) (n = 5 males). Beginning 2 hrs post-LNP-*luc* injection, mice were administered the luciferase substrate, $_D$-Luciferin, and underwent serial BLI. Imaging revealed proper localization of functional luciferase protein to the liver as early as 2 hrs post-LNP-*luc* injection that remained detectable by BLI in some animals up to 36 hrs post-injection (Fig. 2-1A). 72 hrs after the initial LNP-*luc* injection, luciferase protein was undetectable by BLI and an additional IV bolus of 2 mg/kg LNP-*luc* was administered at 73 hrs after the first injection. Repeat serial BLI revealed comparable liver trafficking and luciferase protein translation and stability kinetics to the initial LNP-*luc* injection (Fig. 2-1A-B). Though protein translation kinetics and half-life will be variable and determined by the specific mRNA encapsulated within the LNPs, BLI demonstrated the LNPs ability to reliably and repeatedly deliver mRNA to the liver without overt evidence of short-term abnormalities.

Pharmacokinetic characterization of LNP-encapsulated arginase mRNA in murine livers

A human codon-optimized arginase 1 (h*ARG1*) mRNA was designed, synthesized, and encapsulated within our biodegradable liver-targeting LNPs (LNP-h*ARG1*). To characterize the kinetics of the h*ARG1* mRNA release from the LNPs and stability within the liver, we performed a pharmacokinetic (PK) study in wild type (WT) Arg1$^{flox/flox}$ mice (n = 3 mice per time point). We administered a single IV bolus of 2 mg/kg LNP-h*ARG1* and collected livers at time points 0, 2, 6,

12, and 24 hrs and then daily from day 2 to 7 post-injection. Using quantitative real time-PCR (qRT-PCR) primers specific for the human codon optimized *ARG1* mRNA encapsulated within the LNPs, h*ARG1* mRNA levels in treated livers were determined relative to murine *Gapdh* housekeeping transcript levels. We observed peak and substantial h*ARG1* mRNA levels in the liver at the earliest time point 2 hrs post-injection compared to 0 hr mice that did not receive LNP-h*ARG1* (0 hr: 0.934 ± 9.934 vs 2 hrs: $1.49 \times 10^5 \pm 2.06 \times 10^4$ relative transcript levels; $p < 0.001$) (Fig. 2-1C). After the observed peak at 2 hrs, h*ARG1* mRNA levels significantly decreased by 33.1% by 6 hrs ($p = 0.005$) and 84.2% by 12 hrs ($p < 0.001$) relative to 2 hrs post-injection mRNA levels. By 24 hrs only 4.4% of the 2 hrs post-injection mRNA levels remained ($p < 0.001$) and maintained levels below 0.25% from day 2 to 7 ($p < 0.001$ each day).

Long-term animal survival after systemic delivery of LNP-hARG1

Hepatic loss of murine Arg1 expression leads to hyperargininemia, hyperammonemia, and death in Arg1$^{-/-}$ mice [52]. Previous studies have demonstrated that delivery of the murine Arg1 cDNA by AAVrh10 can rescue a juvenile-lethal arginase deficient murine model, but whose therapeutic efficacy may be limited due to hepatocellular division leading to eventual dilution and a substantial loss of the transgene [27]. To demonstrate the long-term efficacy of LNP-mediated delivery of codon-optimized h*ARG1* mRNA to successfully treat arginase deficiency, adult Arg1$^{flox/flox}$ mice were administered 2.0×10^{11} genome copies of AAV8-thyroxine binding globulin (TBG)-Cre recombinase on day 0 to disrupt hepatic expression of the endogenous functional murine Arg1 by excision of exons 7 and 8. Beginning on day 14 after AAV8-TBG-Cre administration, mice were administered IV either 2 mg/kg LNP-*luc* or LNP-h*ARG1* (n = 10; 5 male, 5 female per group). One group was administered LNP-mRNA weekly and another group every 3 days (q3D). Weight was recorded daily, blood was collected weekly, and livers were collected at the end of the study or at time of euthanasia for humane endpoints or death. Weekly LNP-h*ARG1* mice demonstrated significant life extension compared to the

weekly LNP-*luc* control mice (p < 0.001), but none exhibited long-term survival and stable weights; all weekly LNP-h*ARG1* mice died or were euthanized for humane endpoints by day 62 while all weekly LNP-*luc* mice perished by day 27 (Fig. 2-2A-B). In contrast, q3D LNP-h*ARG1* mice exhibited significant life extension (p < 0.001) with 100% survival and without physiological signs of hyperammonemia or weight loss to beyond day 77 compared to q3D LNP-*luc* mice where all perished by day 22 (Fig. 2-2C-D). These data demonstrate that delivery of 2 mg/kg LNP-h*ARG1* each 3 days is a therapeutic dose and frequency of administration that can successfully extend and maintain long-term survival and health of arginase deficient mice. No period of multi-day loading of LNP-h*ARG1* by daily injections is necessary (Fig. 2-S1).

Functional metabolic recovery of Arg1$^{-/-}$ mice after systemic delivery of LNP-hARG1

To evaluate the metabolic function of conditional Arg1$^{-/-}$ mice in response to LNP-mRNA treatment, plasma was collected over the course of the study and analyzed for various criteria. Due to the transient nature of LNP-mRNA treatment, plasma metabolite levels were expected to fluctuate depending on timing of plasma collection within the therapeutic q3D dosing interval. Therefore, mice (n = 6 per group) were bled every 7 days regardless of timing within the dosing interval to collect time points representing the full spectrum within the dosing interval. In weekly LNP-*luc* mice, plasma ammonia levels were measured on day 0 (183.7 ± 26.9 μM) and demonstrated significantly increased concentrations that peaked at death on day 21 (692.9 ± 23.5 μM; p < 0.001) (Fig. 2-3A). Similarly, significantly increased plasma ammonia concentrations at death compared to day 0 levels was also found in weekly LNP-h*ARG1* mice (day 0: 120.0 ± 17.8 vs. day 42: 1409.6 ± 449.5 μM; p = 0.002) (Fig. 2-3A) and in q3D LNP-*luc* mice (day 0: 174.1 ± 32.6 vs. day 21: 1505.6 ± 414.5 μM; p = 0.003) (Fig. 2-3B). However, q3D LNP-h*ARG1* mice showed good control and no statistically significant increases in plasma ammonia throughout the study compared to day 0 levels, demonstrating amelioration of hyperammonemic episodes induced by hepatic Arg1 disruption (day 0: 112.8 ± 36.7 vs. day 14:

58

146.2 ± 42.2, day 21: 122.2 ± 35.2, day 28: 130.5 ± 33.4, day 42: 146.5 ± 22.7, day 56: 101.3 ±

31.9, day 70: 123.4 ± 24.5, day 77: 163.1 ± 33.7 µM; $p > 0.05$) (Fig. 2-3B). q3D LNP-h*ARG1*

plasma ammonia was measured at days 0, 14, 21, 28, 42, 56, 70 and 77 demonstrating levels

corresponding to 0, 0, 1, 2, 1, 3, 2, and 1 day(s) post last-dose (post-LD), respectively (Fig 3B).

Mice (n = 5 males per group) administered q3D LNP-h*ARG1* on day 72 (1 day post-LD) were

also able to similarly metabolize an ammonium challenge compared to WT control mice after 60

minutes demonstrating adequate ability to handle exogenous nitrogen loading (Fig. 2-3C).

To further confirm recovery of ureagenesis, q3D LNP-h*ARG1* mice on day 72 (1 day

post-LD) and WT control mice (n = 8 per group; 4 male, 4 female) were administered

intraperitoneal ^{15}N ammonium chloride and allowed to metabolize into ^{15}N urea for 60 minutes

before collected blood was measured by GC-MS for ^{15}N urea enrichment (Fig. 2-3D_{Left}); q3D

LNP-h*ARG1* mice metabolized 81.9 ± 11.3% of total WT control ^{15}N urea enrichment levels

demonstrating no statistically significant difference between the two groups ($p > 0.05$) (Fig. 2-

3D_{Right}).

Plasma and liver (n = 6 per group) were also analyzed for selected amino acids critical to

the urea cycle and nitrogen metabolism pathways. Plasma amino acids were measured on day

0, 28, 56, and 77 demonstrating levels corresponding to 0, 2, 3, and 1 day(s) post-LD,

respectively. Plasma arginine and glutamine, both typically found elevated in mice with arginase

deficiency, were significantly increased at time of euthanasia in q3D LNP-*luc* mice compared to

day 0 (ARG_{D0}: 114.6 ± 1.5 µM, vs. ARG_{D21}: 832.5 ± 102.1 µM; $p < 0.001$) (GLN_{D0}: 731.8 ± 47.2

µM vs. GLN_{D21}: 1277.0 ± 243.0 µM; $p = 0.020$) (Fig. 2-4A-B). However, in q3D LNP-h*ARG1*

mice, neither plasma arginine nor glutamine observed any statistically significant increase

throughout the course of the study compared to day 0 (ARG_{D0} 82.3 ± 8.3 µM vs. ARG_{D28} 127.5 ±

12.09 µM, ARG_{D56} 165.2 ± 36.47 µM, ARG_{D77}: 151.2 ± 34.4 µM, $p > 0.05$) (GLN_{D0}: 584.5 ± 19.1

µM vs. GLN_{D28}: 643.4 ± 32.5 µM, GLN_{D56}: 628.0 ± 90.86 µM, GLN_{D77}: 784.2 ± 66.7 µM, p = n.s.)

(Fig. 2-4A-B). Plasma ornithine and lysine were also examined and while neither q3D LNP-*luc*

nor q3D LNP-h*ARG1* groups demonstrated statistically significant increases throughout the study, plasma lysine in q3D LNP-*luc* at time of euthanasia was trending toward statistical significantly increased levels when compared to day 0 (LYS$_{D0}$ 182.5 ± 21.1 μM vs. LYS$_{D21}$ 356.9 ± 103.6 μM, p = 0.096) (Fig. 2-4C-D).

Hepatic amino acids (n = 6 per group unless otherwise noted) were measured for q3D LNP-*luc* mice at time of euthanasia and for q3D LNP-h*ARG1* on day 35 (3 days post-LD) and day 77 (1 day post-LD). Hepatic arginine concentrations in q3D LNP-*luc* mice (34.6 ± 5.7 nmol/mg protein) were significantly higher compared to q3D LNP-h*ARG1* mice on both day 35 (2.6 ± 1.1 nmol/mg protein; p < 0.001, n = 4) and day 77 (3.1 ± 0.2 nmol/mg protein; p < 0.001,) and WT control mice (2.5 ± 0.2 nmol/mg protein; p < 0.001) (Fig. 2-4E). Liver glutamine concentrations in q3D LNP-*luc* mice (9.0 ± 1.2 nmol/mg protein) were significantly lower compared to q3D LNP-h*ARG1* mice on day 77 (26.4 ± 1.8 nmol/mg protein; p < 0.001), but not significantly different from q3D LNP-h*ARG1* mice on day 35 (19.92 ± 4.6 nmol/mg protein; p > 0.05, n = 4) or WT control mice (18.0 ± 3.6 nmol/mg protein; p > 0.05) (Fig. 2-4F); ammonia does result in the short-term activation of hepatic glutaminase [116] and may be the cause of this intracellular glutamine reduction in LNP-*luc* mice as plasma ammonia is markedly elevated in this group (Fig. 2-3B) Hepatic ornithine concentrations, when compared to WT controls (2.0 ± 0.2 nmol/mg protein), were significantly elevated in q3D LNP-*luc* (12.1 ± 2.8 nmol/mg protein; p = 0.003) and q3D LNP-h*ARG1* mice on day 35 (11.0 ± 2.3 nmol/mg protein; p = 0.017, n = 4), but not significantly elevated in q3D LNP-h*ARG1* mice on day 77 (4.1 ± 0.7 nmol/mg protein; p > 0.05) (Fig. 2-4G). Hepatic lysine concentrations in q3D LNP-*luc* mice (36.2 ± 7.6 nmol/mg protein) were significantly higher compared to q3D LNP-h*ARG1* mice on both day 35 (7.7 ± 1.8 nmol/mg protein; p = 0.002, n = 4) and day 77 (5.9 ± 0.6 nmol/mg protein; p < 0.001,) and WT control mice (5.1 ± 0.7 nmol/mg protein; p < 0.001) (Fig. 2-4H).

Guanidino compounds have been found to accumulate in patients with arginase deficiency [14, 16, 117]. Therefore, we quantified the accumulation of guanidinoacetic acid (n =

6 per group unless otherwise stated) in plasma of q3D LNP-*luc* mice at time of euthanasia and for q3D LNP-h*ARG1* on day 35 (3 days post-LD) and day 77 (1 day post-LD). There was no statistically significant increase between q3D LNP-h*ARG1* mice on day 35 (3.9 ± 0.6 nM; n = 4) and on day 77 (3.0 ± 0.4 nM) and WT controls (2.3 ± 0.2 nM); however, GAA levels of q3D LNP-*luc* mice at time of euthanasia were trending toward significantly increased levels (3.8 ± 0.6 nM; $p = 0.100$) compared to the WT controls (Fig. 2-4I).

To support the plasma GAA studies, hepatic levels were also quantified for q3D LNP-*luc* mice at time of euthanasia and for q3D LNP-h*ARG1* on day 35 (3 days post-LD) and 77 (1 day post-LD) (n = 4 per group). Liver GAA levels in q3D LNP-*luc* mice (61.5 ± 12.7 pmol/mg of tissue) were significantly elevated compared to q3D LNP-h*ARG1* mice on day 77 (27.3 ± 6.9 pmol/mg of tissue; $p = 0.047$) and WT controls (18.8 ± 4.3 pmol/mg of tissue; $p = 0.013$); levels were trending toward significance compared to q3D LNP-h*ARG1* mice on day 35 (30.5 ± 5.6 pmol/mg of tissue; $p = 0.077$) (Fig. 2-4J).

To examine for potential liver toxicity induced by long-term administration of LNPs, plasma was examined for levels of ALT (n = 6 per group), a marker of liver injury, of q3D LNP-*luc* mice at time of euthanasia (49.3 ± 17.5 U/L) and q3D LNP-h*ARG1* mice on D77 (1 day post-LD) (33.6 ± 3.8 U/L); differences in levels in both groups were not statistically significant compared to WT control levels (27.3 ± 3.7 U/L) ($p > 0.05$ for both comparisons) (Fig. 2-4K). Altogether, these data demonstrate the ability for this treatment modality to completely and safely recover the metabolic profile of adult arginase-deficient mice.

LNP-hARG1 levels and localization characteristics within Arg1$^{-/-}$ livers

After the completion of our *in vivo* and biochemical studies, LNP-mRNA-treated mice were euthanized and their livers collected, sectioned, and analyzed to characterize LNP-h*ARG1* levels and distribution. h*ARG1* mRNA in LNP-mRNA-treated livers was determined relative to the murine *Gapdh* housekeeping transcript levels (n = 6 per group). The q3D LNP-h*ARG1* mice

were euthanized on day 77 (1 day post-LD). Mice were found to have a markedly and significantly increased level of h*ARG1* mRNA compared to LNP-*luc* and WT control mice (p = 0.022 for both) (Fig. 2-5A). In contrast, weekly LNP-h*ARG1* mice showed levels of h*ARG1* mRNA in large variation and demonstrated no statistically significant differences compared to weekly LNP-*luc* and WT control mice (Fig. 2-S2A).

Liver lysates from LNP-mRNA-treated mice (n = 6 per group) were analyzed for functional ARG1 protein. The q3D LNP-h*ARG1* mice on day 77 (1 day post-LD) recovered 53.6 ± 6.3% functional ARG1 activity relative to WT control mice (p < 0.001) (Fig. 2-5B). In contrast, while weekly LNP-h*ARG1* mice at time of euthanasia recovered 10.9 ± 1.5% functional ARG1 activity relative to WT control mice (p < 0.001), these activity levels were found to be not significant different from weekly LNP-*luc* mice at time of euthanasia with 6.4 ± 0.6% functional ARG1 activity (p > 0.05) whose expression was too low to maintain survival (Fig. 2-S2B). To further confirm these findings, western blot analysis was performed with q3D LNP-h*ARG1* liver collected on day 77 (1 day post-LD) that revealed the strong presence of a single 35 kDa isoform of ARG1 derived from LNP-h*ARG1* compared to WT mouse liver that demonstrates both 35 and 37 kDa endogenous Arg1 isoforms (Fig. 2-5C). Weekly LNP-h*ARG1* livers collected at time of euthanasia demonstrated minimal presence of ARG1 protein (Fig. 2-S2C).

To confirm that any survival extension was due to LNP-h*ARG1* treatment and not maintenance of endogenous murine Arg1 expression, qRT-PCR primers were designed to span the endogenous murine *Arg1* exon 7 and 8 mRNA junction excised after AAV8-TBG-Cre activation. In weekly LNP-mRNA-treated and q3D LNP-*luc*-treated livers collected at time of euthanasia and q3D LNP-h*ARG1*-treated mice on day 77 (1 day post-LD) there was absence of endogenous murine *Arg1* mRNA compared to WT control levels (p > 0.05 for both) (Fig. 2-S2D-E).

Livers collected from weekly LNP-h*ARG1* and q3D LNP-*luc* mice collected at time of euthanasia, and q3D LNP-h*ARG1* mice on day 77 (1 day post-LD) were sectioned and

underwent various imaging analyses. h*ARG1* mRNA presence in LNP-mRNA-treated livers was visualized using *in situ* hybridization (ISH) probes designed specifically for h*ARG1* mRNA that was LNP-encapsulated. ISH of q3D LNP-h*ARG1* livers on day 77 collected 24 hrs after the final LNP-h*ARG1* dose revealed positive but low presence of h*ARG1* mRNA in both hepatocytes and Kupffer cells (Fig 2-6); h*ARG1* mRNA levels were in accordance with previous PK data that demonstrated significant reduction in h*ARG1* mRNA after 24 hrs post-LNP-h*ARG1* injection (Fig 2-1C). Weekly LNP-h*ARG1* mice similarly euthanized 24 hrs after the final LNP-h*ARG1* dose also demonstrated positive but lower presence of h*ARG1* mRNA compared to q3D LNP-h*ARG1* livers by ISH (Fig. 2-S3). Immunofluorescent staining for ARG1 and glutamine synthetase (GS), to differentiate periportal (GS^{Negative}) and perivenous (GS^{Positive}) vasculature, was performed on weekly and q3D LNP-mRNA-treated liver sections to visualize localization of ARG1 expression. For weekly LNP-h*ARG1* livers collected at time of euthanasia, no expression of ARG1 could be visualized, further confirming results from the molecular analysis (Fig. 2-S3). However, q3D LNP-h*ARG1* livers on day 77 (1 day post-LD) revealed strong ARG1 expression primarily localized in the periportal and interportal spaces consistent with LNP-h*ARG1* hepatic entrance via periportal vasculature and diffusion out to peripheral hepatocytes (Fig. 2-6). All liver sections were also stained with H&E revealing no overt pathological hepatic abnormalities or lymphocytic infiltrates, and with Masson's trichrome where absence of dark blue staining indicated lack of hepatic fibrosis or collagen deposition (Fig. 2-6). Furthermore, liver sections were imaged by electron microscopy to reveal intricate subcellular structures. All groups showed regular organization of the hepatic tissue without evidence of accumulation of electron-dense inclusions or bundles of collagen fibers. Hepatocytes demonstrated normal nuclear membranes, rough endoplasmic reticulum and mitochondrial morphology. Compared to the wild type and LNP-h*ARG1*-treated mice, LNP-*luc* hepatocytes did reveal mitochrondria that were slightly enlarged (Fig. 2-6 and Fig. 2-S3) and the occasional presence of a lipid droplet (arrow) (Fig. 2-6).

Discussion

Urea cycle disorders are a family of inherited metabolic conditions of the liver in any of 6 enzymes or 2 transporters which impair ureagenesis and normal nitrogen detoxification produced as a consequence of protein metabolism [118]. They are caused by monogenic loss of enzyme or transporter function, and are combined with straight-forward medical treatments (i.e. protein-restricted diet, ammonia scavengers) that do not address the underlying cause. Urea cycle disorders can result in the rapid development of hyperammonemia characterized by symptoms and signs including headaches, hypo/hyperventilation, seizures, coma and potentially death [5]. Survivors typically have intellectual disabilities and remain vulnerable to repeat episodes of hyperammonemia with their cumulative and permanent neurological injury.

Arginase deficiency (OMIM #207800), caused by biallelic mutations in arginase 1, tends to be recognized in late infancy to early childhood, unlike the other urea cycle disorders where hyperammonemia and related signs often occur within a few days of birth [5, 12]. Often identified by a presentation of spastic paraparesis or quadraparesis, the condition has progressive neurological decline including developmental delays, psychomotor and growth retardation and seizures as characteristic findings [12]. While the potential for diagnosis by newborn screening would enable earlier therapeutic intervention [119], the current treatment is less than fully effective at best, resulting in progressive neurological injury. As such, arginase deficiency is another example of the growing number of metabolic diseases that can be detected by newborn screening but lack fully effective therapies.

In these present studies, we asked the question whether encapsulation of human codon-optimized *ARG1* mRNA within liver-targeting lipid nanoparticles and their systemic delivery to arginase deficient mice can achieve therapeutic recovery of urea cycle function at a reasonable concentration, dosage and frequency and result in normal biochemical parameters. We demonstrate that administration of 2 mg/kg LNP-h*ARG1* every 3 days results in both biochemical and functional efficacy of h*ARG1* mRNA. Unlike arginase 1-deficient mice treated

with a control mRNA (2 mg/kg LNP-*luc* q3D) where all mice perished by day 22, we achieved 100% survival beyond 11 weeks, stable weight, and recovery of urea cycle function with LNP-h*ARG1* as demonstrated in part by maintenance of normal plasma ammonia and urea cycle-related amino acid levels including glutamine. Notably, maintenance of normal plasma ammonia and amino acid levels was sustained throughout the q3D dosing interval with analysis occurring 1, 2 and 3 days post-LD. Importantly, unlike some other metabolic disorders where restored hepatic expression results in incomplete correction due to other metabolite-producing uncorrected tissues [e.g. methylmalonic acidemia [120]], plasma arginine was completely normalized as the urea cycle is exclusive to the liver. In addition, the generation of disease-related metabolites (i.e. GAA) are prevented and repeat administration of h*ARG1* mRNA led to stable weights, an indication of their overall health. The distribution of the exogenous arginase protein was pan-hepatic, as occurs naturally and is in contrast to the other urea cycle enzymes which concentrate in the peri-portal areas.

Pharmacokinetic studies revealed the lipid nanoparticle as an effective delivery vehicle of h*ARG1* mRNA *in vivo* leading to peak levels of h*ARG1* mRNA in the liver shortly after administration. Significant degradation of LNP-mRNA within 24 hours is consistent with other studies [120]. Functionally, whereas control mice demonstrated no hepatic arginase activity and perished, translated ARG1 protein from LNP-h*ARG1* persisted even after significant h*ARG1* mRNA degradation leading to 54% of normal hepatic arginase activity 24 hours after administration. This led to mice (1 day post-LD) being able to completely metabolize an exogenous challenge of ammonia into urea. In addition, ureagenesis was reestablished with similar ^{15}N incorporation in mice (1 day post-LD) compared to wild type mice. While analyses aimed to quantify h*ARG1* mRNA and translated protein levels in the liver as well as *in vivo* efficacy of LNP-h*ARG1* through exogenous ammonia challenges and recovery of ureagenesis were performed on mice 1 day post-LD, a time point expected to have high ARG1 expression, we nonetheless have demonstrated the sustained efficacy of LNP-h*ARG1* throughout the q3D

dosing interval as evidenced by maintenance of normal weight, plasma amino acids and prevention of GAA accumulation in mice 3 days post-LD.

LNP-h*ARG1* also led to normalization of intracellular arginine levels in hepatocytes; this is not achievable with enzyme replacement therapy (presently in clinical trial [NCT03378531]) due to the inability of the PEGylated enzyme to enter hepatocytes [19]. Though further studies need to be performed, we hypothesize that normalization of intrahepatic arginine levels (not only plasma arginine levels) is needed to avoid the accumulation of disease-related metabolites such as GAA.

With concern for long-term toxicity issues related to repeat dosing of LNPs, we demonstrated that at the end of the 11-week study there was no histologic or enzymatic evidence of liver injury. Further examination with electron microscopy demonstrated hepatocytes with normal nuclear membranes, rough endoplasmic reticulum and mitochondrial morphology. Taken together, within the duration and scope of our study, repeat LNP-h*ARG1* dosing allowed for long-term survival and maintenance of normal plasma ammonia without evidence of hepatocellular injury.

We did find better survival and normalization of plasma ammonia during the q3D dosing period than with weekly administration. As human arginase-deficient patients uncommonly have hyperammonemia, the murine model, however, presents with both hyperammonemia and hyperargininemia, with the former leading to death. In this model, the q3D dosing is needed for extended therapeutic efficacy and survival. Along with q3D dosing, we examined 2 mg/kg LNP-h*ARG1* administered weekly and demonstrated significant life extension; however, the weekly-dosed mice exhibited unstable weights, significant increases of plasma ammonia by the end of each week, and eventually they succumbed to hyperammonemia. Notably, some weekly-dosed mice had positive presence of h*ARG1* mRNA by the time of death or euthanasia; however, western blot and a functional assay demonstrated minimal hARG1 protein expression, potentially due to inadequate time for proper protein translation and the progression of disease

66

in the mice. Thus, while further frequency optimization will be necessary for clinical application, human patients may not require the frequency of administration utilized in these murine studies. Though progress has been made by way of advancements with both integrating- and non-integrating viral vector- and non-viral-based technologies to restore enzyme function, these gene therapy methods, for arginase deficiency, generally remain in the pre-clinical stage [27, 28, 80] and exhibit potential disadvantages. These include risk for insertional mutagenesis [101] and limited efficacy due to hepatocellular division [102] with viral-based strategies, lack of availability of cellular- [69] and organ-based strategies [121], and inability for hepatocyte penetrance with PEGylated enzyme replacement [19]. Though highly promising and potentially curative, these strategies must be studied further to ensure effectiveness and safety before consideration of clinical applicability. Delivering mRNA to the liver is an alternative strategy to provide missing or defective enzyme function. With the ability to repeatedly dose lipid nanoparticles that carry h*ARG1* mRNA, supported by the pharmacokinetic studies that demonstrate the rapid onset of expression and the tolerability of multiple dosing, suggests the value and preclinical proof-of-concept efficacy of lipid nanoparticle-based arginase 1 mRNA therapy as an effective therapy for arginase deficiency.
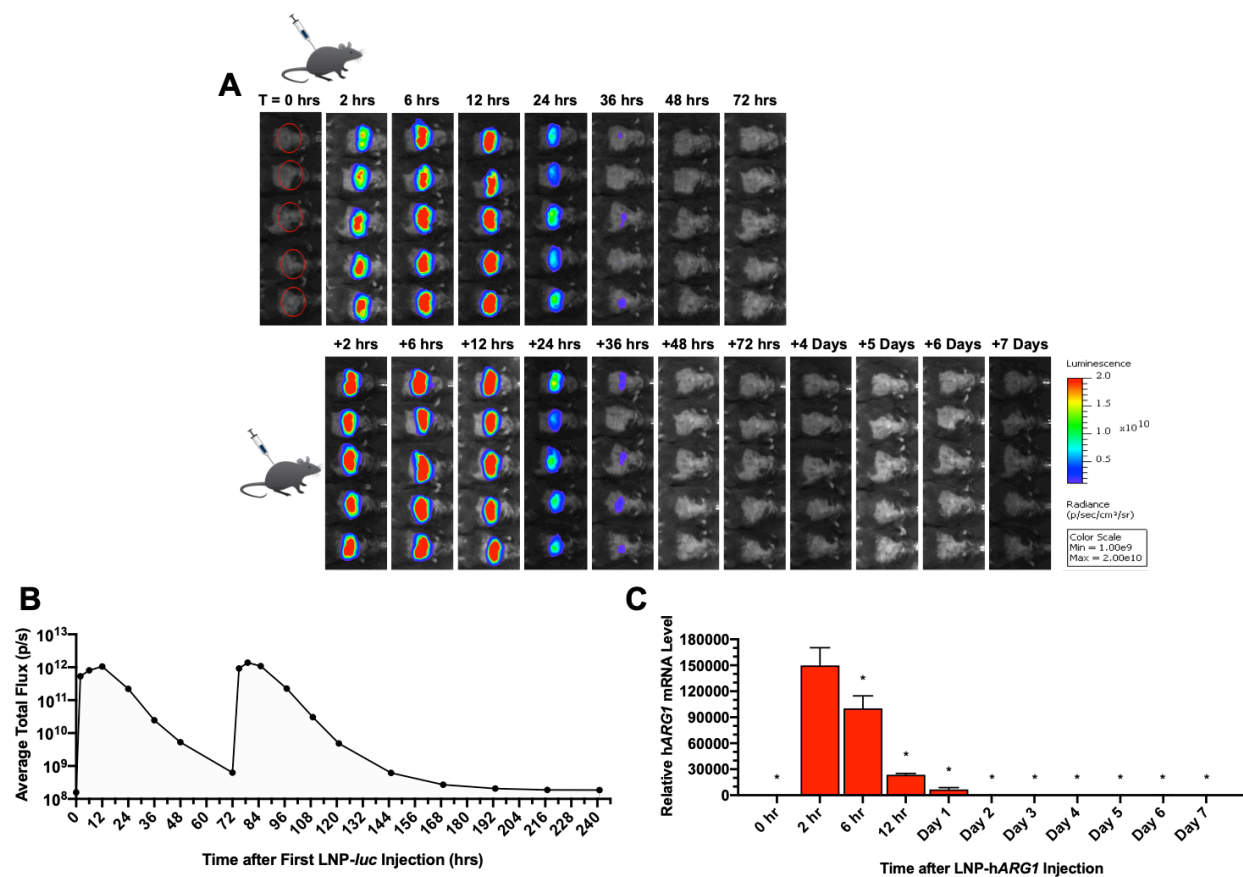
Figure 2-1. Lipid nanoparticle-mediated mRNA delivery to the liver results in repeatable hepatic expression. Wild type conditional arginase 1 knockout mice were administered an intravenous bolus dose of 2 mg/kg of lipid nanoparticle encapsulating mRNA expressing firefly luciferase (LNP-*luc*) **(**or human codon-optimized ARG1 (LNP-h*ARG1*). **(A)** Bioluminescent imaging of hepatic luciferase expression represented by pseudocolor scale was performed at various time points (0, 2, 6, 12, 24, 36, 48, 72 hours) after the first LNP-*luc* dose with repeat imaging after the second bolus administration (2, 6, 12, 24, 36, 48, 72 hours; 4, 5, 6, 7 days; n = 5 mice per time point). All images were acquired and processed with the same settings. **(B)** Quantitation of hepatic expression of firefly luciferase was performed after the initial LNP-*luc* bolus injection and after repeat administration. **(C)** The pharmacokinetics of h*ARG1* mRNA in the liver was determined by quantitative real-time PCR after liver collection at various time points (0, 2, 6, 12, 24 hours; 2, 3, 4, 5, 6, 7 days; n = 3 per time point). P values obtained from

one-way ANOVA with Tukey's multiple comparison's test. (*) represents p < 0.001 compared to 2 hrs post-injection h*ARG1* mRNA levels. Data is presented as mean ± SEM.
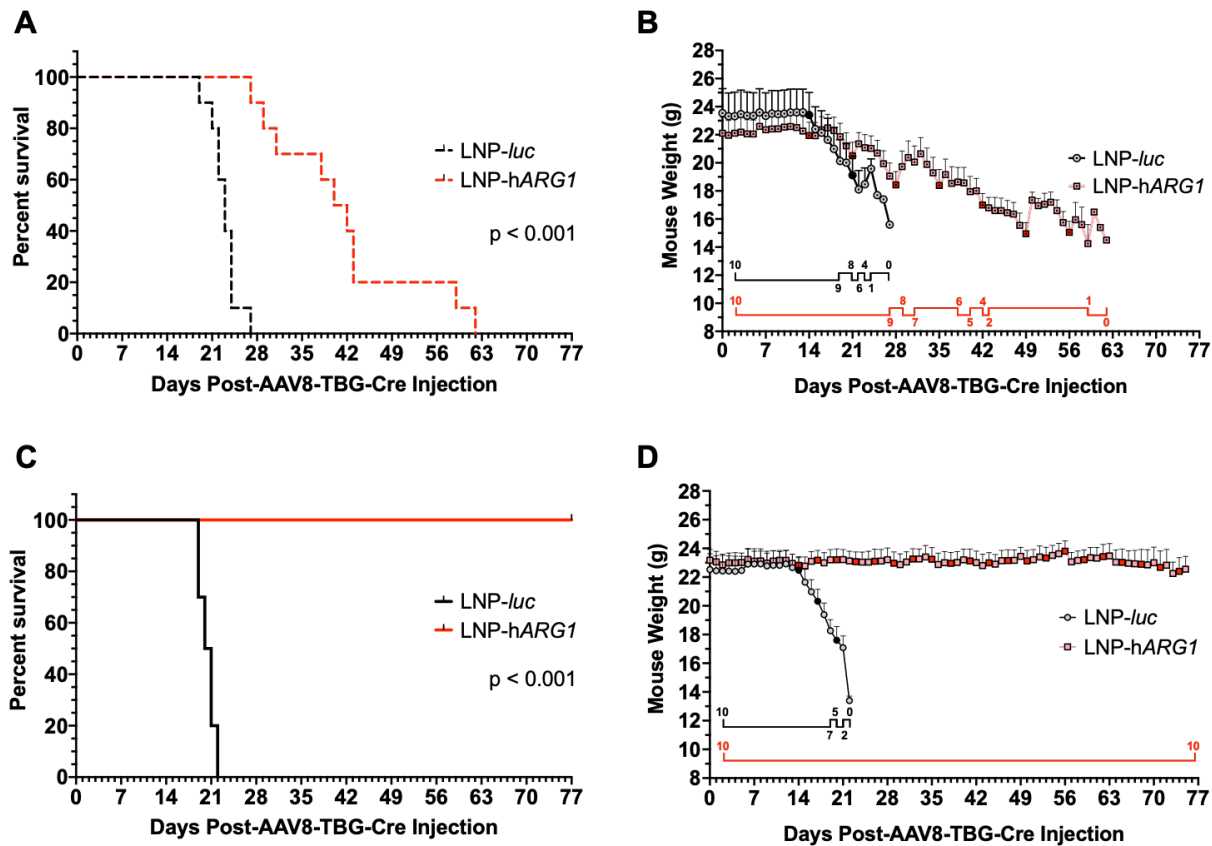

Figure 2-2. Survival and weights of conditional arginase 1 knockout mice were stable long-term in mice administered LNP-formulated h*ARG1* mRNA every 3 days. Conditional arginase knockout mice were administered 2 x 10^{11} genome copies of AAV8-TBG-Cre recombinase (day 0) to induce cre-lox excision in the endogenous murine Arg1 gene resulting in loss-of-function. Mice were administered an IV bolus of 2 mg/kg LNP-*luc* (control, black line) or 2 mg/kg LNP-h*ARG1* (experimental, red line) **(A, B)** weekly or **(C, D)** every 3 days (q3D) beginning on day 14. Mice were monitored for survival and clinical evidence of deterioration in both the weekly-dosed and q3D-dosed groups up to 11 weeks after initiating cre-lox recombination (n = 10 per group, 5 males and 5 females). **(B, D)** Solid black line (LNP-*luc*) and red line (LNP-h*ARG1*) parallel to X-axis of weight logs represent surviving animals in each

treatment study. **(A, C)** p < 0.001 obtained by log-rank. Data is presented as mean ± SEM. (**[B, D]** Day of LNP injection is represented by darkened red square (n) for LNP-h*ARG1* and solid black circle (•) for LNP-*luc*.) (g = gram) (TBG = thyroxine binding globulin promoter; Cre = cre recombinase)
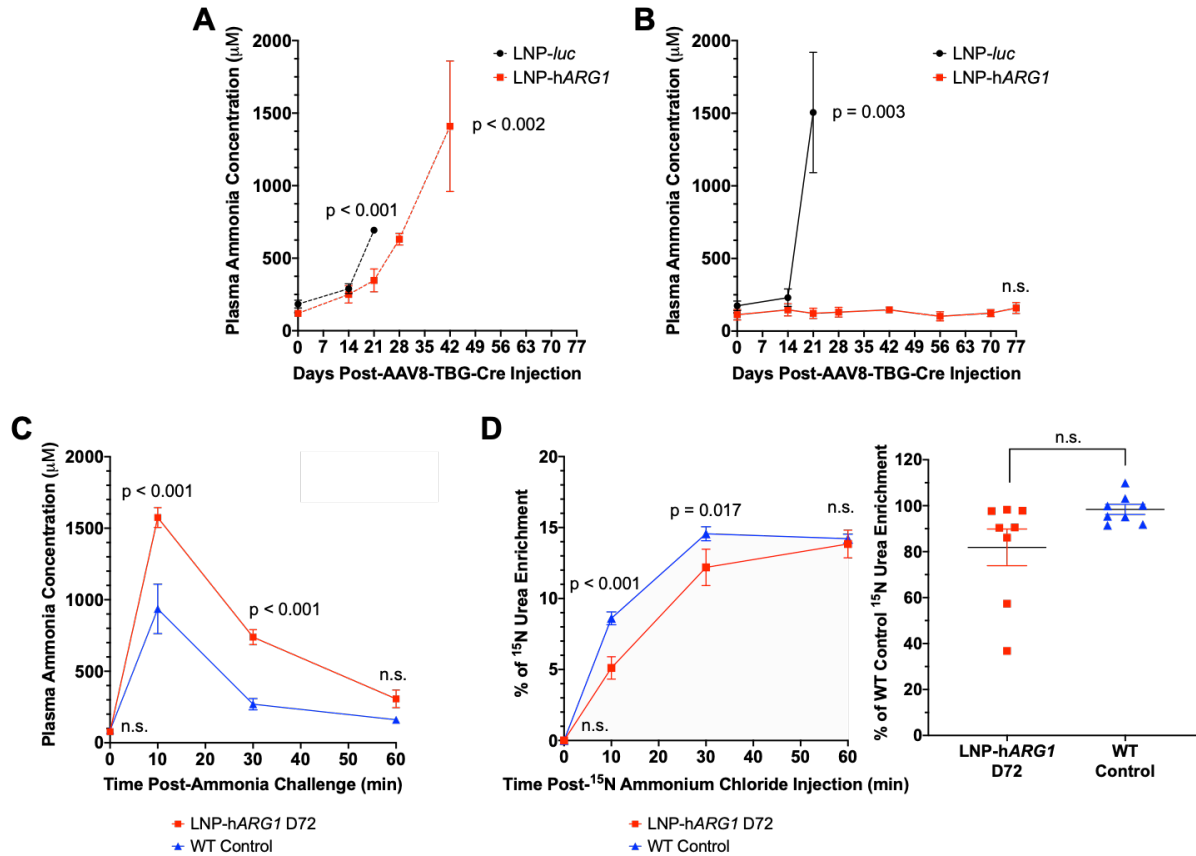
Figure 2-3. Administration of LNP-h*ARG1* every 3 days results in controlled plasma ammonia and near normal ureagenesis. Conditional arginase knockout mice were administered 2 x 10^{11} genome copies of AAV8 TBC-Cre recombinase (day 0) to induce cre-lox excision in the endogenous Arg1. Mice were administered an IV bolus of 2 mg/kg LNP-*luc* (control, black line) or 2 mg/kg LNP-h*ARG1* (experimental, red line) **(A)** weekly or **(B)** every 3 days (q3D) (n = 6 per group) beginning on day 14. **(A)** Plasma ammonia was measured in weekly-dosed mice on day 0, 14, 21, 28 and 42 in the morning before subsequent injection of LNP-mRNA in the afternoon (n = 6 per group). **(B)** Plasma ammonia was measured in q3D-

dosed mice on days 0, 14, 21, 28, 42, 56, 70 and 77 demonstrating levels corresponding to 0, 0, 1, 2, 1, 3, 2, and 1 day(s) post-last-dose (post-LD), respectively (n = 6 per group). **(C)** q3D LNP-h*ARG1*-treated mice on day 72 (1 day post-LD) (red line; n = 6) and wild-type (WT) controls (Arg1$^{flox/flox}$; blue line; n = 6) were administered 0.4 M ammonium chloride IP and plasma ammonia was measured 10, 30, and 60 minutes post-challenge. **(D)** Ureagenesis was assessed at 10, 30 and 60 minutes after IP administration of 0.4 M ^{15}N ammonium chloride on day 72 (1 day post-LD) in q3D LNP-h*ARG1* and WT control mice by ^{15}N urea enrichment quantitation by GC-MS (n = 8 per group). Left graph demonstrates progression of ^{15}N urea enrichment at each time point. Right graph demonstrates total calculated area under the curve to depict total accumulated quantity of ^{15}N urea enrichment of each group. Right graph values are normalized to average total area under the curve value of WT control mice. P values obtained from (A-B) one-way ANOVA with Tukey's multiple comparison's test, (C, D$_{Left}$) two-way ANOVA with Sidak's multiple comparison's test, and (D$_{Right}$) unpaired T-test. Data is presented as mean ± SEM. (TBG = thyroxine binding globulin promoter; Cre = cre recombinase; n.s. = not significant)
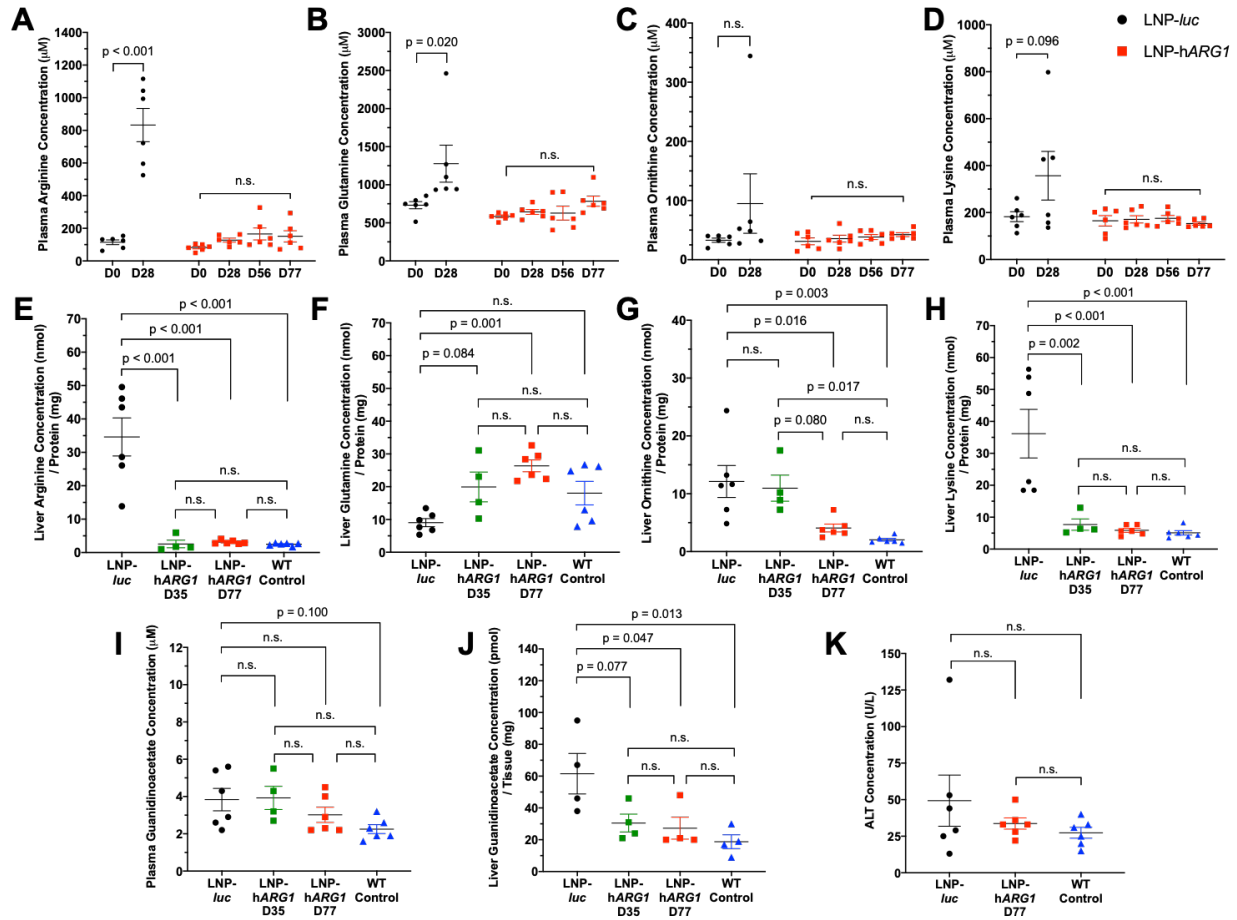
Figure 2-4. LNP-h*ARG1* administration every 3 days prevents elevated plasma and hepatic arginine, controls plasma glutamine and prevents guanidinoacetic acid accumulation in the plasma. (A) Plasma arginine, **(B)** glutamine, **(C)** ornithine and **(D)** lysine were assessed in every 3 day (q3D) control LNP-*luc* mice (n = 6; black) at day 0 and 28 and in q3D LNP-h*ARG1* mice (n = 6; red) at day 0, 28, 56, and 77 demonstrating levels corresponding to 0, 2, 3, and 1 day(s) post-last-dose (post-LD), respectively. **(E)** Hepatic arginine, **(F)** glutamine, **(G)** ornithine and **(H)** lysine were similarly assessed in control q3D LNP-*luc* mice at time of euthanasia (n = 6; black) and in q3D LNP-h*ARG1* mice on day 35 (3 days post-LD; n = 4; green) and on day 77 (1 day post-LD; n = 6; red) and compared with wild type (WT) control liver (n = 6; blue). **(I)** Plasma guanidino compounds, represented by guanidinoacetic acid, was assessed in q3D LNP-h*ARG1* mice on day 35 (3 days post-LD; n = 4; green) and on day 77 (1

72

day post-LD; n = 6; red) and compared with q3D LNP-*luc* (n = 6; black) and WT controls (n = 6; blue). **(J)** Liver guanidinoacetic acid was assessed similarly to **(I)** (n = 4 per group). **(K)** Plasma ALT was assessed in q3D LNP-h*ARG1* on day 77 (1 day post-LD; n = 6; red) and compared with q3D LNP-*luc* at time of euthanasia (n = 6; black) and WT controls (n = 6; blue). P values obtained from one-way ANOVA with Tukey's multiple comparison's test. Data is presented as mean ± SEM. (n.s. = not significant)
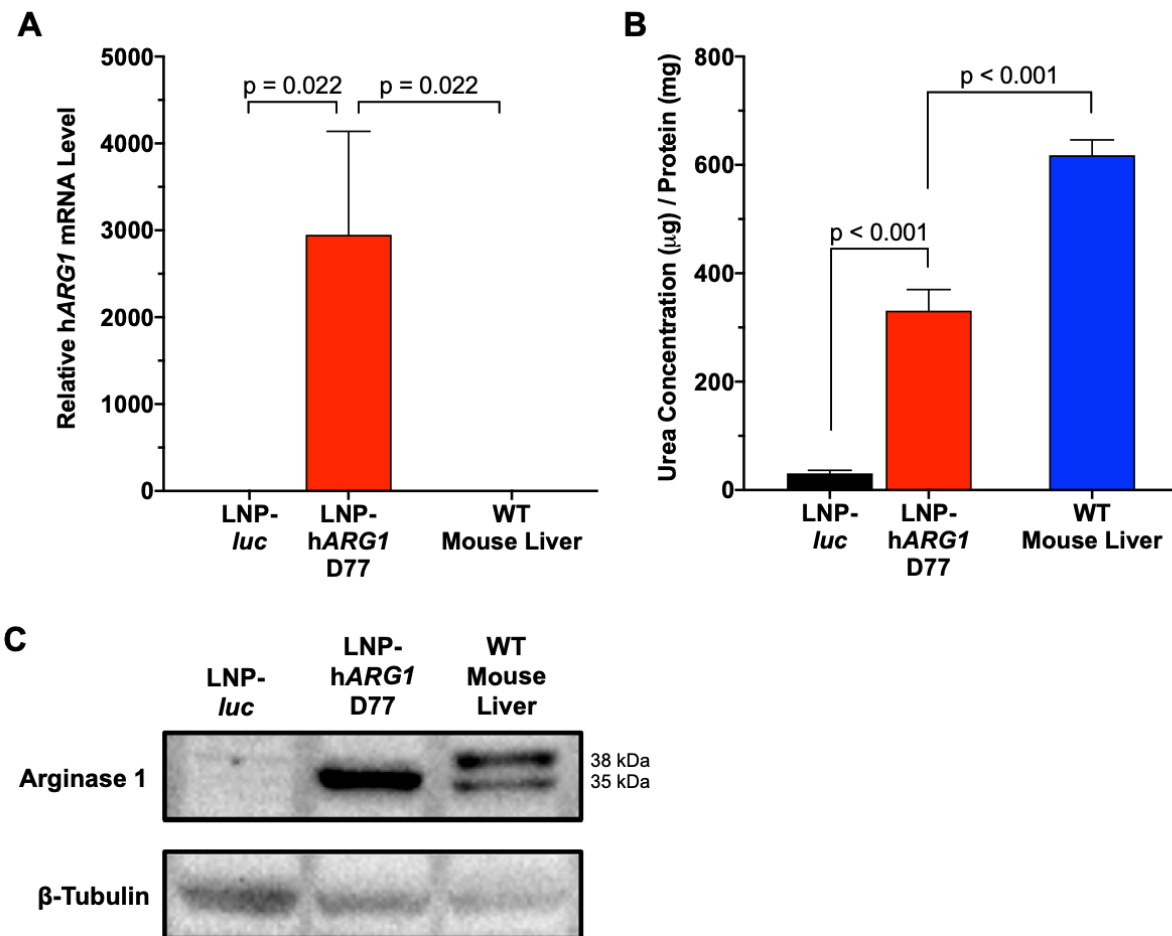

Figure 2-5. LNP-h*ARG1* administration results in restoration of hepatic arginase mRNA and protein. (A) h*ARG1* mRNA hepatic levels relative to murine Gapdh housekeeping gene was assessed by quantitative real-time PCR and **(B)** functional hepatic ARG1 activity was assessed by a biochemical functional arginase assay in every 3 day (q3D) LNP-h*ARG1* mice on day 77 (1 day post-last-dose) and compared with q3D LNP-*luc* at time of euthanasia and wild
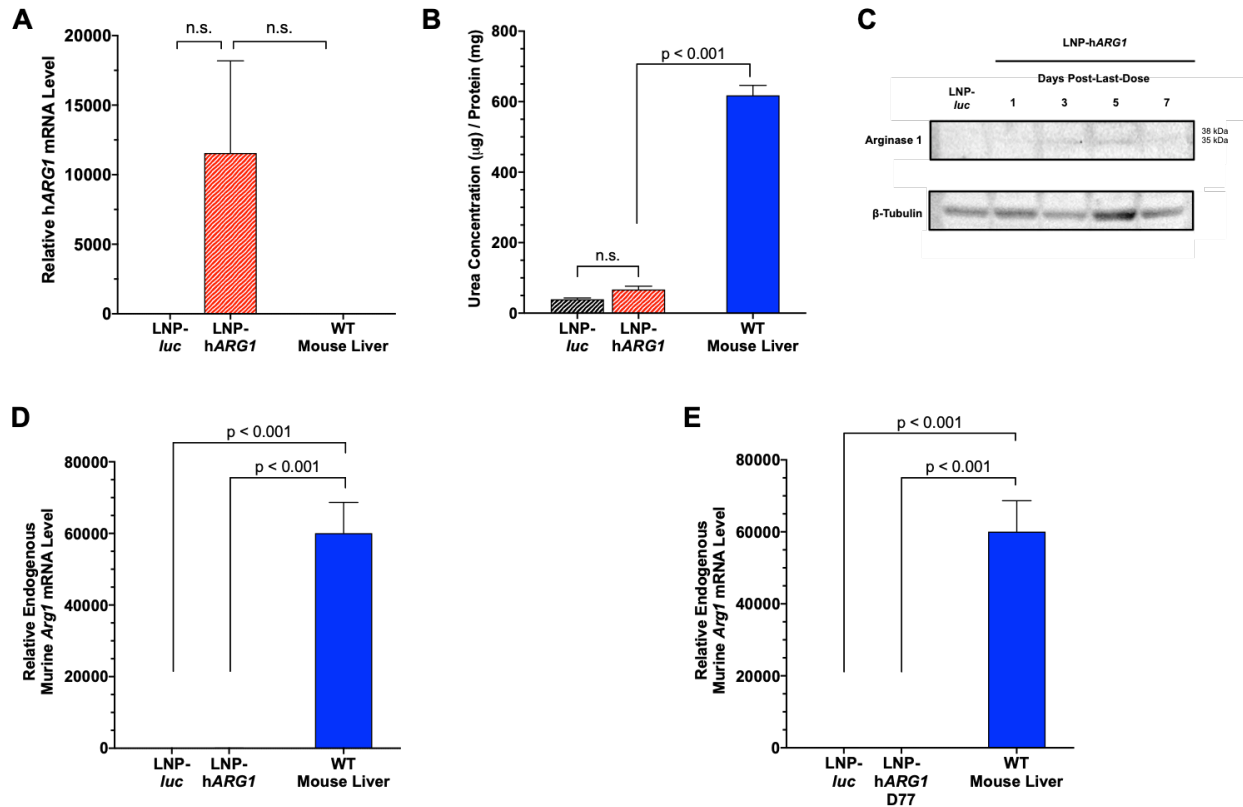
type (WT) controls (n = 6 per group). **(C)** Western blot analysis of hepatic ARG1 transgene expression in q3D LNP-h*ARG1* mice on day 77 (1 day post-last-dose) was compared with q3D LNP-*luc* at time of euthanasia and WT control liver. P values obtained from one-way ANOVA with Tukey's multiple comparison's test. Data is presented as mean ± SEM.
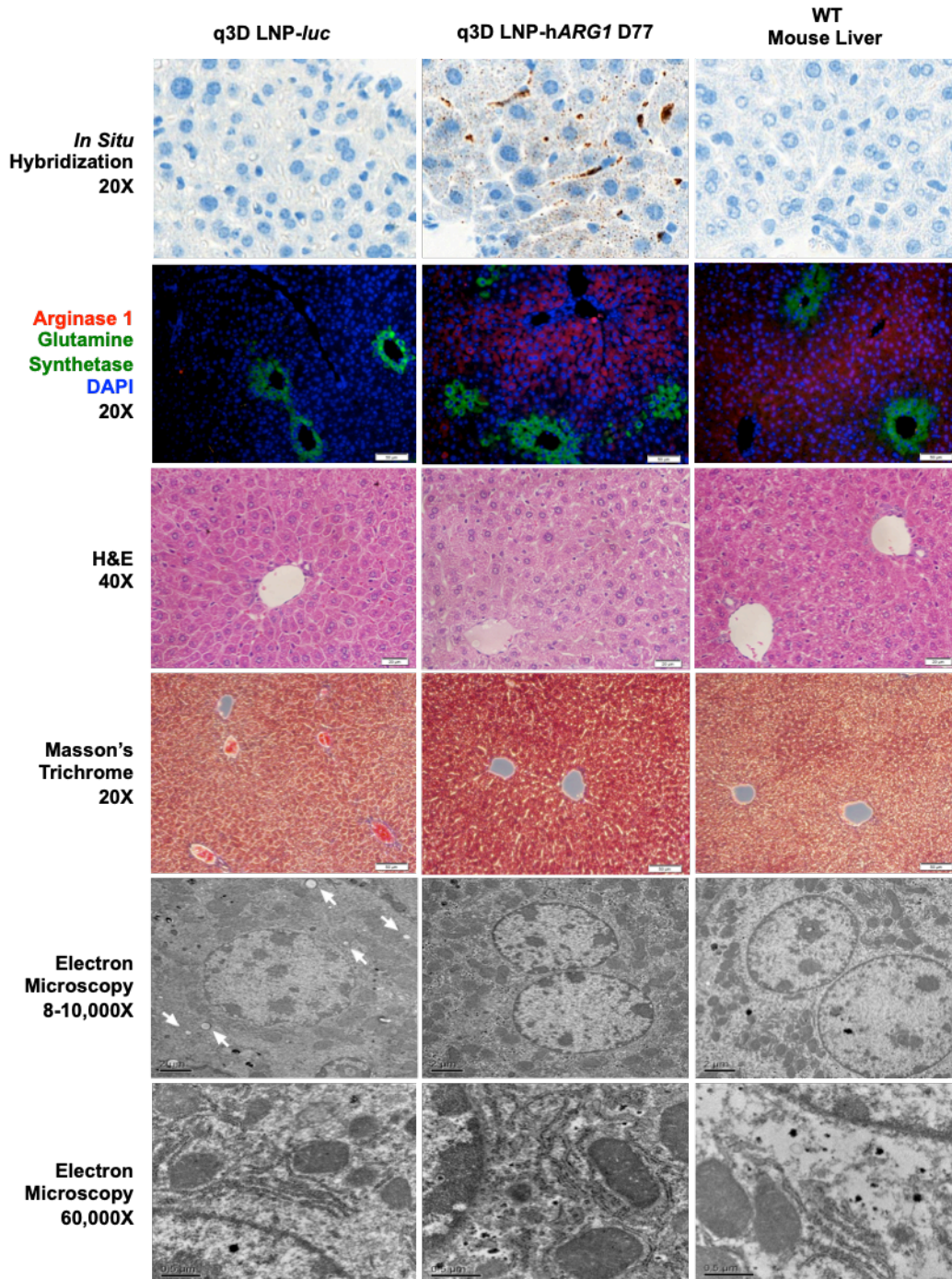
Figure 2-6. LNP-h*ARG1*-mediated protein is detected in the liver when administered by lipid nanoparticle without evidence of inflammatory infiltrates, fibrosis, or subcellular injury. Liver sections of representative images of every 3 day (q3D) LNP-*luc* mice at time of euthanasia, q3D LNP-h*ARG1* mice on day 77 (1 day post-last-dose), and wild type (WT) control mice were examined for: h*ARG1* mRNA presence by *in situ* hybridization (RNAscope®) (top row-20X magnification); ARG1 transgene expression with greater perivenous vascular localization by immunostaining for ARG1 (red) and glutamine synthase (green) (2nd row-20X magnification); hepatic histology by hematoxylin and eosin (H&E) staining (3rd row-40X magnification); examination for collagen deposition/fibrosis by Masson's trichrome staining (4th row-20X magnification); and electron microscopy (5th row-8-10,000X magnification, 6th row-60,000X magnification). (arrows denote lipid droplets)
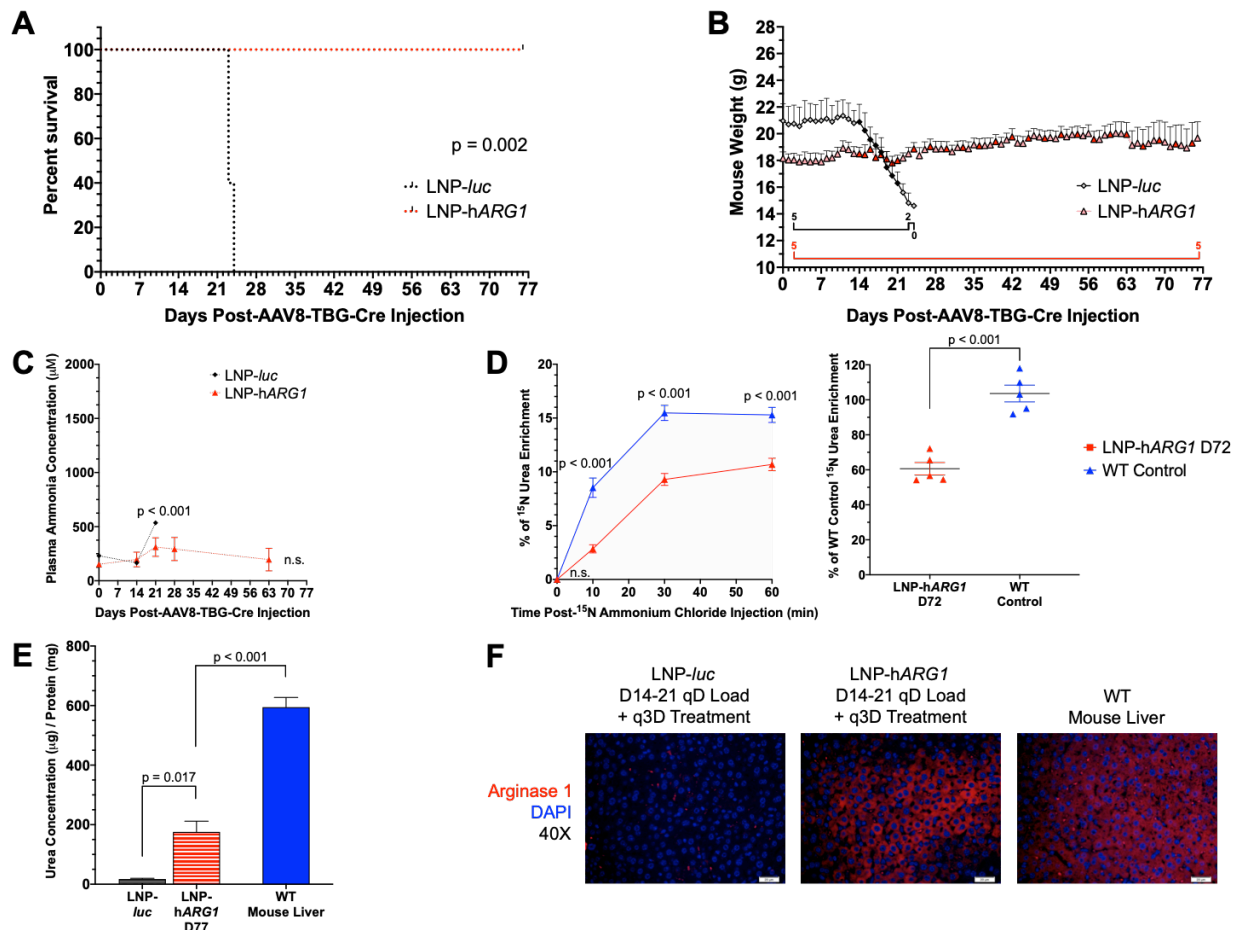
Fig. 2-S1. Conditional arginase knockout mice were administered 2 x 10^{11} genome copies of AAV8-TBG-Cre (day 0) to induce cre-lox excision in endogenous murine Arg1 resulting in loss-of-function. (A) Mice were administered a multi-day loading of 2 mg/kg LNP-*luc* (control, black line) or 2 mg/kg LNP-h*ARG1* (experimental, red line) every day beginning on day 14 to 21 and then dose frequency reduced to every 3 days (D14-21 qD Load + q3D). (A, B) Mice were monitored for survival and clinical evidence of deterioration up to 11 weeks after initiating cre-lox recombination (n = 5 females). (B) Solid black line (LNP-*luc*) and red line (LNP-h*ARG1*) beneath weight log illustrates number of mice remaining in treatment study. (C) Plasma ammonia was measured on days 0, 14, 21, 28, and 63 corresponding to 0, 0, 1, 1, and 3 days post-last-dose (post-LD) (n = 2 females). (D) Ureagenesis was assessed at 10, 30 and 60 minutes after IP administration of 0.4 M ^{15}N ammonium chloride on day 72 (1 day post-LD) in D14-21 qD Load + q3D and wild type (WT) control mice by ^{15}N urea enrichment quantitation. Left graph demonstrates progression of ^{15}N urea enrichment at each time point. Right graph demonstrates total calculated area under the curve to depict total accumulated quantity of ^{15}N urea enrichment of each group. Right graph values are normalized to average total area under the curve value of WT control mice (n = 5 females per group). (E) Hepatic arginase activity was assessed by a biochemical functional arginase assay in D14-21 qD Load + q3D LNP-*luc* at time of euthanasia, D14-21 qD Load + q3D LNP-h*ARG1* on day 72 (1 day post-LD), and WT control livers (n = 3 females) (F) Liver sections of representative images of D14-21 qD Load + q3D LNP-*luc* at time of euthanasia, D14-21 qD Load + q3D LNP-h*ARG1* on day 72 (1 day post-LD), and WT control livers were examined for ARG1 transgene expression by immunostaining for ARG1. P values obtained by (A) log-rank, (C, E) one-way ANOVA with Tukey's multiple comparison's test, (D$_{Left}$) two-way ANOVA with Sidak's multiple comparison's test, and (D$_{Right}$) unpaired T-test. Data is presented as mean ± SEM. ([B] Day of LNP injection is represented by darkened red square **(n)** for LNP-h*ARG1* and solid black circle (•) for LNP-*luc*.) (g = gram) (TBG = thyroxine binding globulin promoter; Cre = cre recombinase)

Fig. 2-S2. (A) h*ARG1* mRNA hepatic levels relative to murine Gapdh housekeeping gene was assessed by quantitative real-time PCR and (B) hepatic arginase activity was assessed by a biochemical functional assay in weekly LNP-h*ARG1* mice and compared with weekly LNP-*luc* and wild type (WT) controls (n = 6 per group). (C) Western blot analysis of hepatic ARG1 transgene expression in weekly LNP-h*ARG1* mice that were euthanized for humane endpoints at 1, 3, and 5 days or found dead 7 days after the last LNP-h*ARG1* dose and compared with weekly LNP-*luc* and WT control liver. Residual endogenous *Arg1* mRNA levels relative to murine Gapdh housekeeping gene was assessed by quantitative real-time PCR in (D) weekly LNP-h*ARG1*, weekly LNP-*luc*, and WT control mice (n = 6 per group) and in (E) every 3 day (q3D) LNP-h*ARG1* on day 77 (1 day post-last-dose), q3D LNP-*luc*, and WT control mice (n = 6 per group). P values obtained from one-way ANOVA with Tukey's multiple comparison's test. Data is presented as mean ± SEM.
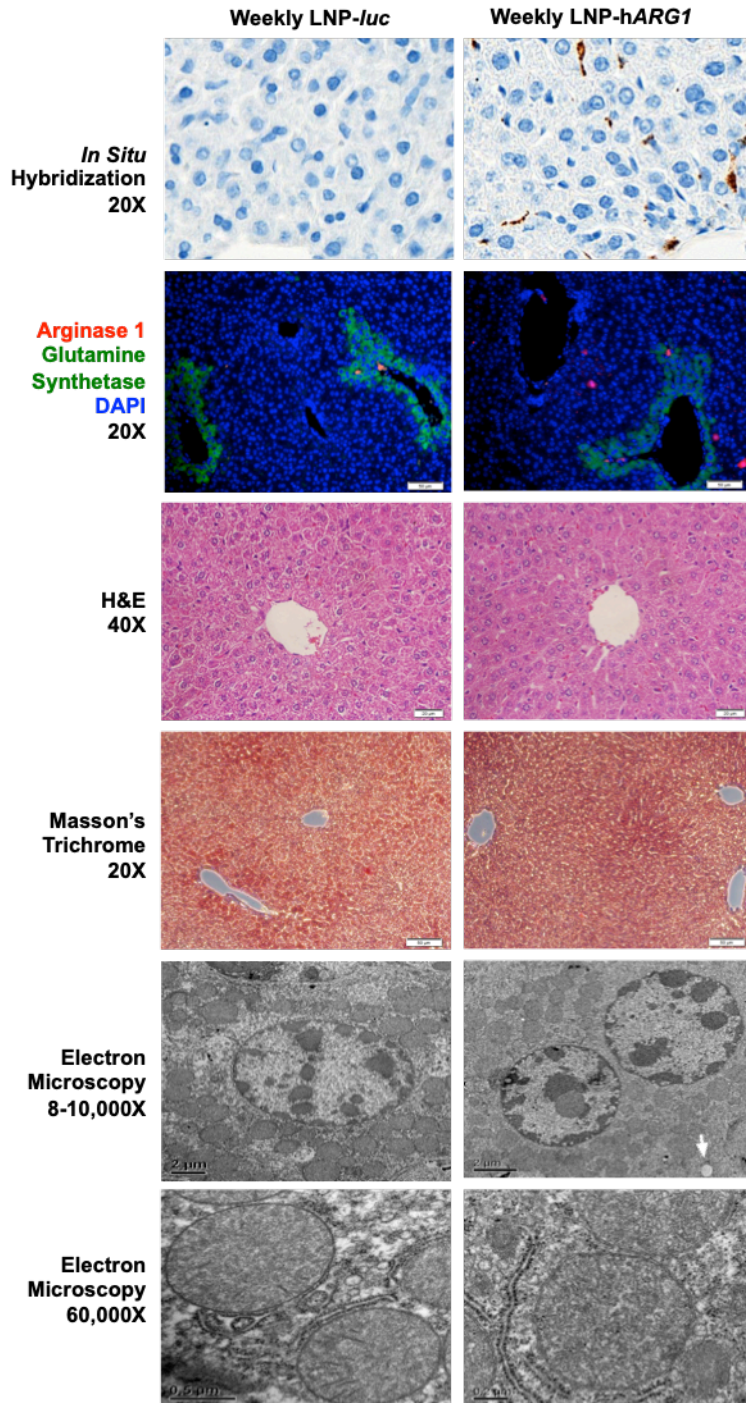
Fig. 2-S3. Liver sections of representative images of weekly LNP-h*ARG1*, weekly LNP-*luc*, and wild type (WT) control mice were examined for: h*ARG1* mRNA presence by *in situ* hybridization (RNAscope®) (top row-20X magnification); h*ARG1* transgene expression with perivenous vascular localization by immunostaining for ARG1 and glutamine synthase (2nd row-20X

magnification); hepatic histology by hematoxylin and eosin (H&E) staining (3rd row-40X magnification); collagen deposition/fibrosis examination by Masson's trichrome staining (4th row-20X magnification); and electron microscopy (5th row-8-10,000X magnification, 6th row-60,000X magnification).

CONCLUSIONS AND FUTURE DIRECTIONS

The urea cycle is an essential pathway for ammonia detoxification and for the regulation and disposal of excess nitrogen in mammals. Its disregulation by way of inherited UCDs, though uncommon, have significant consequences as afflicted infants and newborns are at substantial risk for brain injury and death with standard of care being more prophylactic than curative. Arginase deficiency presents in late infancy with chronic therapy often being ineffective at preventing the progressive and relentless nature of intellectual decline. Liver transplantation is the only known cure, but is an extreme alternative with limited availability. Though our group has demonstrated preclinical data supporting an AAV-based strategy for treatment of arginase deficiency, its clinical application is hampered by concerns for eventual transgene dilution as pediatric patient livers grow. Therefore, the work presented here aimed to develop a proof-of-concept of a personalized cellular-based approach that could grow with the patient. However, recognizing the preclinical nature and lengthy preparation time of the approach, we investigated LNP-encapsulated mRNA that can treat the patient while the more curative cellular approach is prepared.

Restoring Ureagenesis in Hepatocytes by CRISPR/Cas9-mediated Genomic Addition to Arginase-Deficient Induced Pluripotent Stem Cells

The purpose of this study was to determine if hiPSCs could be derived from three genetically distinct arginase deficient patients and whether integration of a human codon-

optimized arginase mediated by a CRISPR/Cas9 nickase system could produce *in vitro* functional arginase after differentiation into hepatocyte-like derivatives for potential use in autologous cellular therapy. After obtaining skin punch biopsies from two arginase deficient patients and a fibroblast sample from third, we demonstrated that hiPSCs could be successfully derived from the diseased lines. We developed a genomic modification system using CRISPR/Cas9 nickases to facilitate significant restoration of arginase enzyme function integrating into the HPRT safe harbor locus with minimal observed off-target effects. We then established a protocol to differentiate our gene-added hiPSCs into HLCs that demonstrated significant arginase enzyme function.

However, after differentiation to HLCs, a significant reduction of arginase RNA and functional activity was observed, but nonetheless, >40% of functional arginase activity was maintained relative to the human fetal liver controls; this decrease also raised concerns of continued transgene reduction upon post-transplantation *in vivo*. We hypothesized that this transgene reduction was due to the use of the hEF1α promoter as it has been shown to undergo silencing post-differentiation. Efforts were performed to determine if pairing the hEF1α promoter with a UCOE could better maintain post-differentiation transgene expression, but similar levels of silencing were observed. Therefore, future arginase expression cassettes should use promoters expressed highly in the liver such as the albumin promoter. Additionally, instead of targeting the HPRT locus, the arginase transgene could target the endogenous albumin locus by integration either directly behind the endogenous promoter or linked to the 3' end of the albumin gene by a self-cleaving 2A peptide.

Additionally, further efforts were performed to derive more mature HLCs where different differentiation protocols and an AFP-Reporter/Selection Construct (ARC) were examined. An updated differentiation protocol based on the Carpentier *et. al.* protocol established a more mature HLC phenotype, though low expression of urea cycle enzymes still indicated fetal-like characteristics. Therefore, additional protocols should be further investigated utilizing 2D-based

80

strategies and also 3D-based liver bud protocols [39, 122]. An ARC was also examined to be able to select for AFP-positive expressing cells to remove non-hepatic derivatives from a heterogeneous population of HLCs. Though selection by antibiotic resistance slightly enriched for an AFP-positive population, it caused significant loss of hepatic morphology and gene expression. However, selection by FACS did modestly improve the hepatic gene expression, but clinical application would be limited due FACS machine constraints such as throughput and application of adverse cellular mechanical stress. Therefore, future reporter constructs should likely be based on albumin expression and also use an alternative and gentler antibiotic such as neomycin or puromycin.

To determine if our gene-added HLCs could contribute to *in vivo* urea cycle function, we developed an immunosuppressed arginase deficient mouse model. However, at present, we have not been able to successfully engraft and repopulate the murine livers with our hiPSC-derived HLCs though we have demonstrated successful engraftment and repopulation of murine livers with intrasplenic injection of 1×10^6 primary human hepatocytes. Future engraftment and repopulation studies will try to determine if lack of engraftment potential is due to hiPSC-derived HLC lack of maturity or potentially a need to transplant more cells per animal.

Lipid Nanoparticle Targeted mRNA Therapy as a Treatment for the Inherited Metabolic Liver Disorder Arginase Deficiency

Though there is promising progression being made in the field to develop a patient-specific pluripotent stem cell-based gene therapy approach for treatment of UCDs such as arginase deficiency and other monogenic liver disorders, these therapies remain in the preclinical stage. Even if established, deriving patient-specific genomically modified HLCs is time consuming. Consequently, during the several months of cellular therapy preparation, patients can remain vulnerable to the progressive intellectual deterioration as conventional

standard of care can prove to be ineffective. Therefore, we were determined to investigate a readily available treatment strategy to bridge the gap.

Delivery of mRNA encapsulated in LNPs for *in vivo* systemic delivery for uptake by hepatocytes is an alternative strategy to provide missing or defective enzyme function. In this study, we systemically administered LNPs targeting the liver that were encapsulating human codon optimized *ARG1* mRNA and were able to achieve functional expression of the enzyme in a conditional knockout model of arginase deficiency. Metabolically, this resulted in maintaining normal plasma ammonia and arginine, preventing the buildup of excessive hepatic arginine, and obviated the development of guanidino compounds, a hallmark of this enzyme deficiency. Unlike controls, repeat dosing of LNPs led to long-term survival without evidence of toxicity, restoration of ureagenesis and the ability to handle toxic ammonia loading.

Though we did not detect any hepatotoxicity, adverse immune responses, or accumulation of lipids in the liver through the duration of our experiment, the dosing frequency and concentration of 2 mg/kg q3D is relatively high compared to other studies treating as low as 0.5 mg/kg weekly [112]. However, since our conditional knockout model does not perfectly recapitulate the human pathobiology, optimization of dosage and frequency of LNP-h*ARG1* in a clinical human disease context will be required. Alternatively, further modifications to the chemically modified mRNA to optimize mRNA stability and translation efficiency or to the LNP formulation to enhance hepatocyte uptake and endosomal escape may also help reduce the dosage and frequency.

As these studies evaluating LNP-h*ARG1* were performed in an adult conditional knockout model of arginase deficiency, additional studies should be performed in the constitutive knockout model [27]. Though we demonstrated by qRT-PCR the absence of any residual endogenous arginase after administration of AAV8-TBG-Cre recombinase, the constitutive knockout model will allow us to determine if treatment with LNP-h*ARG1* can lead to long-term survival in this juvenile lethal arginase deficient mouse model [27]. Additionally, as the

conditional knockout model's immune system has been exposed and tolerized to the wild-type endogenous arginase protein, the constitutive knockout may serve as an appropriate model to examine any potential immune response to the foreign human protein. Additionally, dosage and frequency of administration will need to be optimized as hepatocellular division is rapid in newborn mice and enzymatic requirements may increase as the mice grow. Furthermore, route of LNP-h*ARG1* administration will need to be carefully considered and optimized as IV injections in newborn mice may not be feasible until ~P13, approximately the period when this mouse model perishes or requires euthanasia. However, alternative routes of injections may cause significant shifts in pharmacokinetics and biodistribution of the LNP-h*ARG1* and thereby alter dosage and frequency requirements. These findings and future studies have implications for therapy of arginase deficiency, which is presently inadequately treated and leads to progressive neurological decline.

References

1.   Summar, M.L., et al., *The incidence of urea cycle disorders.* Mol Genet Metab, 2013. **110**(1-2): p. 179-80.

2.   Deignan, J.L., S.D. Cederbaum, and W.W. Grody, *Contrasting features of urea cycle disorders in human patients and knockout mouse models.* Mol Genet Metab, 2008. **93**(1): p. 7-14.

3.   Uchino, T., et al., *Molecular basis of phenotypic variation in patients with argininemia.* Hum Genet, 1995. **96**(3): p. 255-60.

4.   Ah Mew, N., et al., *Urea Cycle Disorders Overview*, in *GeneReviews(R)*, R.A. Pagon, et al., Editors. 1993: Seattle (WA).

5.   Ah Mew, N., et al., *Urea Cycle Disorders Overview*, in *GeneReviews((R))*, M.P. Adam, et al., Editors. 1993: Seattle (WA).

6.   Foschi, F.G., et al., *Urea cycle disorders: a case report of a successful treatment with liver transplant and a literature review.* World J Gastroenterol, 2015. **21**(13): p. 4063-8.

7.   Cooper, A., *Role of glutamine in cerebral nitrogen metabolism and ammonia neurotoxicity.* Ment Retard Dev Disabil Res Rev, 2001. **7**(4): p. 280-286.

8.   Ah Mew, N., et al., *Clinical outcomes of neonatal onset proximal versus distal urea cycle disorders do not differ.* J Pediatr, 2013. **162**(2): p. 324-329.

9.   Perito, E., et al., *Pediatric liver transplantation for urea cycle disorders and organic acidemias: United Network for Organ Sharing data for 2002-2012.* Liver Transpl, 2014. **20**(1): p. 89-99.

10.   Shepherd, R., et al., *Risk Factors for Rejection and Infection in Pediatric Liver Transplantation*
. Am J Transplant, 2008. **8**(2).

11.   Cederbaum, S.D., et al., *Arginases I and II: do their functions overlap?* Mol Genet Metab, 2004. **81 Suppl 1**: p. S38-44.

12.   Carvalho, D.R., et al., *Clinical features and neurologic progression of hyperargininemia.* Pediatr Neurol, 2012. **46**(6): p. 369-74.

13.   Deignan, J.L., et al., *Guanidino compound levels in blood, cerebrospinal fluid, and post-mortem brain material of patients with argininemia.* Mol Genet Metab, 2010. **100 Suppl 1**: p. S31-6.

14.   Marescau, B., et al., *Guanidino compounds in plasma, urine and cerebrospinal fluid of hyperargininemic patients during therapy.* Clin Chim Acta, 1985. **146**(1): p. 21-7.

15.   Mizutani, N., et al., *Guanidino compounds in hyperargininemia.* Tohoku J Exp Med, 1987. **153**(3): p. 197-205.

16.   Wiechert, P., et al., *Excretion of guanidino-derivates in urine of hyperargininemic patients.* J Genet Hum, 1976. **24**(1): p. 61-72.

17.   Wiechert, P., et al., *Hyperargininemia, epilepsy and the metabolism of guanidino compounds.* Padiatr Grenzgeb, 1989. **28**(2): p. 101-6.

18.   Deignan, J.L., et al., *Increased plasma and tissue guanidino compounds in a mouse model of hyperargininemia.* Mol Genet Metab, 2008. **93**(2): p. 172-8.

19.   Burrage, L.C., et al., *Human recombinant arginase enzyme reduces plasma arginine in mouse models of arginase deficiency.* Hum Mol Genet, 2015. **24**(22): p. 6417-27.

20.   Santos Silva, E., et al., *Liver transplantation in a case of argininaemia.* J Inherit Metab Dis, 2001. **24**(8): p. 885-7.

21.   Silva, E.S., et al., *Liver transplantation prevents progressive neurological impairment in argininemia.* JIMD Rep, 2013. **11**: p. 25-30.

22.   Prakash, V., M. Moore, and R. Yanez-Munoz, *Current Progress in Therapeutic Gene Editing for Monogenic Diseases*
. Mol Ther, 2016. **24**(3): p. 465-474.

23.   Anguela, X. and K. High, *Entering the Modern Era of Gene Therapy.* Annu Rev Med, 2019. **70**: p. 273-288.

24.   Lundstrom, K., *Viral Vectors in Gene Therapy.* Diseases, 2018. **6**(2): p. 42.

25.   Iyer, R.K., et al., *Mouse model for human arginase deficiency.* Mol Cell Biol, 2002. **22**(13): p. 4491-8.

26.   Gau, C.L., et al., *Short-term correction of arginase deficiency in a neonatal murine model with a helper-dependent adenoviral vector.* Mol Ther, 2009. **17**(7): p. 1155-63.

27.   Lee, E.K., et al., *Long-term survival of the juvenile lethal arginase-deficient mouse with AAV gene therapy.* Mol Ther, 2012. **20**(10): p. 1844-51.

28.   Hu, C., et al., *Myocyte-mediated arginase expression controls hyperargininemia but not hyperammonemia in arginase-deficient mice.* Mol Ther, 2014. **22**(10): p. 1792-802.

29.   Iansante, V., et al., *Human hepatocyte transplantation for liver disease: current status and future perspectives.* Pediatr Res, 2018. **83**(1-2): p. 232-240.

30.   Takahashi, K., et al., *Induction of pluripotent stem cells from adult human fibroblasts by defined factors.* Cell, 2007. **131**(5): p. 861-72.

31.   Takahashi, K. and S. Yamanaka, *Induction of pluripotent stem cells from mouse embryonic and adult fibroblast cultures by defined factors.* Cell, 2006. **126**(4): p. 663-76.

32.   Idelson, M., et al., *Directed differentiation of human embryonic stem cells into functional retinal pigment epithelium cells.*
. Cell Stem Cell, 2009. **5**(4): p. 396-408.

33.   Schuldiner, M., et al., *Induced neuronal differentiation of human embryonic stem cells.* Brain Res, 2001. **913**(2): p. 201-205.

34.   Lian, X., et al., *Robust cardiomyocyte differentiation from human pluripotent stem cells via temporal modulation of canonical Wnt signaling.* Proc Natl Acad Sci U S A, 2012. **109**(27): p. E1848-1857.

35.   Hay, D., et al., *Efficient Differentiation of Hepatocytes from Human Embryonic Stem Cells Exhibiting Markers Recapitulating Liver Development In Vivo.* Stem Cells, 2008. **26**(4): p. 894-902.

36.   Carpentier, A., et al., *Hepatic differentiation of human pluripotent stem cells in miniaturized format suitable for high-throughput screen.* Stem Cell Res. , 2016. **16**(3): p. 640-650.

37.   Chen, Y.F., et al., *Rapid generation of mature hepatocyte-like cells from human induced pluripotent stem cells by an efficient three-step protocol.* Hepatology, 2012. **55**(4): p. 1193-203.

38.   Song, Z., et al., *Efficient generation of hepatocyte-like cells from human induced pluripotent stem cells.* Cell Res, 2009. **19**(11): p. 1233-42.

39.   Ang, L., et al., *A Roadmap for Human Liver Differentiation from Pluripotent Stem Cells.* Cell Rep, 2018. **22**(8): p. 2190-2205.

40.   !!! INVALID CITATION !!! [36, 39, 40].

41.   Dave, U., N. Jenkins, and N. Copeland, *Gene therapy insertional mutagenesis insights.* Science, 2004. **303**(5656): p. 333.

42.   Marraffini, L. and E. Sontheimer, *CRISPR interference: RNA-directed adaptive immunity in bacteria and archaea.* Nature Reviews, 2010. **11**(3): p. 181-190.

43.   Mali, P., et al., *RNA-guided human genome engineering via Cas9.* Science, 2013. **339**(6121): p. 823-826.

44.   Qi, L., et al., *Repurposing CRISPR as an RNA-guided platform for sequence-specific control of gene expression.* Cell, 2013. **152**(5): p. 1173-1183.

45.   Cong, L., et al., *Multiplex genome engineering using CRISPR/Cas systems.* Science, 2013. **339**(6121): p. 819-823.

46.   Young, C.S., et al., *A Single CRISPR-Cas9 Deletion Strategy that Targets the Majority of DMD Patients Restores Dystrophin Function in hiPSC-Derived Muscle Cells.* Cell Stem Cell, 2016. **18**(4): p. 533-40.

47.   Li, S., et al., *Efficient generation of hiPSC neural lineage specific knockin reporters using the CRISPR/Cas9 and Cas9 double nickase system.* J Vis Exp, 2015. **99**: p. e52539.

48.   Lee, P., et al., *Restoring ureagenesis in hepatocytes by CRISPR/Cas9-mediated genomic addition to arginase-deficient induced pluripotent stem cells.* Mol Ther Nucleic Acids, 2016. **5**(11): p. e394.

49.   Chien, K., L. Zangi, and K. Lui, *Synthetic Chemically Modified mRNA (modRNA): Toward a New Technology Platform for Cardiovascular Biology and Medicine.* Cold Spring Harb Perspect Med, 2015. **5**(1): p. a014035.

50.   Yam, Y., S. Chen, and P. Cullis, *Advances in Lipid Nanoparticles for siRNA Delivery.* Pharmaceutics, 2013. **5**(3): p. 498-507.

51.   Jain-Ghai, S., et al., *Arginase I deficiency: severe infantile presentation with hyperammonemia: more common than reported?* Mol Genet Metab, 2011. **104**(1-2): p. 107-11.

52.   Kasten, J., et al., *Lethal phenotype in conditional late-onset arginase 1 deficiency in the mouse.* Mol Genet Metab, 2013. **110**(3): p. 222-30.

53.   Luiking, Y.C., M.P. Engelen, and N.E. Deutz, *Regulation of nitric oxide production in health and disease.* Curr Opin Clin Nutr Metab Care, 2010. **13**(1): p. 97-104.

54.   Byrne, J.A., H.N. Nguyen, and R.A. Reijo Pera, *Enhanced generation of induced pluripotent stem cells from a subpopulation of human fibroblasts.* PLoS One, 2009. **4**(9): p. e7118.

55.   Lowry, W.E., et al., *Generation of human induced pluripotent stem cells from dermal fibroblasts.* Proc Natl Acad Sci U S A, 2008. **105**(8): p. 2883-8.

56.   Yu, J., et al., *Induced pluripotent stem cell lines derived from human somatic cells.* Science, 2007. **318**(5858): p. 1917-20.

57.   Zhang, Z., et al., *Impact of immune response on the use of iPSCs in disease modeling.* Curr Stem Cell Res Ther, 2015. **10**(3): p. 236-44.

58.   Jinek, M., et al., *A programmable dual-RNA-guided DNA endonuclease in adaptive bacterial immunity.* Science, 2012. **337**(6096): p. 816-21.

59.   Karumbayaram, S., et al., *From skin biopsy to neurons through a pluripotent intermediate under Good Manufacturing Practice protocols.* Stem Cells Transl Med, 2012. **1**(1): p. 36-43.

60.   Durruthy-Durruthy, J., et al., *Rapid and efficient conversion of integration-free human induced pluripotent stem cells to GMP-grade culture conditions.* PLoS One, 2014. **9**(4): p. e94231.

61.   Sommer, C.A., et al., *Induced pluripotent stem cell generation using a single lentiviral stem cell cassette.* Stem Cells, 2009. **27**(3): p. 543-9.

62.   Levitt, N., et al., *Definition of an efficient synthetic poly(A) site.* Genes Dev, 1989. **3**(7): p. 1019-25.

63.   Somers, A., et al., *Generation of transgene-free lung disease-specific human induced pluripotent stem cells using a single excisable lentiviral stem cell cassette.* Stem Cells, 2010. **28**(10): p. 1728-40.

64.   Baxter, M., et al., *Phenotypic and functional analyses show stem cell-derived hepatocyte-like cells better mimic fetal rather than adult hepatocytes.* J Hepatol, 2015. **62**(3): p. 581-9.

65.   Müller-Kuller, U., et al., *A minimal ubiquitous chromatin opening element (UCOE) effectively prevents silencing of juxtaposed heterologous promoters by epigenetic remodeling in multipotent and pluripotent stem cells. .* Nucleic Acids Res, 2015. **43**(3): p. 1577-1592.

66.   Yin, Y., et al., *AFP+, ESC-Derived Cells Engraft and Differentiate into Hepatocytes in Vivo.* Stem Cells, 2002.

67.   Carpentier, A., et al., *Engrafted human stem cell–derived hepatocytes establish an infectious HCV murine model.* J Clin Invest., 2014. **124**(11): p. 4953-4964.

68.   Sadelain, M., E. Papapetroul, and F. Bushman, *Safe harbours for the integration of new DNA in the human genome.* Nature Reviews Cancer, 2012. **12**: p. 51-58

69.   Angarita, S.A.K., et al., *Human hepatocyte transplantation corrects the inherited metabolic liver disorder arginase deficiency in mice.* Mol Genet Metab, 2018. **124**(2): p. 114-123.

70.   Strulovici, Y., et al., *Human embryonic stem cells and gene therapy.* Mol Ther, 2007. **15**(5): p. 850-66.

71.   Meyburg, J. and G.F. Hoffmann, *Liver, liver cell and stem cell transplantation for the treatment of urea cycle defects.* Mol Genet Metab, 2010. **100 Suppl 1**: p. S77-83.

72.   Bachmann, C., *Outcome and survival of 88 patients with urea cycle disorders: a retrospective evaluation.* Eur J Pediatr, 2003. **162**(6): p. 410-6.

73.   Enns, G.M., et al., *Survival after treatment with phenylacetate and benzoate for urea-cycle disorders.* N Engl J Med, 2007. **356**(22): p. 2282-92.

74.   Schambach, A., et al., *Generation and genetic modification of induced pluripotent stem cells.* Expert Opin Biol Ther, 2010. **10**(7): p. 1089-103.

75.   Liu, H., et al., *In vivo liver regeneration potential of human induced pluripotent stem cells from diverse origins.* Sci Transl Med, 2011. **3**(82): p. 82ra39.

76.   Gerecht-Nir, S. and J. Itskovitz-Eldor, *Human embryonic stem cells: a potential source for cellular therapy.* Am J Transplant, 2004. **4 Suppl 6**: p. 51-7.

77.   Giudice, A. and A. Trounson, *Genetic modification of human embryonic stem cells for derivation of target cells.* Cell Stem Cell, 2008. **2**(5): p. 422-33.

78.   Yusa, K., et al., *Targeted gene correction of alpha1-antitrypsin deficiency in induced pluripotent stem cells.* Nature, 2011. **478**(7369): p. 391-4.

79.   Musunuru, K., *Genome editing of human pluripotent stem cells to generate human cellular disease models.* Dis Model Mech, 2013. **6**(4): p. 896-904.

80.   Hu, C., et al., *Minimal ureagenesis is necessary for survival in the murine model of hyperargininemia treated by AAV-based gene therapy.* Gene Ther, 2015. **22**(2): p. 111-5.

81.   Lee, E.K., et al., *AAV-based gene therapy prevents neuropathology and results in normal cognitive development in the hyperargininemic mouse.* Gene Ther, 2013. **20**(8): p. 785-96.

82.   Silverman, L.J., W.N. Kelley, and T.D. Palella, *Genetic analysis of human hypoxanthine-guanine phosphoribosyltransferase deficiency.* Enzyme, 1987. **38**(1-4): p. 36-44.

83.   Liao, S., M. Tammaro, and H. Yan, *Enriching CRISPR-Cas9 targeted cells by co-targeting the HPRT gene.* Nucleic Acids Res, 2015. **43**(20): p. e134.

84.   Swann, P.F., et al., *Role of postreplicative DNA mismatch repair in the cytotoxic action of thioguanine.* Science, 1996. **273**(5278): p. 1109-11.

85.   Shaw-White, J.R., et al., *Expression of the lacZ gene targeted to the HPRT locus in embryonic stem cells and their derivatives.* Transgenic Res, 1993. **2**(1): p. 1-13.

86.   Narsinh, K.H. and J.C. Wu, *Gene correction in human embryonic and induced pluripotent stem cells: promises and challenges ahead.* Mol Ther, 2010. **18**(6): p. 1061-3.

87.   Hong, S., et al., *Functional analysis of various promoters in lentiviral vectors at different stages of in vitro differentiation of mouse embryonic stem cells.* Mol Ther, 2007. **15**(9): p. 1630-9.

88.   Soltys, K.A., et al., *Barriers to the successful treatment of liver disease by hepatocyte transplantation.* J Hepatol, 2010. **53**(4): p. 769-74.

89.   Bhatia, S.N., et al., *Cell and tissue engineering for liver disease.* Sci Transl Med, 2014. **6**(245): p. 245sr2.

90.   Fox, I.J., et al., *Treatment of the Crigler-Najjar syndrome type I with hepatocyte transplantation.* N Engl J Med, 1998. **338**(20): p. 1422-6.

91.   Puppi, J., et al., *Hepatocyte transplantation followed by auxiliary liver transplantation--a novel treatment for ornithine transcarbamylase deficiency.* Am J Transplant, 2008. **8**(2): p. 452-7.

92.   Dhawan, A., et al., *Hepatocyte transplantation for inherited factor VII deficiency.* Transplantation, 2004. **78**(12): p. 1812-4.

93.   Horslen, S.P., et al., *Isolated hepatocyte transplantation in an infant with a severe urea cycle disorder.* Pediatrics, 2003. **111**(6 Pt 1): p. 1262-7.

94.   Muraca, M., et al., *Hepatocyte transplantation as a treatment for glycogen storage disease type 1a.* Lancet, 2002. **359**(9303): p. 317-8.

95.   Sokal, E.M., et al., *Hepatocyte transplantation in a 4-year-old girl with peroxisomal biogenesis disease: technique, safety, and metabolic follow-up.* Transplantation, 2003. **76**(4): p. 735-8.

96.   Lipshutz, G.S., et al., *Short-term correction of factor VIII deficiency in a murine model of hemophilia A after delivery of adenovirus murine factor VIII in utero.* Proc Natl Acad Sci U S A, 1999. **96**(23): p. 13324-9.

97.   DeWeerdt, S., *Prenatal gene therapy offers the earliest possible cure.* Nature, 2018. **564**(7735): p. S6-S8.

98.   Hu, C. and G.S. Lipshutz, *AAV-based neonatal gene therapy for hemophilia A: long-term correction and avoidance of immune responses in mice.* Gene Ther, 2012. **19**(12): p. 1166-76.

99.   Waddington, S.N., et al., *Fetal and neonatal gene therapy: benefits and pitfalls.* Gene Ther, 2004. **11 Suppl 1**: p. S92-7.

100. Cantero, G., et al., *Rescue of the Functional Alterations of Motor Cortical Circuits in Arginase Deficiency by Neonatal Gene Therapy.* J Neurosci, 2016. **36**(25): p. 6680-90.

101. Chandler, R.J., et al., *Vector design influences hepatic genotoxicity after adeno-associated virus gene therapy.* J Clin Invest, 2015. **125**(2): p. 870-80.

102. Hu, C., R.W. Busuttil, and G.S. Lipshutz, *RH10 provides superior transgene expression in mice when compared with natural AAV serotypes for neonatal gene therapy.* J Gene Med, 2010. **12**(9): p. 766-78.

103. Wang, Z., et al., *Adeno-associated virus serotype 8 efficiently delivers genes to muscle and heart.* Nat Biotechnol, 2005. **23**(3): p. 321-8.

104. Cunningham, S.C., et al., *Gene delivery to the juvenile mouse liver using AAV2/8 vectors.* Mol Ther, 2008. **16**(6): p. 1081-8.

105. Fausto, N. and J.S. Campbell, *The role of hepatocytes and oval cells in liver regeneration and repopulation.* Mech Dev, 2003. **120**(1): p. 117-30.

106. Magami, Y., et al., *Cell proliferation and renewal of normal hepatocytes and bile duct cells in adult mouse liver.* Liver, 2002. **22**(5): p. 419-25.

107. Ramaswamy, S., et al., *Systemic delivery of factor IX messenger RNA for protein replacement therapy.* Proc Natl Acad Sci U S A, 2017. **114**(10): p. E1941-E1950.

108. An, D., et al., *Systemic Messenger RNA Therapy as a Treatment for Methylmalonic Acidemia.* Cell Rep, 2018. **24**(9): p. 2520.

109. Kormann, M.S., et al., *Expression of therapeutic proteins after delivery of chemically modified mRNA in mice.* Nat Biotechnol, 2011. **29**(2): p. 154-7.

110. Zatsepin, T.S., Y.V. Kotelevtsev, and V. Koteliansky, *Lipid nanoparticles for targeted siRNA delivery - going from bench to bedside.* Int J Nanomedicine, 2016. **11**: p. 3077-86.

111. Gustafsson, C., S. Govindarajan, and J. Minshull, *Codon bias and heterologous protein expression.* Trends Biotechnol, 2004. **22**(7): p. 346-53.

112. An, D., et al., *Systemic Messenger RNA Therapy as a Treatment for Methylmalonic Acidemia.* Cell Rep, 2017. **21**(12): p. 3548-3558.

113. Khoja, S., et al., *Conditional disruption of hepatic carbamoyl phosphate synthetase 1 in mice results in hyperammonemia without orotic aciduria and can be corrected by liver-directed gene therapy.* Mol Genet Metab, 2018. **124**(4): p. 243-253.

114. Sun, Q. and W.E. O'Brien, *Diagnosis of creatine metabolism disorders by determining creatine and guanidinoacetate in plasma and urine.* Methods Mol Biol, 2010. **603**: p. 175-85.

115. Allegri, G., et al., *A simple dried blood spot-method for in vivo measurement of ureagenesis by gas chromatography-mass spectrometry using stable isotopes.* Clin Chim Acta, 2017. **464**: p. 236-243.

116.   Chung-Bok, M.I. and M. Watford, *Characterization of the hepatic glutaminase promoter.* Contrib Nephrol, 1997. **121**: p. 43-7.

117.   Amayreh, W., U. Meyer, and A.M. Das, *Treatment of arginase deficiency revisited: guanidinoacetate as a therapeutic target and biomarker for therapeutic monitoring.* Dev Med Child Neurol, 2014. **56**(10): p. 1021-4.

118.   Jichlinski, A., et al., *"Cerebral Palsy" in a Patient With Arginase Deficiency.* Semin Pediatr Neurol, 2018. **26**: p. 110-114.

119.   Therrell, B.L., et al., *Newborn screening for hyperargininemia due to arginase 1 deficiency.* Mol Genet Metab, 2017. **121**(4): p. 308-313.

120.   Chandler, R.J., et al., *Metabolic phenotype of methylmalonic acidemia in mice and humans: the role of skeletal muscle.* BMC Med Genet, 2007. **8**: p. 64.

121.   Hsu, E.K., et al., *Analysis of Liver Offers to Pediatric Candidates on the Transplant Wait List.* Gastroenterology, 2017. **153**(4): p. 988-995.

122.   Takebe, T., et al., *Massive and Reproducible Production of Liver Buds Entirely from Human Pluripotent Stem Cells.*
. Cell Rep, 2017. **21**(10): p. 2661-2670.